

**REAL-TIME IMPLEMENTATION OF SOME
ATTITUDE ESTIMATION ALGORITHMS ON A
QUADROTOR UAV**

by

Siddhant Nayak

Under the Supervision of Dr. Abdelhamid Tayebi

A Thesis Submitted in Partial Fulfillment
of the Requirements for the Degree of
Master of Science
in Control Engineering

Lakehead University, Thunder Bay, Ontario, Canada

November 2013

ProQuest Number: 10611963

All rights reserved

INFORMATION TO ALL USERS

The quality of this reproduction is dependent upon the quality of the copy submitted.

In the unlikely event that the author did not send a complete manuscript and there are missing pages, these will be noted. Also, if material had to be removed, a note will indicate the deletion.



ProQuest 10611963

Published by ProQuest LLC (2017). Copyright of the Dissertation is held by the Author.

All rights reserved.

This work is protected against unauthorized copying under Title 17, United States Code
Microform Edition © ProQuest LLC.

ProQuest LLC.
789 East Eisenhower Parkway
P.O. Box 1346
Ann Arbor, MI 48106 - 1346

Abstract

The recent developments in research pertaining to the field of Unmanned Aerial Vehicles (UAVs) is motivated by its technical challenges as well as its practical implications in areas where human presence is inefficient, redundant or dangerous. The absence of human interference requires more robust and precise control techniques. However, most modern attitude control techniques require the knowledge of the current orientation of the body. There is no sensor available that explicitly measures the attitude of a rigid body and hence, for small scale UAVs, it must be estimated using inertial vector measurements from low-cost and low-weight Micro-Electro-Mechanical System (MEMS) sensors like gyroscopes, accelerometers and magnetometers.

The predominant attitude representation formulations of a rigid body in three-dimensional space are recapitulated to elucidate the dynamical model of a quadrotor UAV. Low-cost MEMS are prone to significant noise effects from temperature change, vibrations, on-board magnetic fields generated by motors and currents. To improve the accuracy of the measurements sensor calibration techniques are explored. Primitive attitude estimation techniques like TRIAD, Davenport's q-method, QUEST, FOAM, SVD method, etc. (which were aimed to be static optimization solutions to Wahbas Problem) were reviewed. These algorithms were extended to incorporate filtering techniques like Kalman-type, to handle the measurement noise, and complementary filtering, where sensor measurements are fused to reconstruct the orientation of a rigid body. The latest nonlinear observers are also discussed for implementation purposes.

Practical implementation and performance comparison of various attitude estimation algorithms has been conducted on a small-scale quadrotor UAV, consisting of an inertial measurement unit (3-axis gyroscope, accelerometer and magnetometer), microcontroller, brushless motors, electronic speed controllers, on-board power supply and necessary frame constructs.

Acknowledgments

Foremost, I would like to express my sincere gratitude to my Supervisor Dr. Abdelhamid Tayebi for the continuous support of my study and research, for his patience, motivation, enthusiasm, and immense knowledge. His guidance helped me throughout my research and writing of this thesis. I could not have imagined having a better advisor and mentor for my masters degree.

I would like to thank Dr. Xiaoping Liu, Dr. Wilson Wang and Dr. Krishnamoorthy Natarajan, whom I have had the privilege and pleasure to learn from while at Lakehead University. My sincere thanks also goes to Mr. Warren Paju, Mr. Bruce Misner and Mr. Kailash Bhatia for their help and innovative ideas throughout the process.

I thank my fellow graduate students Kurtis Schram, Nirav Patel and Bhavin Patel, for the stimulating discussions, their insightful comments and suggestions and for all the fun we have had in the last two years.

I would like to express my deepest gratitude to my family for, their endless love and support, encouragement to pursue higher education in engineering and supporting me spiritually throughout my life.

Finally, I would like to thank Tarz, for her continued love and belief in me to succeed.

Siddhant Nayak

Contents

List of Figures	v
List of Abbreviations	viii
1 Introduction	1
1.1 Problem Statement	2
1.2 Brief History of Quadrotors	3
1.3 Motivation	5
2 Attitude Representations and Model Preliminaries	7
2.1 Attitude Formalisms	7
2.1.1 Direction Cosine Matrix	8
2.1.2 Euler Angles	9
2.1.3 Unit Quaternion	10
2.2 Quadrotor Mathematical Model	12

2.3	Inertial Sensors and Measurements	15
2.3.1	Gyroscope	15
2.3.2	Accelerometer	16
2.3.3	Magnetometer	16
3	Experimental Apparatus and Calibration Techniques	18
3.1	APM 2.5	19
3.1.1	Atmel Atmega2560	20
3.1.2	Atmel Atmega32U2	20
3.1.3	Invensense MPU-6000	21
3.1.4	Honeywell HMC5883L	22
3.2	Radio and Telemetry	22
3.3	Power Module and Actuators	23
3.4	Microstrain Inc. 3DM-GX1	23
3.5	Gyroscope and Accelerometer Calibration	25
3.6	Magnetometer Calibration	26
4	Static Attitude Estimation	32
4.1	TRIAD	33
4.2	Q-Method	34
4.3	QUEST	35

4.4	SVD	36
4.5	FOAM	37
4.6	Experimental Results	38
5	Dynamic Attitude Estimation	50
5.1	Filter QUEST	51
5.2	Kalman Filter	52
5.2.1	Extended Kalman Filter	53
5.2.2	Multiplicative EKF	54
5.2.3	Additive EKF	58
5.3	Complementary Filter	62
5.3.1	Linear Complementary Filter	62
5.3.2	Non-linear Complementary Filter	65
5.4	Globally Exponentially Stable Observers Non-evolving in SO3	67
5.5	Experimental Results	72
6	Conclusion	86

List of Figures

2.1	Quadrotor aircraft	12
3.1	Arducopter platform	20
3.2	ArduPilotMega controller (a) with enclosure and (b) without enclosure	21
3.3	3DM-GX1 Module	24
3.4	Accelerometer output at 260 Hz filtering	27
3.5	Accelerometer output at 184 Hz filtering	27
3.6	Accelerometer output at 94 Hz filtering	28
3.7	Accelerometer output at 44 Hz filtering	28
3.8	Accelerometer output at 21 Hz filtering	29
3.9	Magnetometer calibration results	31
4.1	TRIAD result 1	39
4.2	Q-method result 1	39
4.3	QUEST result 1	40

4.4	SVD Method result 1	40
4.5	FOAM result 1	41
4.6	TRIAD result 2	41
4.7	Q-method result 2	42
4.8	QUEST result 2	42
4.9	SVD Method result 2	43
4.10	FOAM result 2	43
4.11	TRIAD result with accelerometer measurements filtering	45
4.12	Q-method result with accelerometer measurements filtering	45
4.13	QUEST result with accelerometer measurements filtering	46
4.14	SVD Method result with accelerometer measurements filtering	46
4.15	FOAM result with accelerometer measurements filtering	47
4.16	TRIAD result with accelerometer measurements filtering and simulated motion	47
4.17	Q-method result with accelerometer measurements filtering and simulated motion	48
4.18	QUEST result with accelerometer measurements filtering and simulated motion	48
4.19	SVD Method result with accelerometer measurements filtering and simulated motion	49
4.20	FOAM result with accelerometer measurements filtering and simulated motion	49
5.1	Linear complementary filter	64
5.2	Filter QUEST result 1	74

5.3	MEKF result 1	74
5.4	AEKF result 1	75
5.5	Linear complementary filter result 1	75
5.6	Nonlinear complementary filter result 1	76
5.7	Globally exponentially stable Observer result 1	76
5.8	Filter QUEST result 2	77
5.9	MEKF result 2	77
5.10	AEKF result 2	78
5.11	Linear complementary filter result 2	78
5.12	Nonlinear complementary filter result 2	79
5.13	Globally exponentially stable Observer result 2	79
5.14	Filter QUEST result 3	82
5.15	MEKF result 3	82
5.16	AEKF result 3	83
5.17	Linear complementary filter result 3	83
5.18	Nonlinear complementary filter result 3	84
5.19	Globally exponentially stable Observer result 3	84
5.20	Globally exponentially stable Observer result 4	85
5.21	Globally exponentially stable Observer result 5	85

List of Abbreviations

UAV	- Unmanned Aerial Vehicle.
DCM	- Direction Cosine Matrix.
ESC	- Electronic Speed Controller.
MEMS	- Micro-Electro-Mechanical System.
SDK	- Software Development Kit.
APM	- ArduPilotMega.
SPI	- Serial Peripheral Interface.
IGRF	- International Geomagnetic Reference Field.
WMM	- World Magnetic Model.
TRIAD	- TRI-axial Attitude Determination.
QUEST	- QUaternion ESTimator.
SVD	- Singular Value Decomposition.
EKF	- Extended Kalman Filter.
MEKF	- Multiplicative Extended Kalman Filter.
SPARS	- Space Precision Attitude Reference System.
AEKF	- Additive Extended Kalman Filter.
ESQ	- ESTimation of Optimal Quaternion.
FOAM	- Fast Optimal Attitude Matrix.
PWM	- Pulse Width Modulation.
PPM	- Pulse Position Modulation.
ADC	- Analog-to-Digital Converter.
EMF	- Electro Motive Force.
IMU	- Inertial Measurement Unit.
GPS	- Global Positioning System.
SONAR	- SOund Navigation and Ranging.
UDP	- User Datagram Protocol.
GES	- Globally Exponentially Stable.
CPU	- Central Processing Unit.
DC	- Direct Current.
AC	- Alternate Current.

Chapter 1

Introduction

In the past, unmanned aerial vehicles (UAVs) have been primarily the subject of investment for different fields including military and rescue operations, reconnaissance, investigation, aeronautical, remote mapping, etc. However, this has changed in the past few years, as these vehicles have gained immense popularity among the researchers and hobbyists.

In order to achieve autonomous stable flight, various configurations have evolved over the years. The rotary wing class of aircrafts has been a popular structure in this domain due to its maneuverability and the capability to land / take off vertically. In comparison to conventional helicopters, quadrotor aircraft possess some desirable attributes, making them ideal for research applications. The quadrotor model owing to its fixed-pitch rotors as well as the elimination of the tail rotor is a simpler and efficient design to control. In the past decade, academic research teams have particularly shown a rising interest in quadrotor UAV platforms majorly due to the birth of MEMS technology and consequently, the availability of miniature sized inertial sensors. From a theoretical perspective, many authors have investigated control strategies to maintain a stable hovering condition for UAVs. In practice, the noise and uncertainties due to inaccurate sensor measurements and the inherent instability of aerial robots make it an exciting and interesting field of research.

1.1 Problem Statement

Attitude estimation and attitude stabilization are two main tasks associated with developing an autonomous quadrotor aerial robot. The lack of a human pilot complicates the problem of attitude stabilization and requires more sophisticated and advanced control algorithms, which should not only control the flight dynamics but also perform the desired task at hand. However, the main difficulty of the attitude stabilization problem is obtaining accurate estimates of the systems attitude. Most modern controllers presume that the precise attitude information is known. As a result of this, the key focus of this thesis is to explore, implement and compare the popular attitude estimation algorithms.

The prenominal requirement to achieve attitude balance is an accurate estimation of the vehicle orientation. The theory of the kinematics of motion suggests that if the rigid body's exact angular velocity is known, its attitude can be calculated. However, in practice there are many flaws in the measurements by gyroscopic sensors used for angular velocity. Specifically, in long-term missions, gyros often drift and uncertainties over time cause errors to accumulate, making the integration of kinematic equations an impractical way to estimate the attitude. This fact reveals the challenging side of attitude estimation problem. Another problem is that the orientation must be efficiently and clearly parameterized.

Various engineering disciplines, including aerial or under water robotics, aeronautics and space engineering all experience a similar crucial problem of determining the orientation of a rigid body relative to an inertial frame of reference. This problem has been studied extensively over the past years. Euler angles, Rodriguez Parameterization, Rotation Matrix and Quaternion Formulation are among the common attitude representation methods used to represent the orientation of an object. A large number of publications have been found in the literature discussing attitude representation techniques and their advantages and drawbacks [1], [2], [3].

A common approach to obtain relatively accurate attitude estimation is using inertial sensors; accelerometers and magnetometers in addition to gyroscopes. Combination of inertial measurements from a multitude of sensors to develop attitude observers has been the subject of many

valuable discussions in the literature [4], [5], [6].

Low cost inertial sensors measurements are contaminated with noise, biases and misalignments. Thus, reducing noise and compensating for measurement uncertainties are added tasks when dealing with the attitude estimation process. Low pass filtering method is a well-known solution to minimize the effect of measurement noise. However, since there is a compromise between measurement bandwidth and sensor response time, the limitation in bandwidth must be taken into account.

1.2 Brief History of Quadrotors

Quadrotor design history can generally be defined in two main generations. The earlier generations were developed majorly for military missions. The latest quadrotor design generation consists of model sized aircraft capable of autonomous flight possible due to existence of low cost and lightweight MEMS sensors. In the past decade, quadrotors have been used mainly as a popular test bed to design an unmanned aerial vehicle because of their small size, agile maneuverability, low cost, simple maintenance and the capability of flight indoor as well as outdoor.

The history of quadrotor design dates back more than a century. Gyroplane, an X-shaped steel constructed quadrotor built by Louis and Jacques Breguet in association with Professor Charles Richet in summer of 1907, was introduced only four years after the Wright brothers recorded the first controllable flight by an airplane [7]. A four-blade rotor was mounted at the end of each arm. One pair of diagonally opposed rotors rotated in a clockwise direction while the other pair rotated counter-clockwise. All rotors were driven by a 40/45 hp Antoinette piston-engine mounted in the rectangular central chassis which was considered to protect pilot and engine. Pilot M. Volumard was chosen for flight tests in which the vehicle took off with success and could hover at low altitudes. The Breguet-Richet quadrotor aircraft was not the first free flight, as during experiments, each rotor was kept in a steady condition with assistance of a man. However, it was the first quadrotor aircraft to experiment a vertical take-off with the help of a pilot [7].

The first distance flight by a quadrotor was recorded on April 14, 1924 in France for Etienne Oemichens second helicopter. This quadrotor was built in 1920, an X-shaped frame with one large propeller at the end of each arm. Five small horizontal propellers were added to achieve lateral stability as well as one mounted at the nose for steering and another couple of propellers for forward motion. All propellers were driven by a single 120hp Le Rhone rotary engine. This quadrotor showed a considerable degree of stability and controllability, considering the limited facilities available at the time. However, Oemichen was dissatisfied with the limited altitude the aircraft could reach during several experiments, resulting in the abandonment of the multi rotor schemes to concentrate on single rotor layouts [8].

Around same time in 1922, the US army funded the experiments of Dr.George De Bothezat to build a four rotor aircraft powered by one main engine [9]. The frame was X-shaped with arms slightly inclined inward. The aircraft could record stable flight of 90 seconds despite being heavy weight (see for instance, [7] and [10]). Unfortunately, due to high cost and relatively insufficient performance, the US army gradually lost interest in the project, hindering any possible achievements.

The ten years following World War II witnessed the start and stop of a large number of companies attempting to manufacture and sell a variety of helicopter configurations. D. H. Kaplan's quadrotor project was sponsored by Convertawings Company in Amityville, New York [11]. This model was an H-shaped configuration with four rotors mounted at the very end of arms. The system was designed such that almost all movements could be achieved using the four rotors. For instance, increasing the pitch of two rotors on one side while decreasing those of the two rotors on the other side would lead to roll movement. For moving right or left, the four rotors would be inclined slightly inward from the vertical position. The designer and test pilot, D. H. Kaplan successfully flew the quadrotor on Long Island in 1956. However, this project was terminated later as there were not sufficient orders made for commercial or military versions.

As mentioned earlier, the recent interest in building small sized quadrotors as unmanned aircraft has generated from the availability of the lightweight miniature electronics. In 1996 Area Fifty One Technologies built the first modern quadrotor, later improved and manufactured as the com-

mercial radio controlled aerial robot called Draganflyer by the well-known Canadian company, RCToys [12], [13]. Since then, a large number of groups and individuals have worked on the development of the quadrotor aerial robot. The quadrotor makes the perfect choice as a test bed to validate different new flight control and stabilization algorithms developed by academic research teams due to its low maintenance requirement and the symmetrical mechanical configuration. For instance, in 2001, a very small-scaled quadrotor aerial robot was initially developed in the Mesicopter project [14] sponsored by Stanford University, investigating the challenging control and manufacture of this aircraft. A vision based control algorithm was used through this particular project leading to successful hovering. STAR- MAC project was another successor in the modern generation of quadrotor aerial robots widely known for aggressive maneuverability and successful multi-agent flights [15].

For more than a decade now, the unmanned aerial vehicles have been the subject of research in the Automatic Control lab, at Lakehead University [16], [17], [18]. The objective of some previous projects was to investigate the challenging concept of design and implementation of a quadrotor aerial robot seeking the required attitude stabilization for a hovering flight.

1.3 Motivation

As discussed earlier, there are a large number of solutions to the attitude estimation problem. However, there has been very little focus on the comparison and evaluation of these algorithms under varying conditions. This issue was first addressed in 1999 by F. L. Markley and D. Mortari [19]. It was a comparison of the static attitude estimation techniques prevalent at that time and considered that the vector measurements were accurate and did not present any challenges in terms of noise and misalignments. The algorithms were simulated in MATLAB [20] and compared in terms of accuracy and speed of execution. Another survey of non-linear attitude estimation methods was conducted to explore the modern filtering methods available for attitude estimation under the assumption that vector measurements are affected by a considerable amount of noise [4]. While it was successful in enlisting and discussing the advantages and drawbacks of a large number of dynamic attitude estimation techniques, simulations or practical results were

not provided.

In May 2013, through the thesis work of N. Madinehi [21], a wide variation of static as well as dynamic attitude estimation techniques were studied. Theoretical background, supported by simulations in MATLAB and SIMULINK provided a much clearer view of the limitations and convenience of the algorithms under review.

With these precursors in view, there was a need to validate these results on a practical system. A large number of attitude estimation techniques have been tested and implemented on various models of flying and aquatic robots. However, these results cannot be used for the purpose of a comparative study as the parameters, environments and experimental setups used vary extensively. This thesis focuses on the implementation of a few prominent attitude estimation techniques on a common apparatus for the purpose of an unbiased and reasonable comparison. Attitude representations and model preliminaries are examined in Chapter 2. The choice and setup of the experimental apparatus is elucidated in Chapter 3 and the theoretical review with implementation and results are discussed in Chapters 4 and 5.

Chapter 2

Attitude Representations and Model Preliminaries

Attitude parameterization is crucial to determine the motion of a rigid body in space with respect to an inertial frame of reference. This chapter aims to summarize the commonly used attitude representations and their relative advantages and disadvantages in section (2.1). It is a common area of study and has been dealt with in a variety of texts (see for example [2], [22] and [23]).

One of the primary aims of this research is to establish a comparison of attitude estimation algorithms on a quadrotor UAV. Therefore, the dynamical model of the quadrotor has been reviewed in brief. This helps us to understand the special groups that represent the rotational and dedicated to this aim. Since, the application is heavily reliant on inertial sensor measurements in attitude estimation problems, the sensors are reviewed from a theoretical perspective in section (2.3).

2.1 Attitude Formalisms

In order to describe a rotation, two frames of reference, namely the inertial and body-fixed frame of reference, are used. The inertial frame of reference is considered to be stationary and is rigidly attached to a certain location on earth, the sun or a star. For the purpose of our research, this

frame of reference was chosen to have its origin at latitude 48.42 North, longitude 89.26 West at an altitude of 211m from sea level. The second frame of reference, as the name suggests, is attached to the center of mass of the rigid body under consideration.

Several existing methods are available to represent the orientation of a rigid body and relating inertial and non-inertial coordinates. Each of these methods has a number of advantages and disadvantages, making them useful depending on the application they are used for. The rotation matrix and the unit-quaternion are constrained parameterizations with redundant elements. Euler angles, Rodrigues parameters and modified Rodrigues parameters are examples of unconstrained minimal parameterizations.

For the purpose of this thesis, we summarize the commonly used attitude representations: Direction Cosine Matrix, Euler Angles and Unit Quaternions. The notations used in this thesis denote \mathcal{I} as the inertial (fixed) frame and \mathcal{B} as the body-attached frame. The orientation (attitude) of a rigid body is defined as the orientation of frame \mathcal{B} with respect to frame \mathcal{I} .

2.1.1 Direction Cosine Matrix

The Direction Cosine Matrix (DCM), also known as rotation matrix, is possibly the most natural way of describing the attitude of a body. It can be described as a matrix that must be multiplied to a vector in the inertial frame in order to convert it to the body frame. For example, let $a_{\mathcal{I}}$ be a vector expressed in the inertial frame \mathcal{I} and $a_{\mathcal{B}}$ be the vector projection of $a_{\mathcal{I}}$ in the body frame \mathcal{B} . Then,

$$a_{\mathcal{B}} = R^T a_{\mathcal{I}} \quad (2.1)$$

where R is the rotation matrix describing the orientation of frame \mathcal{B} with respect to frame \mathcal{I} . Mathematically, DCM belongs to the Lie group $SO(3)$, Special Orthogonal group of dimension 3.

$$SO(3) = \{R \in R^{3 \times 3} | R^T R = R R^T = I_{3 \times 3}, \det(R) = 1\} \quad (2.2)$$

The product of two rotation matrices belonging to $SO(3)$, is also a rotation matrix belonging to $SO(3)$. A special case of this property is where the rotation matrix R is multiplied by its transpose R^T or inverse R^{-1} resulting in the identity matrix I . This identity matrix represents a

null rotation or a condition where the two frames of reference are coincident. Another definition of rotation matrix R , describing the orientation of frame \mathcal{I} with respect to frame \mathcal{B} , can also be found in the literature. In this case one has

$$a_{\mathcal{B}} = Ra_{\mathcal{I}} \quad (2.3)$$

Note that the rotation matrix is non-singular and unique representation of the orientation.

2.1.2 Euler Angles

The Euler angles were introduced by Leonhard Euler to describe the orientation of a rigid body. To describe such an orientation in 3-dimensional Euclidean space, three parameters were required. Many such three-dimensional attitude parameterizations have been presented over the years (refer to [24] and [2]), but Euler angles have been the most popular. However, similar to the other parameterizations, it can be shown that it cannot be both non-singular and unique.

In common terminology, the Euler angles $[\phi, \theta, \psi]$ are known as roll, pitch and yaw of the rigid body, where ϕ , θ and ψ define a positive rotation about x , y and z axes respectively. The rotation matrix can be defined in terms of three consecutive rotations about the given axes in the specific order of rotation. The order of rotations in this case is $z \rightarrow y \rightarrow x$.

$$\begin{aligned} R &= R_z(\psi)R_y(\theta)R_x(\phi) \\ &= \begin{bmatrix} c\psi & -s\psi & 0 \\ s\psi & c\psi & 0 \\ 0 & 0 & 1 \end{bmatrix} \begin{bmatrix} c\theta & 0 & s\theta \\ 0 & 1 & 0 \\ -s\theta & 0 & c\theta \end{bmatrix} \begin{bmatrix} 1 & 0 & 0 \\ 0 & c\phi & -s\phi \\ 0 & s\phi & c\phi \end{bmatrix} \\ &= \begin{bmatrix} c\theta c\psi & s\theta s\phi c\psi - s\psi c\phi & s\theta c\phi c\psi + s\psi s\phi \\ c\theta s\psi & s\theta s\phi s\psi + c\psi c\phi & s\theta c\phi s\psi - c\psi s\phi \\ -s\theta & c\theta s\phi & c\theta c\phi \end{bmatrix} \end{aligned} \quad (2.4)$$

where s and c denote the sine and cosine of the respective angles.

The extraction of the Euler angles from the rotation matrix, results in a singularity at $\theta = \pm\pi/2$. There is no unique solution for yaw and roll at this singular configuration. Therefore, we can say that Euler angles formalism is not a global parameterization of the attitude. However, it is easier

to imagine the orientation of a rigid body when the values of roll, pitch and yaw are provided. The DCM and quaternion representation fail to provide such insight to the actual orientation.

2.1.3 Unit Quaternion

Another globally non-singular representation of the attitude consists of using four-dimensional vectors Q , called unit-quaternion, evolving in the three-sphere \mathbb{S}^3 , embedded in \mathbb{R}^4 , $\mathbb{S}^3 = \{Q \in \mathbb{R}^4 \mid Q^T Q = 1\}$.

A unit-quaternion $Q = (q_0, q^T)^T$ is composed of a scalar component $q_0 \in \mathbb{R}$ and a vector component $q \in \mathbb{R}^3$, such that $q_0^2 + q^T q = 1$. A rotation matrix R describing a rotation by an angle θ about the unit-vector $\hat{k} \in \mathbb{R}^3$, can be represented by the unit-quaternion Q or $-Q$ such that $q_0 = \cos(\theta/2)$ and $q = \sin(\theta/2)\hat{k}$. Note that the mapping from $SO(3)$ to \mathbb{S}^3 is not a one-to-one mapping as there are two unit quaternion that represent the rotation matrix R . The rotation matrix can be constructed from the unit quaternion by using Rodrigues formula

$$\begin{aligned} R(Q) &= I_3 + 2S(q)^2 - 2q_0S(q) \\ &= \begin{bmatrix} q_0^2 + q_1^2 - q_2^2 - q_3^2 & 2q_0q_3 + 2q_1q_2 & -2q_0q_2 + 2q_1q_3 \\ -2q_0q_3 + 2q_1q_2 & q_0^2 - q_1^2 + q_2^2 - q_3^2 & 2q_0q_1 + 2q_2q_3 \\ 2q_0q_2 + 2q_1q_3 & -2q_0q_1 + 2q_2q_3 & q_0^2 - q_1^2 - q_2^2 + q_3^2 \end{bmatrix} \end{aligned} \quad (2.5)$$

where $S(x)$ is the skew-symmetric matrix associated with $x \in \mathbb{R}^3$. The skew-symmetric matrix can be defined as

$$S(x) = \begin{bmatrix} 0 & -x_3 & x_2 \\ x_3 & 0 & -x_1 \\ -x_2 & x_1 & 0 \end{bmatrix} \quad (2.6)$$

with $x = [x_1, x_2, x_3]^T \in \mathbb{R}^3$. Given a rotation matrix R and two vectors $x, y \in \mathbb{R}^3$, we have the following useful properties: $S(x)y = -S(y)x = x \times y$, $S(x)x = 0$, $S(x)S(y) = yx^T - (x^T y)I_3$ and $S(Rx) = RS(x)R^T$, where \times denotes the vector cross product [25].

If the unit quaternion is described by a rotation angle θ and a rotation axis \hat{k} , then the transformation to rotation matrix is given by

$$R(\theta, \hat{k}) = I_3 - \sin(\theta)S(\hat{k}) + (1 - \cos(\theta))S(\hat{k})^2 \quad (2.7)$$

To preserve the definition of a quaternion, quaternion multiplication is much different from linear algebra employed for rotation matrices. As with rotation matrices, quaternion multiplication can be used to combine two or more quaternions to describe the overall attitude of a moving body. It is also used to transform a vector from one frame to another. Let $Q_x = (q_{0,x}, q_x)$ and $Q_y = (q_{0,y}, q_y)$, be two unit quaternions. Then the quaternion product $Q_z = (q_{0,z}, q_z)$ is given by

$$Q_z = Q_x \odot Q_y = \begin{pmatrix} q_{0,x}q_{0,y} - q_x^T q_y \\ q_{0,x}q_y + q_{0,y}q_x + q_x \times q_y \end{pmatrix} \quad (2.8)$$

where (\odot) denotes the quaternion multiplication and (\times) denotes the cross product. Similar to the DCM, unit quaternion multiplication is non-commutative.

The inverse of a unit quaternion $Q = (q_0, q)$ is denoted by $Q^{-1} = (q_0, -q)$, where

$$Q \odot Q^{-1} = Q^{-1} \odot Q = (1, \mathbf{0}) \quad (2.9)$$

The quaternion representation $Q = (1, \mathbf{0})$ is equivalent to the null rotation observed in DCM.

As discussed earlier, the unit quaternion multiplication can also be used to transform a vector from one frame of reference to another. Let a_I be a vector expressed in the inertial frame I and a_B be the vector projection of a_I in the body frame B. Then,

$$\bar{a}_B = Q \odot \bar{a}_I \odot Q^{-1} \quad (2.10)$$

where $\bar{x} = (0, x)$, $x \in \mathbb{R}^3$

The quaternion representation has some distinct advantages over other attitude formalisms. Its minimal representation makes it more suited for implementation on practical systems. As opposed to the rotation matrix, which has 9 elements, the quaternion works with 4 elements to reduce computational load. The Euler angles while computationally more efficient than the unit quaternion representation is ineffective as it is a non-global representation.

The unit quaternion is a non-singular representation of attitude. However, despite its strong advantages, there are certain drawbacks. The quaternion representation is an over-parameterization of the rotation space $SO(3)$. As a result, both unit quaternions Q and $-Q$ signify the same rotation matrix $R(Q) = R(-Q)$. Therefore, the unit quaternion representation lacks uniqueness.

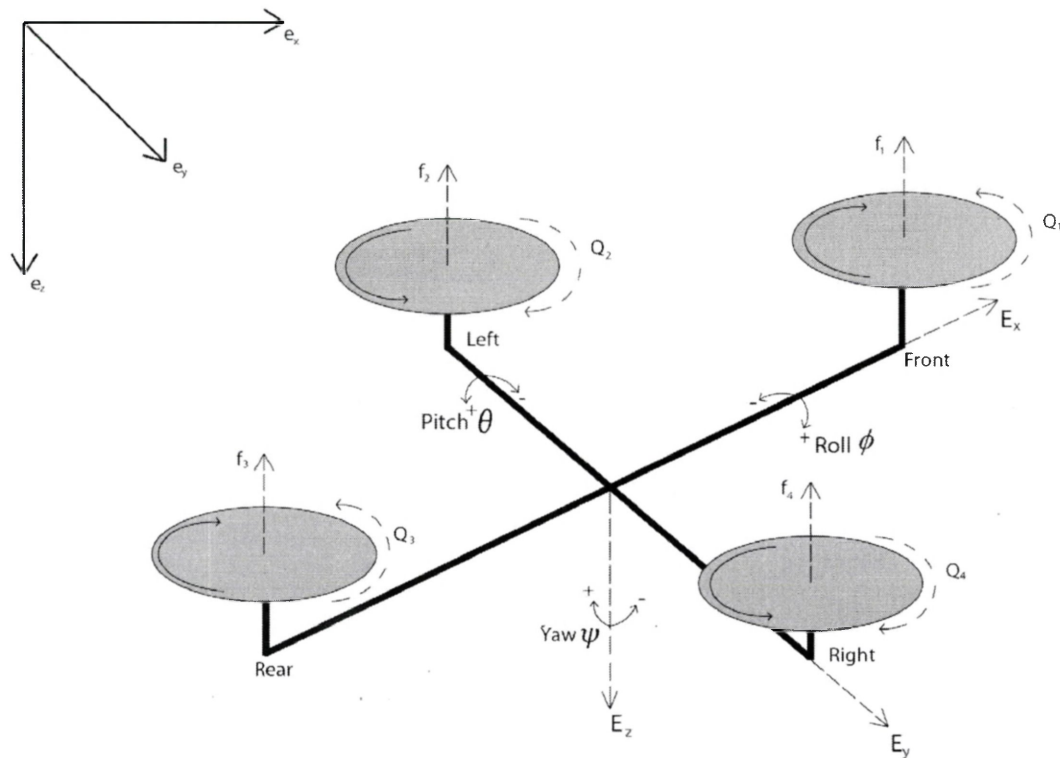


Figure 2.1: Quadrotor aircraft

2.2 Quadrotor Mathematical Model

The quadrotor UAV consists of a rigid frame of four arms joined at the center. At the ends of each arm is a rotor as shown in Figure 2.1. The motion of the quadrotor is a combination of variations in angular velocity of individual motors. Each rotor generates an upward thrust and a torque about its center of rotation. Each propeller produces a drag force opposite to the vehicle's direction of flight. If individual rotor angular velocities are the same, with left and right rotors rotating clockwise and front and rear rotors counterclockwise, the angular acceleration about the yaw axis is exactly zero. This implies that the yaw stabilizing rotor of conventional helicopters is not needed.

Each pair of blades rotating in the same direction controls one axis for roll and pitch. Roll and pitch action is produced by changing the relative angular velocity of the rotors with the

same direction of rotation, without changing the overall thrust produced by the pair. Therefore, individual angular accelerations about the pitch and roll axes can be achieved without disturbing the yaw axis. Yaw is induced by mismatching the cumulative angular velocities of two pairs of blades. This way, fixed pitch blades can maneuver the quadrotor in all dimensions. Translational acceleration is achieved by maintaining a non-zero pitch or roll angle.

Let $\mathcal{I} = \{e_x, e_y, e_z\}$ denote an inertial frame, and $\mathcal{B} = \{E_x, E_y, E_z\}$ denote a frame rigidly attached to the aircraft as shown in Figure 2.1. Then the dynamical model of a quadrotor as described in [26] and [27] is given by

$$\dot{p} = v \quad (2.11)$$

$$\dot{v} = ge_z - \frac{1}{m}TRe_z \quad (2.12)$$

$$\dot{R} = RS(\Omega) \quad (2.13)$$

$$I_f \dot{\Omega} = -\Omega \times I_f \Omega - G_a + \tau_a \quad (2.14)$$

$$I_r \dot{\omega}_i = \tau_i - Q_i, \quad i \in 1, 2, 3, 4 \quad (2.15)$$

$$T = \sum_{i=1}^4 |f_i| = b \sum_{i=1}^4 \omega_i^2 \quad (2.16)$$

$$G_a = \sum_{i=1}^4 I_r (\Omega \times e_z) (-1)^{i+1} \omega_i \quad (2.17)$$

$$Q_i = k\omega_i^2 \quad (2.18)$$

The notations used in equations 2.11 to 2.18 are defined in Table 2.1. Equation (2.13) can be re-written in quaternion representation as,

$$\dot{Q} = \frac{1}{2}Q \odot \begin{bmatrix} 0 \\ \omega \end{bmatrix} \quad (2.19)$$

and as Euler angles representation,

$$\begin{aligned} \dot{\phi} &= \omega_1 + \omega_2 \sin \phi \tan \theta + \omega_3 \cos \phi \tan \phi \\ \dot{\theta} &= \omega_2 \cos \phi - \omega_3 \sin \phi \\ \dot{\psi} &= \omega_2 \sin \phi \sec \theta + \omega_3 \cos \phi \sec \theta \end{aligned} \quad (2.20)$$

Notation	Represents
m	mass of airframe
g	acceleration due to gravity
e_z	$(0, 0, 1)^T$ unit vector in I
p	position of the origin of the body fixed frame B with respect to I
v	linear velocity vector of the origin of B
T	total thrust generated by the four motors
R	orientation of the airframe
$S(x)$	skew symmetric operator as given by Equation (2.6)
Ω	angular velocity of the airframe in the body-fixed frame
I_f	symmetric positive-definite constant inertia matrix of the airframe with respect to the frame B whose origin is at the center of mass
\times	vector cross product
G_a	gyroscopic torques due to the combination of the rotation of the airframe and the four rotors
τ_a	airframe torques generated by the rotors
ω_i	angular velocity of motor i (direction does not change)
τ_i	torque produced by motor i
Q_i	reactive torque generated in free air by rotor i due to rotor drag
k	positive proportionality constant that relates reactive torque its respective angular velocity
b	positive proportionality constant that relates total thrust to the sum of angular velocity
f_i	lift generated by rotor i in free air

Table 2.1: Notations used

2.3 Inertial Sensors and Measurements

As mentioned in earlier sections, inertial sensors used individually are not reliable for attitude reconstruction. The three types of sensors commonly used for attitude estimation are gyroscopes, accelerometers and magnetometers. The accelerometers ideally provide the linear acceleration of the rigid body in the body-fixed frame of reference B . The magnetometers measure the surrounding magnetic field in the body frame. The gyroscopes measure the angular velocity in the body frame. Tri-axial sensors are generally used for measurements on all the three orthogonal axes.

This section discusses the characteristics of inertial sensors, considering possible sources of biases and uncertainties in measurements by these type of sensors. Due to the heavy reliance of attitude estimations techniques on inertial sensors, it is necessary to understand the theoretical aspect of the nature of operation of inertial sensors. These issues have been addressed in [28] and [29].

2.3.1 Gyroscope

MEMS gyroscopes are based on the Coriolis effect. This can be observed as a deflection of moving objects when they are viewed with respect to a rotating frame of reference. In MEMS gyroscopes two vertically driven vibrating masses form the core for each axis of observation. When the sensor is rotated, the Coriolis phenomena triggers the masses in opposite directions. This leads to an orthogonal vibration that can be sensed by a capacitive pickoff. The resulting signal is then amplified, demodulated and filtered to produce a measurement that is proportional to the angular rate.

The gyroscope output ω_m can be modeled as,

$$\omega_m = \omega + b_g + n_\omega \quad (2.21)$$

where ω is the exact system body-referenced angular velocity, affected by the constant sensor bias b_g and white noise n_ω .

Apart from a constant sensor bias and white noise, the gyro readings are also contaminated with bias drift, which takes effect at lower frequencies, and self heating of the device to produce faulty

readings.

The gyroscope signals can be easily measured at rest to provide the constant bias. However, the bias drift and white noise cannot be known *a priori*.

2.3.2 Accelerometer

An accelerometer is a device that measures the apparent acceleration. The linear acceleration measured by an accelerometer is not necessarily the gravity vector measured in the body-frame of reference. If $g = (0, 0, 9.8)^T m/s^2$ is the gravity vector and $a \in \mathbb{R}^3$ is the acceleration of the rigid body due to translational motion in the inertial frame, then the accelerometer reading A_m , in the body frame, is given by

$$A_m = R^T (a - g) + b_a + n_a \quad (2.22)$$

where, R , b_a and n_a are the rotation matrix defining the orientation of the rigid body with respect to the inertial frame, constant bias and random noise respectively. For quasi-stationary flights, the linear acceleration of the system can be assumed to be much smaller than the gravity vector and we can say that $a \approx 0$.

The MEMS accelerometer is a polysilicon surface-micromachined structure built on top of a silicon wafer. The structure is suspended by polysilicon springs over the surface of the wafer and provide a resistance against acceleration forces. The measurement corresponds to a deflection of the surface using a differential capacitor that consists of independent fixed plates and plates attached to the moving mass. Out-of-phase (180°) square waves drive the fixed plates. The moving mass is deflected by the acceleration that unbalances the differential capacitor resulting in a sensor output. The magnitude and direction of the acceleration are determined by phase-sensitive demodulation techniques. For more details about construction and operational theory of MEMS accelerometer refer to [28] and [30].

2.3.3 Magnetometer

A magnetometer is an instrument to measure the strength and direction of the surrounding magnetic field. Magnetometers are widely used for measuring the Earth's magnetic field and in

geophysical surveys to detect magnetic anomalies of various types. In aerospace applications, they are primarily used to compute the yaw or heading of the aircraft. However, due to the distortion D , the sensor bias b_m and the measurement white noise n_m , the magnetometer reading M_m , in the body frame, is given by

$$M_m = DR^T m_I + b_m + n_m \quad (2.23)$$

where R is the rotation matrix and m_I is the earth's magnetic field at the specified location.

A typical MEMS magnetometer is a surface-mount multi-chip module designed for low-field magnetic sensing. The magnetoresistive circuit forms a trio of sensors to measure magnetic fields. The magnetoresistive sensors are made of a nickel-iron (Permalloy) thin-film and shaped to form a resistive bridge. Resistance of the bridge elements changes in the presence of a magnetic field and causes a corresponding change in voltage across the bridge outputs [31].

Chapter 3

Experimental Apparatus and Calibration Techniques

The development of MEMS inertial sensors led to mass production of low-cost research platforms and hobby-grade quadrotors. Various commercially available quadrotors and open source platforms were considered as a candidate for practical implementation. The criteria for selection were:

1. On-board inertial sensors consisting of 3-axis gyroscope, accelerometer and magnetometer.
2. Suitable microcontroller.
3. Open-source programs and product support.
4. Reliability of the platform.
5. Versatility in terms of use and performance.
6. Cost.

With the above criteria in mind, the following options were explored further:

1. **Arducopter** [32] is an open-source quadrotor autopilot project based on the Arduino framework. It has an onboard 3-axis magnetometer, accelerometer and gyroscope, and altimeter. It is easily programmable and configurable. The project is supported by a large community of researchers and hobbyists around the world. Many options for purchase of spare parts and upgradeable sensors like GPS, SONAR and optical flow are easily available.
2. **Pelican** [33] from Ascending Technologies is one of the most popular quadrotor platforms used in the field of research. Its light weight tower structure helps to mount diverse payloads and easily access all electronics. It is programmable through their proprietary Software Development Kit (SDK) and AstTec Simulink toolkit. It is equipped with a powerful dual-core CPU. Due to price considerations, it was not considered for the current project.
3. **Phantom, Draganflyer X4 and Parrot ARDrone** [34–36] are popular commercially available quadrotors being manufactured and sold as standalone systems. They do not allow for any modification to the proprietary code and hence weren't considered as viable options to be used as a testbed.

Arducopter platform proved to be the most suitable option in the list. A comparative study of some popular platforms is given in [37]. The quadrotor used as the experimental apparatus was purchased from 3DR-robotics. It includes the inertial sensors, micro-controllers, electronic speed controllers, actuators and necessary frame parts.

3.1 APM 2.5

The ArduPilotMega (APM) is the main controller board used in the Arducopter quadrotor. It uses an Atmega2560 microcontroller as the primary controller for processing control and estimation algorithms. The secondary microcontroller is an Atmega 32U-2 used for the purpose of radio communication, telemetry and motor control. A tri-axial gyroscope and accelerometer (Invensense MPU-6000) and a 3-axis magnetometer (Honeywell HMC5883L) are embedded on-board. A barometer (Measurement Specialties MS5611) provides the temperature compensated altitude. These components are discussed briefly in the following sub-sections.



Figure 3.1: Arducopter platform

3.1.1 Atmel Atmega2560

Atmega2560 is a high-performance, low-power Atmel 8-bit AVR RISC-based microcontroller with 256KB flash memory, 8KB SRAM and 4KB EEPROM to meet our processing requirements. It has 86 general purpose I/O lines, 4 USARTs, serial peripheral interface (SPI) and I²C interface to communicate with the sensors and peripherals. Real time counters, six flexible timer/counters with compare modes and hardware and software generated PWM for generating motor outputs and demodulating input radio signals. The device operates at 16 MHz between 4.5-5.5 volts input source voltage which is sufficient for the implementation of estimation and control algorithms as well as communication functions. For more details refer to [38].

3.1.2 Atmel Atmega32U2

Atmega32U2 is a secondary microcontroller on-board the APM. Its primary functions are to offload the radio inputs and motor output generation from Atmega2560. Up to eight radio input channels can be fed to the general purpose pins of 32U2 and are converted to PPM signal to be decoded by Atmega2560. It also acts as the in-line programmer for the Atmega2560. The 32U2

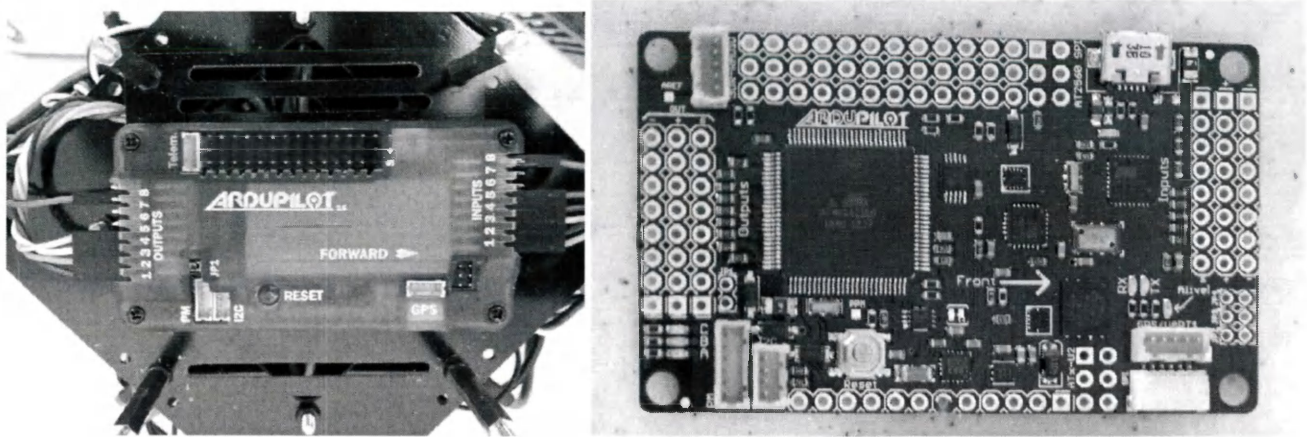


Figure 3.2: ArduPilotMega controller (a) with enclosure and (b) without enclosure

is connected to a USB header and can serve as a programmer via the UART0 pins of the 2560. It is the main source of communication between the base-station computer and the APM2.5. Further details are provided in [39].

3.1.3 InvenSense MPU-6000

MPU-6000 from InvenSense Inc. combines a 3-axis accelerometer and gyroscope, and a digital motion processor on a single chip. It is connected to the Atmega2560 through the SPI lines and is fully programmable. It is a highly versatile device offering a large variety of gyroscope full-scale range of ± 250 , ± 500 , ± 1000 , and ± 2000 degrees/sec (dps) and a user-programmable accelerometer full-scale range of $\pm 2g$, $\pm 4g$, $\pm 8g$, and $\pm 16g$ [40].

The output of the accelerometer is sampled by a 16-bit ADC on each axis and conditioned by a low pass filter with variable configuration. Another set of integrated 16-bit ADCs sample each gyroscope axis from 8000 to 1000 samples per second and a configurable low-pass filter can be set to a wide range of cut-off frequencies. Both the gyroscope and accelerometer readings are stored in data registers and can be retrieved by Atmega2560 via SPI protocol.

3.1.4 Honeywell HMC5883L

The Honeywell HMC5883L magnetometer is a magnetoresistive sensor circuit forming a triad of orthogonal axes to measure its surrounding magnetic field [41]. The magnetoresistive sensors are essentially a nickel-iron thin-film patterned as a resistive strip element. In the presence of a magnetic field, the bridge elements produce a change in the voltage across the bridge corresponding to a change in the bridge resistive elements. Thus, the sensor produces a differential voltage output based on the incident magnetic field in the sensitive axis directions. This voltage is then amplified and sampled on-chip by a 12-bit ADC. The reading is stored in a data register and accessed by the Atmega2560 through I²C protocol.

These resistive elements are aligned together to have a common sensitive axis that will provide positive voltage change with magnetic fields increasing in the sensitive direction. Because the output is only proportional to the magnetic field component along its axis, additional sensor bridges are placed at orthogonal directions to permit accurate measurement of magnetic field in any orientation.

The HMC5883L has a full scale reading of ± 8 gauss that is scalable through a 3-bit gain control ranging the output from ± 1 gauss to ± 8 gauss. Output rates can be varied from 0.75 Hz to 75 Hz with the default being 15 Hz. However, the quadrotor platform is designed for agile performance and the objective is to test the performance of attitude estimation algorithms with noisy measurements. Therefore, the magnetometer is configured to run at maximum output rate of 75 Hz.

3.2 Radio and Telemetry

The transmitter and receiver set used for radio communication is a 2.4 GHz RF system with 8 channels. Initially, a 72 MHz 4 channel FM radio system was used to provide user input to the quadrotor aircraft. It was plagued with erroneous spikes, interference and sudden signal loss that couldn't be explained or corrected. The 2.4 GHz radio system exhibits much better performance and is immune to interference from its surroundings. Also, the added channels allow for more

versatility of input commands to the quadrotor.

The telemetry unit comprises of a transreceiver at the base-station computer as well as one connected to the APM to relay information and send commands. It has an operating radio frequency of 915 MHz. Due to time limitations, implementation of the telemetry unit has not been conducted.

3.3 Power Module and Actuators

The entire platform is powered by a 2700 mAh 3-cell lithium polymer battery. Maximum continuous current that can be drawn from the battery is 121.5 A, allowing up to 243 A of current in short bursts. The battery voltage when fully charged is 12.6 V, and 9.9 V when discharged.

The brushless motor and electronic speed controller (ESC) pairs serve as actuators for the quadrotor. The ESCs are driven by the PWM signal sent from the APM and convert the input DC voltage from the battery to 3-phase AC current to drive the motors at the desired speed. Since, the ESC controls the speed of the motor, a feedback from the motor is required. Earlier speed controllers employed Hall effect sensors but more recent ones measure the back-EMF generated in the un-driven coils. The motor A2830 is an outrunner brushless motor produced by 3DR-robotics. It's specifications as provided by the manufacturer are given in Table 3.1.

Voltage	KV(rpm/V)	Max Pull	Weight	Max power	ESC
7.4-15 V	850	880g	52g	200watt	20A

Table 3.1: Motor Specifications

3.4 Microstrain Inc. 3DM-GX1

Implementation and comparison of attitude estimation algorithms on a practical system is the main objective of this thesis work. However, the Arducopter platform did not include any reference basis to compare various attitude estimation techniques. Hence, the basis of comparison



Figure 3.3: 3DM-GX1 Module

needs to be defined clearly. The estimated attitude from various algorithms need to be objectively viewed with respect to a precise source. The most accurate systems employ an array of motion tracking cameras around the quadrotor, to produce reliable attitude information. However, these motion tracking systems are not cost effective for the task at hand. Another alternative is to use robust, high-performance IMUs for the purpose of generating reliable attitude information. The 3DM-GX1 from Microstrain Inc. is used for this purpose [42].

The 3DM-GX1 contains three angular rate gyros with three orthogonal DC accelerometers and three orthogonal magnetometers. Combined with a multiplexer, 16 bit A/D converter, and embedded microcontroller, it produces the dynamic and static orientation of the module. It can produce outputs in DCM, quaternion and Euler angles format in 360 degrees of angular motion on all three axes with a static accuracy of ± 0.5 degrees and a dynamic accuracy of ± 2 degrees. The digital serial output from an RS-232 connector can also provide temperature compensated, calibrated data from all nine orthogonal sensors at update rates of upto 350 Hz.

The full scale range for angular rate is ± 300 degrees/sec with a resolution of 0.01 degrees/sec. Accelerometer has a range of ± 5 g with a resolution of 0.5 mg. The magnetometer output deflects to ± 1.2 Gauss with a resolution of 0.2 mGauss. Output modes and software filter parameters

are user programmable. Programmed parameters and calibration data are stored in nonvolatile memory. The 3DM-GX1 module is attached rigidly to the body frame, to provide attitude estimates of the quadrotor.

3.5 Gyroscope and Accelerometer Calibration

The accelerometer and gyroscope ranges were set to default operations as specified in the datasheet of MPU6000 [40]. Gyroscope range is set to ± 250 degrees per second with a resolution of 7.63×10^{-3} degrees per second. The typical range for the accelerometer is given as ± 2 g. However, this seemed to be insufficient due to the fact that during take-off the linear acceleration of the quadrotor would be capped off by the accelerometer. Therefore, the range for the accelerometer was selected as ± 4 g with a resolution of 1.22×10^{-4} g.

Both the accelerometer and the gyroscopes models (Equations (2.21) and (2.22)) possess a constant bias term that can be easily compensated. While the system is at rest on a leveled surface, the output data from accelerometer and gyroscope can be collected and averaged for each individual axis to provide estimates of b_g and b_a . The corrected measurements ω_c and A_c can be written as

$$\omega_c = \omega_m - b_g \quad (3.1)$$

$$A_c = A_m - b_a \quad (3.2)$$

The MPU6000 output is filtered by a digital filter. The cut-off frequency of the filter can be selected as per Table 3.2.

Acc. cut-off (Hz)	Acc. delay (ms)	Gyro. cut-off (Hz)	Gyro. delay (ms)
260	0	256	0.98
184	2.0	188	1.9
94	3.0	98	2.8
44	4.9	42	4.8
21	8.5	20	8.3
10	13.8	10	13.4
5	19.0	5	18.6

Table 3.2: Accelerometer and gyroscope cut-off frequencies and delay

Since, response of the quadrotor to changes in attitude was of prime importance, delays over 10 ms were unacceptable and only the first five filters were considered. The accelerometer is much more susceptible to vibrations from the motors. Figures 3.4 to 3.8 show the output of the three axes of the accelerometer under different filters.

The filters progressively reduce the effect of vibrations on the accelerometer as the cut-off frequency is decreased. However, the objective of the thesis is to consider the performance of the attitude estimation algorithms under noisy sensor measurements. Therefore, to preserve the originality of sensor signals, cut-off frequency of the digital filter for the accelerometer is set to 260 Hz.

3.6 Magnetometer Calibration

The magnetometer measures the magnetic field of its surrounding environment including disturbances from structural steel, ferrous metal parts, electric motors and power lines. This leads to untrustworthy magnetometer readings attempting to read the earth's magnetic field. As seen in Equation (2.23), disturbances can be categorized into sources that lead to an offset in the magnetometer readings and those that produce a distortion in the magnetic field measured.

An offset or bias in readings is caused by zero bias shift, hard-iron effect and difference in

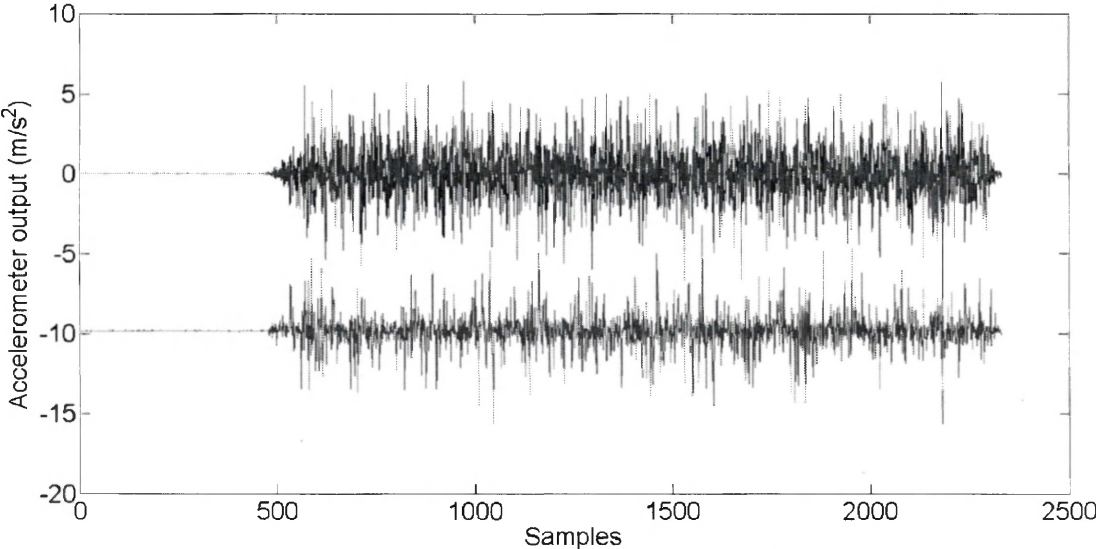


Figure 3.4: Accelerometer output at 260 Hz filtering

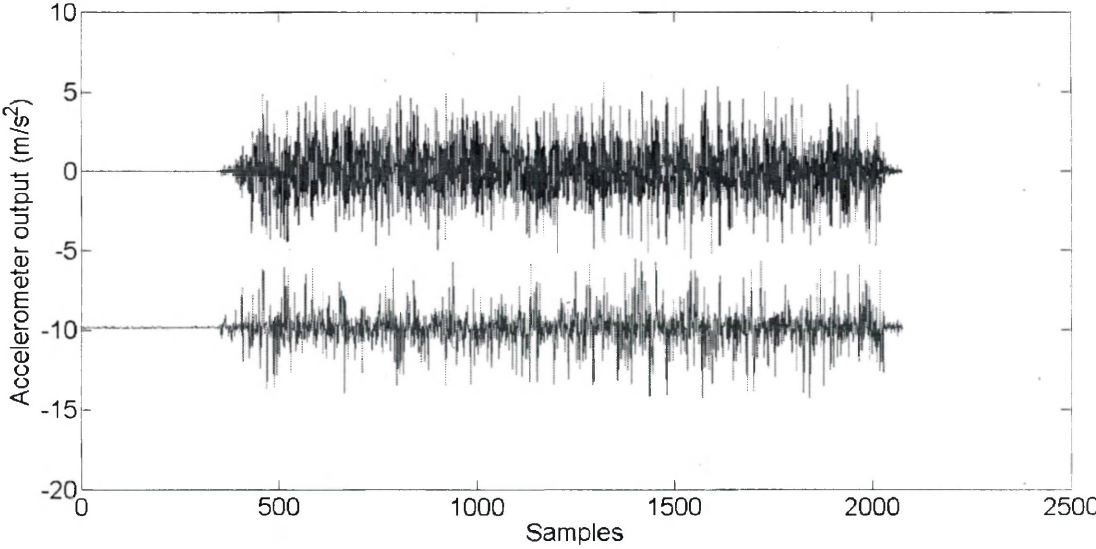


Figure 3.5: Accelerometer output at 184 Hz filtering

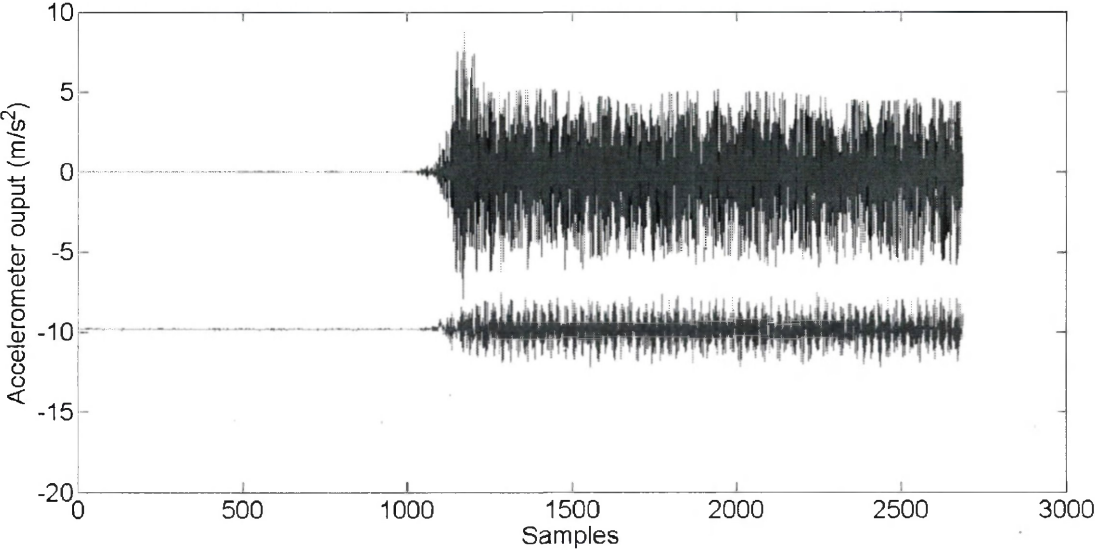


Figure 3.6: Accelerometer output at 94 Hz filtering

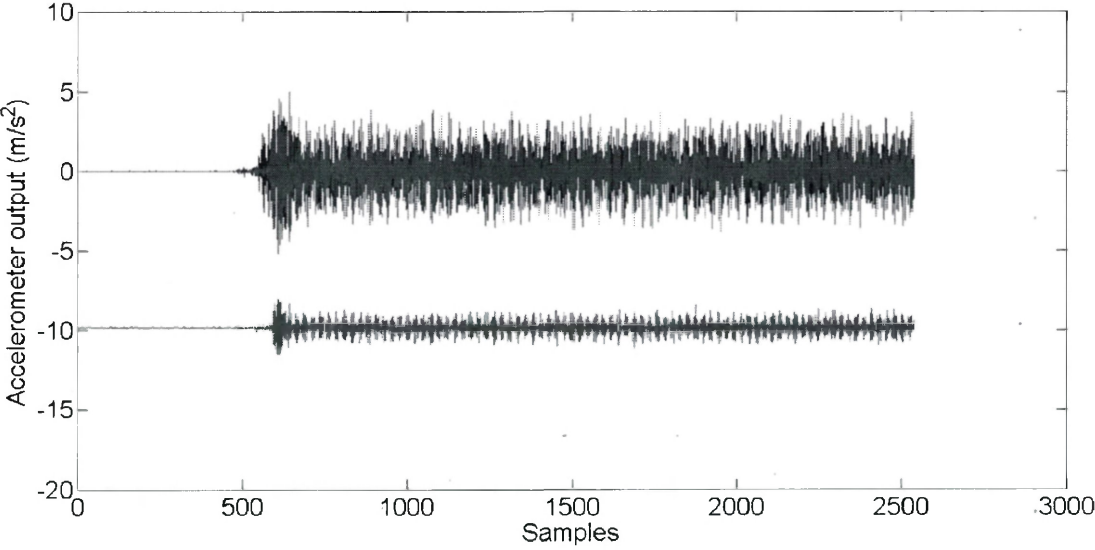


Figure 3.7: Accelerometer output at 44 Hz filtering

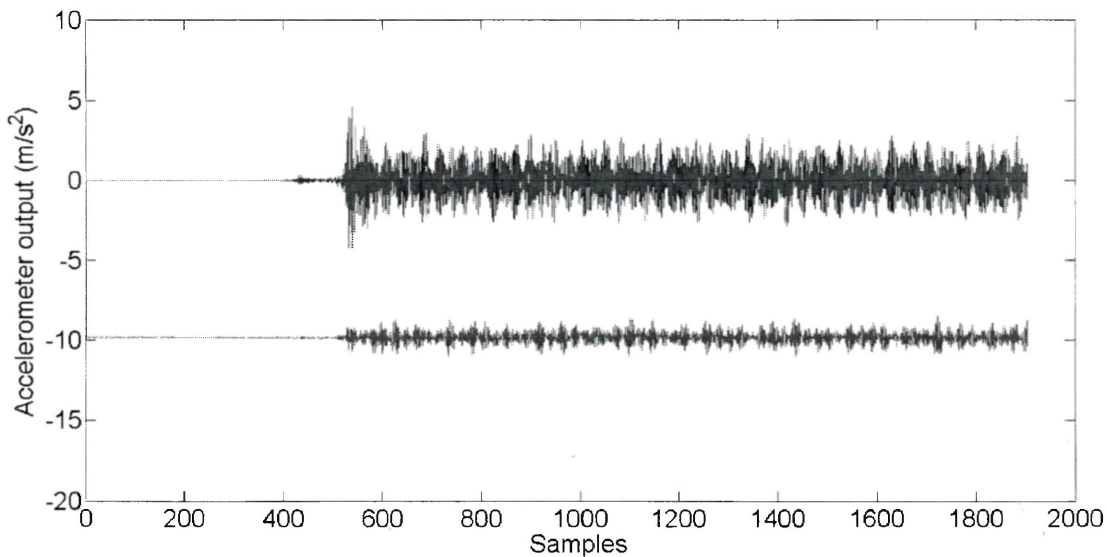


Figure 3.8: Accelerometer output at 21 Hz filtering

sensitivity of the three magnetometer axes. Theoretically, the magnetic field vector m is constant and the collected data points should map out a 3-D sphere centered at zero with radius $|m|$. The offset affects the center of the sphere and shifts it to a non-zero coordinate. A simple approach is to compute $b_m = \text{mean}(\{M_m\})$ based on an appropriate magnetometer data set $\{M_m\}$ and use it to correct future measurements as $M_m - b_m$. The advantage of this method is that it doesn't require any knowledge of the local magnetic field amplitude and involves simple calculations.

Distortions in the measured magnetic field are caused by sensor scaling errors $(\alpha_x, \alpha_y, \alpha_z)$, sensor misalignment angles $(\beta_x, \beta_y, \beta_z)$ and the sensor offsets $(\gamma_x, \gamma_y, \gamma_z)$ on the individual axes. These distortions require more rigorous calibration techniques like [43]. The magnetometer model as proposed in the paper is given as

$$M_m = \begin{bmatrix} \alpha_x & 0 & 0 \\ \alpha_y \sin \beta_x & \alpha_y \cos \beta_x & 0 \\ \alpha_z \sin \beta_y \cos \beta_z & \alpha_z \sin \beta_z & \alpha_z \cos \beta_y \cos \beta_z \end{bmatrix} m_B + \begin{bmatrix} \gamma_x \\ \gamma_y \\ \gamma_z \end{bmatrix} = Dm_B + b_m \quad (3.3)$$

where m_B is the earth's magnetic field in the body frame of reference. Equation (3.3) is a simplification of Equation (2.23), where the effects of white noise are not considered. Equation (3.3) is rearranged to give

$$m_B = D^{-1} (M_m - b_m) \quad (3.4)$$

and substituted in $|m_B|^2 = m_x^2 + m_y^2 + m_z^2$ to result in

$$\begin{aligned} C_1 M_{mx} M_{mx} + C_2 M_{mx} M_{my} + C_3 M_{mx} M_{mz} + C_4 M_{my} M_{my} + C_5 M_{my} M_{mz} + C_6 M_{mz} M_{mz} \\ + C_7 M_{mx} + C_8 M_{my} + C_9 M_{mz} = C_{10} \end{aligned} \quad (3.5)$$

where the coefficients C_k ($1 \leq k \leq 10$) are defined as functions of α, β, γ and $|m_B|$. Assuming that the data set $\{M_m\}$ has N data points, Equation (3.5) can be re-written as

$$\begin{bmatrix} M_{x,1}^2 & M_{mx,1} M_{my,1} & \cdots & M_{mz,1} \\ \vdots & \vdots & \ddots & \vdots \\ M_{x,N}^2 & M_{mx,N} M_{my,N} & \cdots & M_{mz,N} \end{bmatrix} \begin{bmatrix} C_1/C_{10} \\ \vdots \\ C_9/C_{10} \end{bmatrix} = \begin{bmatrix} 1 \\ \vdots \\ 1 \end{bmatrix} \quad (3.6)$$

Note that for $\alpha = [1, 1, 1]$, $\beta = [0, 0, 0]$ and $\gamma = [0, 0, 0]$, it can be shown that $M_m = m_B$, which is the ideal case. Considering this as the initial condition, a least-squares solution for the numerical values of $C_1/C_{10} \dots C_9/C_{10}$ is performed. This produces a system of nine nonlinear equations in nine unknowns α , β and γ , which can be solved numerically. The calibrated measurements M_c can be corrected as

$$M_c = D^{-1} (M_m - b_m) \quad (3.7)$$

The earth's magnetic field for the location specified in Section 2.1 can be found on a particular date from the International Geomagnetic Reference Field (IGRF) [44] or World Magnetic Model (WMM) [45]. Implementation of the above calibration technique resulted in the following values when the unit of readings is Gauss

$$\alpha = \begin{bmatrix} 0.8183 \\ 0.8291 \\ 0.7344 \end{bmatrix} \quad \beta = \begin{bmatrix} 0.0029 \\ 0.0202 \\ -0.0618 \end{bmatrix} \quad \gamma = \begin{bmatrix} 0.0210 \\ 0.0576 \\ 0.0014 \end{bmatrix}$$

Figure 3.9 shows the result of calibration. It can be clearly seen that the offset has been removed and the calibrated values form a circle in all three planes as opposed to ellipses formed by the raw, uncalibrated data set.

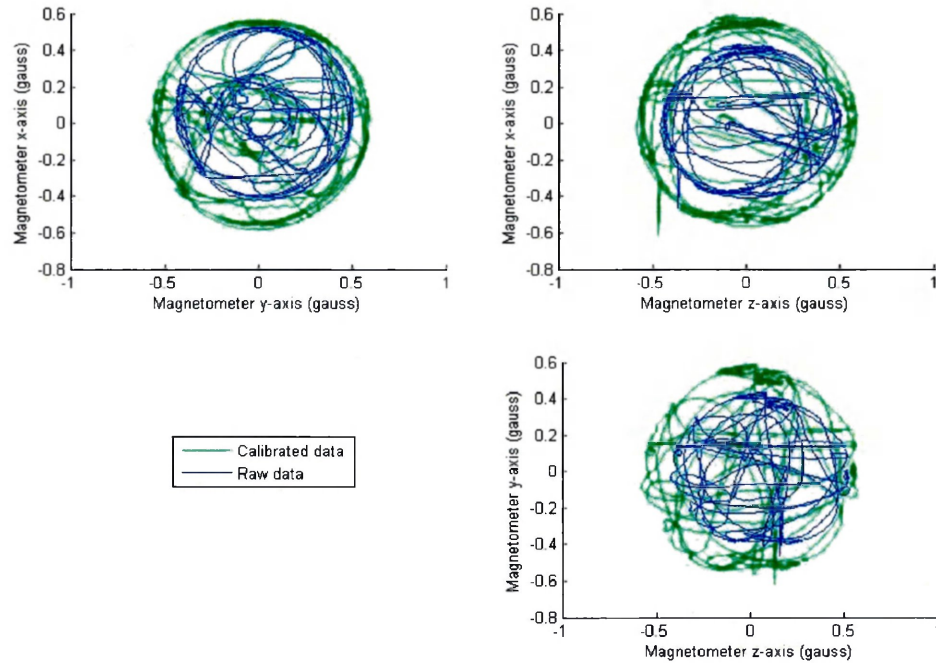


Figure 3.9: Magnetometer calibration results

Chapter 4

Static Attitude Estimation

Static attitude estimation originated in spacecraft attitude systems, where measurements of magnetic fields, sun position and star constellations are accurately available as vector observations. This class of attitude estimation techniques takes advantage of the body vector observations to numerically determine the attitude without necessarily considering its kinematics.

One of the earliest algorithms to be developed was TRIAD, by Harold D. Black in 1964 [46]. It was used in spacecraft attitude estimation for nearly two decades. With the advent of Wahba's problem [47], it was supplanted by the QUEST algorithm [48]. These algorithms were early optimization methods, aimed to solve Wahba's problem. It seeks to find a rotation matrix R between two coordinate systems from a set of weighted vector observations. The cost function that Wahba's problem proposes to minimize is as follows:

$$J(R) = \frac{1}{2} \sum_{i=1}^N a_i \|b_i - Rr_i\|^2 \quad (4.1)$$

where r_i is a set of vectors in the reference frame, b_i is the corresponding set of vectors in the body frame and $\{a_i\}$ is an optional set of weights for each observation. It can be conveniently shown that the cost function can be re-written as

$$J(R) = \sum_{i=1}^N a_i - \text{tr}(RB^T) \quad (4.2)$$

where tr denotes the trace operator and matrix B is defined as

$$B = \sum_{i=1}^N a_i b_i r_i^T \quad (4.3)$$

A number of solutions to the problem have appeared in literature, notable amongst them are [49], [50], [51], and [52]. However, none of these were as widely applied as Paul Davenport's q-method [53].

4.1 TRIAD

TRIAD or TRI-axial Attitude Determination played a key role in the development of the guidance, navigation and control of the U.S. Navy's transit satellite system at Johns Hopkins Applied Physics Laboratories. As evident from the literature, TRIAD represents the state of practice in spacecraft attitude determination, well before the advent of the Wahba's problem and its several optimal solutions. Given the knowledge of two vectors in the reference and body frames, the TRIAD algorithm obtains the direction cosine matrix relating both frames. Covariance analysis for Black's classical solution was subsequently provided by Markley in [19].

We consider the linearly independent reference vectors b_1 and b_2 are measured vectors in the body frame. r_1, r_2 are the reference vectors in the inertial frame. Then they are related by the equations,

$$b_i = R r_i \quad (4.4)$$

for $i = 1, 2$, where R is a rotation matrix that transforms vectors in the inertial frame into vectors expressed in the body frame.

TRIAD proposes an estimate of the direction cosine matrix as a solution to the linear system of equations given by

$$\begin{bmatrix} b_1 & b_2 & (b_1 \times b_2) \end{bmatrix} = \hat{R} \begin{bmatrix} r_1 & r_2 & (r_1 \times r_2) \end{bmatrix} \quad (4.5)$$

The solution presented above works well in the noise-free case. However, in practice, the measurements are noisy and the orthogonality condition of the attitude matrix (or the direction cosine matrix) is not preserved by the above procedure. As proposed in [54], TRIAD incorporates the

following elegant procedure to redress this problem. To this end, we define unit vectors

$$\hat{S} = \frac{b_1}{\|b_1\|} \quad (4.6)$$

$$\hat{s} = \frac{r_1}{\|r_1\|} \quad (4.7)$$

$$\hat{M} = \frac{b_1 \times b_2}{\|b_1 \times b_2\|} \quad (4.8)$$

$$\hat{m} = \frac{r_1 \times r_2}{\|r_1 \times r_2\|} \quad (4.9)$$

Their cross product is used as the third column in the linear system of equations obtaining a proper orthogonal matrix for the spacecraft attitude given by

$$[\hat{S} \ \hat{M} \ (\hat{S} \times \hat{M})] = \hat{R}[\hat{s} \ \hat{m} \ (\hat{s} \times \hat{m})] \quad (4.10)$$

Thus an estimate of the spacecraft attitude is given by the proper orthogonal matrix as

$$\hat{R} = [\hat{S} \ \hat{M} \ (\hat{S} \times \hat{M})][\hat{s} \ \hat{m} \ (\hat{s} \times \hat{m})]^T \quad (4.11)$$

Note that computational efficiency has been achieved in this procedure by replacing the matrix inverse with a transpose. This shows that the matrices used for computing attitude are each composed of an orthogonal triad of basis vectors. TRIAD derives its name from this observation.

4.2 Q-Method

Paul Davenport provided the real breakthrough in applying Wahbas problem to spacecraft attitude determination. He proposed that the solution to Wahba's problem R can be parameterized by a unit quaternion $Q = (q_0, q_1, q_2, q_3)^T$. This is computationally more efficient as opposed to the numerical calculation for the solution of a 3×3 matrix R . Equation (2.5) suggests that the representation of the rotation matrix is a homogeneous quadratic function of Q . Hence, we have

$$tr(RB^T) = Q^T K Q \quad (4.12)$$

where

$$K = \begin{bmatrix} S - I_3 \text{tr}(B) & Z \\ Z^T & \text{tr}(B) \end{bmatrix}, \quad (4.13)$$

$$S = B + B^T, \quad (4.14)$$

$$Z = \sum_{i=1}^N a_i b_i \times r_i \quad (4.15)$$

It is straight-forward to show from Equation (4.2) that the optimal unit quaternion is the normalized eigenvector of K with the largest eigenvalue. Mathematically, it is equivalent to finding the solution of

$$KQ_{opt} = \lambda_{max}Q_{opt} \quad (4.16)$$

Solutions to the symmetric eigenvalue problem can be found in robust algorithms suggested in [55] and [56]. The main problem arises when there is no unique solution *i.e.*, the two largest eigenvalues of K are equal. Thus, the focus of works such as ESOQ (ESTimation of Optimal Quaternion) [57–59], has been to find the optimal quaternion Q_{opt} .

4.3 QUEST

Shuster's QUEST (QUaternion ESTimator) algorithm [48] was one of the most popular and widely used solutions to Walha's problem. It was developed as an algorithm to solve for the optimal quaternion given in Equation (4.16). Therefore, it does not require the minimization of the cost function given in Equation (4.1) and is considerably faster than the primitive algorithms attempting to solve for Q_{opt} .

The Cayley-Hamilton theorem [55] for a general 3×3 matrix G states that

$$G^3 - (\text{tr}G)G^2 + [\text{tr}(\text{adj}G)]G - (\det G)I = 0 \quad (4.17)$$

where $\text{adj}G$ is the classical adjoint of G . This can be used to express the adjoint as

$$\text{adj}G = G^2 - (\text{tr}G)G + [\text{tr}(\text{adj}G)]I \quad (4.18)$$

This can be used to express the matrix S as

$$S^3 = \text{tr}(S)S^2 - [\text{tr}(\text{adj}S)]S + \det(S)I_3 \quad (4.19)$$

Let $X = (\alpha I + \beta S + S^2)Z$, then the optimal quaternion Q_{opt} as given by [48] is

$$Q_{opt} = \frac{1}{\sqrt{\gamma^2 + X^2}} \begin{bmatrix} \gamma \\ X \end{bmatrix} \quad (4.20)$$

where

$$\gamma = (\lambda_{max} + trS) \alpha - detS \quad (4.21)$$

$$\alpha = \lambda_{max}^2 - (trS)^2 + tr(adjS) \quad (4.22)$$

$$\beta = \lambda_{max} - trB \quad (4.23)$$

It is visible that the above computations rely on the knowledge of λ_{max} . This can be obtained from the characteristic equation $det(K - \lambda_{max}I_4) = 0$, which can be written as

$$\lambda_{max}^4 - (a + b) \lambda_{max}^2 - c\gamma + (ab + \frac{c}{2}trS - d) \quad (4.24)$$

where

$$a = \left(\frac{1}{2}trS\right)^2 - tr(adjS), \quad (4.25)$$

$$b = \left(\frac{1}{2}tr(S)\right)^2 + Z^T Z \quad (4.26)$$

$$c = detS + Z^T SZ, \quad (4.27)$$

$$d = Z^T S^2 Z \quad (4.28)$$

Shuster analysed that λ_{max} is approximately equal to $\lambda_0 = \sum_{i=1}^N a_i$, if the loss function $J(R_{opt})$ is small. Hence, λ_{max} can be obtained by Newton-Raphson iterations, starting with λ_0 as the initial estimate. However, it is well established that solving the characteristic equation to find eigenvalues is one of the least reliable methods. Thus, QUEST is believed to be less robust than other static attitude estimation techniques as has been conclusively proven in [19].

4.4 SVD

Singular Value Decomposition (SVD) method is one of the most robust estimators for minimizing Wahba's cost function. It is based upon the algorithm proposed in [52] and was formally introduced by Markley in [60]. It presents that the matrix B given in Equation (4.3) has a singular

value decomposition given by

$$B = U\sigma V^T = U \text{diag}(\sigma_1, \sigma_2, \sigma_3) V^T \quad (4.29)$$

where U and V are orthogonal matrices and σ is a singular value diagonal matrix constrained by the inequalities $\sigma_1 \geq \sigma_2 \geq \sigma_3 \geq 0$. In order to minimize the loss function in Equation (4.2), the trace must be maximized. This can be achieved when

$$U^T R_{opt} V = \text{diag}(1, 1, (\det U)(\det V)) \quad (4.30)$$

where $\det U = \pm 1$ and $\det V = \pm 1$. Thus, the optimal rotation matrix proposed in [60] is given as

$$R_{opt} = U \text{diag}(1, 1, (\det U)(\det V)) V^T \quad (4.31)$$

4.5 FOAM

The Fast Optimal Attitude Matrix (FOAM) algorithm was introduced in [61] as an alternative to the SVD method. They are intrinsically similar and using the properties of matrix B , R_{opt} in Equation (4.31) can be re-written as

$$R_{opt} = [(\kappa + \|B\|^2) B + \lambda \text{adj} B^T - B B^T B] / \xi, \quad (4.32)$$

where adj is the adjoint of a matrix and κ , λ , ξ and $\|B\|$ are defined as

$$\kappa = \sigma_2 \sigma_3 + \sigma_3 \sigma_2 + \sigma_1 \sigma_2 \quad (4.33)$$

$$\lambda = \sigma_1 + \sigma_2 + \sigma_3 \quad (4.34)$$

$$\xi = (\sigma_2 + \sigma_3)(\sigma_3 + \sigma_1)(\sigma_1 + \sigma_2) \quad (4.35)$$

$$\|B\|^2 = \sigma_1^2 + \sigma_2^2 + \sigma_3^2 \quad (4.36)$$

and σ_1, σ_2 and σ_3 retain their definition from Equation (4.29). The coefficients in Equation (4.32) can be calculated without performing the singular value decomposition. This is the main advantage of the FOAM over the SVD method. It can be shown algebraically that

$$\kappa = \frac{1}{2} (\lambda^2 - \|B\|^2) \quad (4.37)$$

$$\xi = \kappa \lambda - \det B \quad (4.38)$$

We observe from Equations (4.32), (4.37) and (4.38) that R_{opt} can be expressed as a function of λ and B . So λ described by Equation (4.34) is given by

$$\lambda = tr(R_{opt}B^T) \quad (4.39)$$

and can be computed as a solution of the equation

$$(\lambda^2 - \|B\|^2)^2 - 8\lambda detB - 4\|adjB\|^2 = p(\lambda) = 0 \quad (4.40)$$

It is evident that λ has four real roots and they are the eigenvalues of the matrix K given in Q-method. The key innovation of this method is that it takes advantage of an iterative computational strategy to avoid finding σ_1 , σ_2 and σ_3 . This defines a sequence of estimates of λ by

$$\lambda_i = \lambda_{i-1} - p(\lambda_{i-1})/p'(\lambda_{i-1}), \quad i = 1, 2, \dots \quad (4.41)$$

where $p'(\lambda)$ is the derivative of $p(\lambda)$ with respect to λ .

4.6 Experimental Results

The attitude estimation algorithms discussed in this chapter have been implemented on the experimental apparatus in Chapter 3. The quadrotor platform is configured and calibrated as discussed. Performance of static estimation algorithms under the effect of noisy sensor measurements is shown. The actuators were run at fifty per cent capacity with the propeller removed. This produced the necessary vibrations and magnetic disturbances to simulate an actual flight. The results are compared to the attitude provided by the 3DM-GX1 IMU as discussed earlier. The results were visualized in SIMULINK by transmitting the data via UDP packets, in real-time. The estimated attitude is indicated in blue color and the attitude measurement from 3DM-GX1 module is shown in red color.

Figures 4.1 to 4.5 show the output yaw, pitch and roll of the attitude estimation algorithms as discussed in this chapter. The variation in steady state estimation error Δ of an angle α , in degrees, can be defined as

$$\Delta(\alpha) = |\max(\alpha) - \min(\alpha)| \quad (4.42)$$

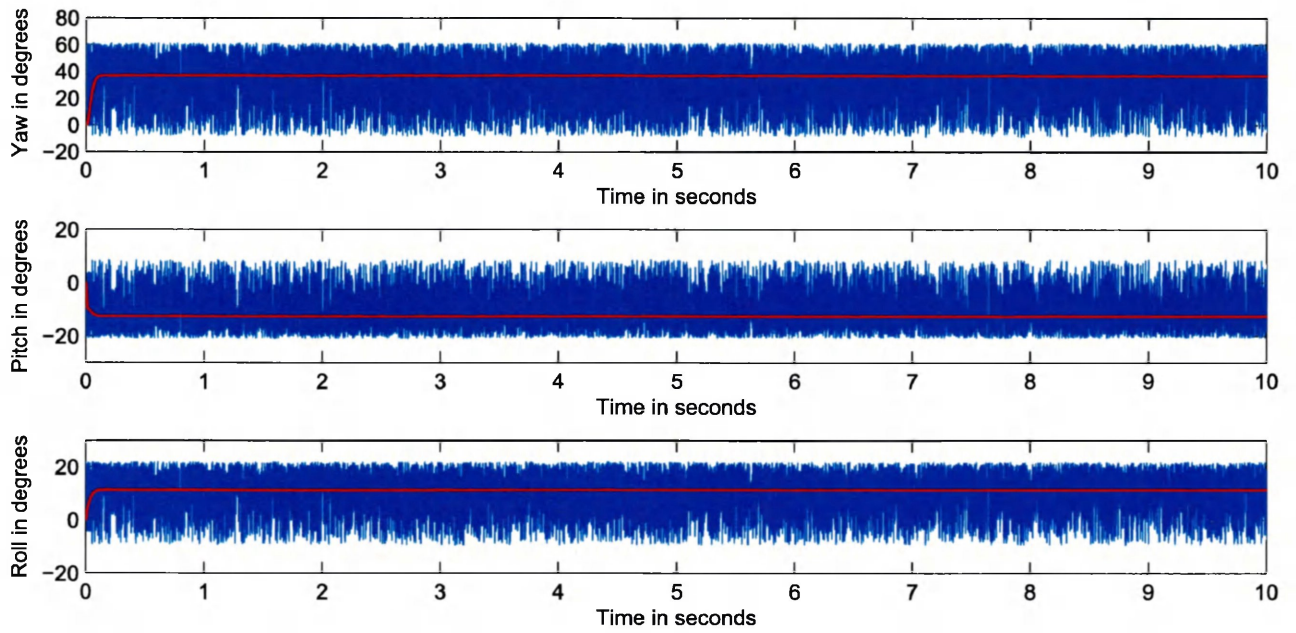


Figure 4.1: TRIAD result 1

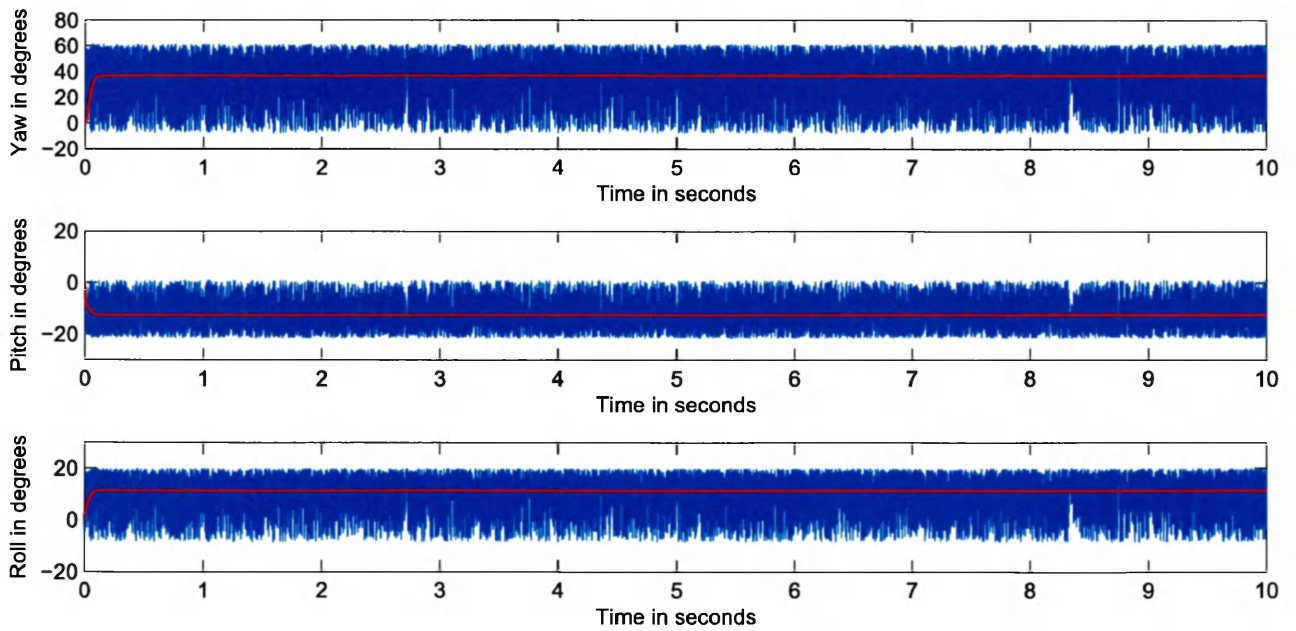


Figure 4.2: Q-method result 1

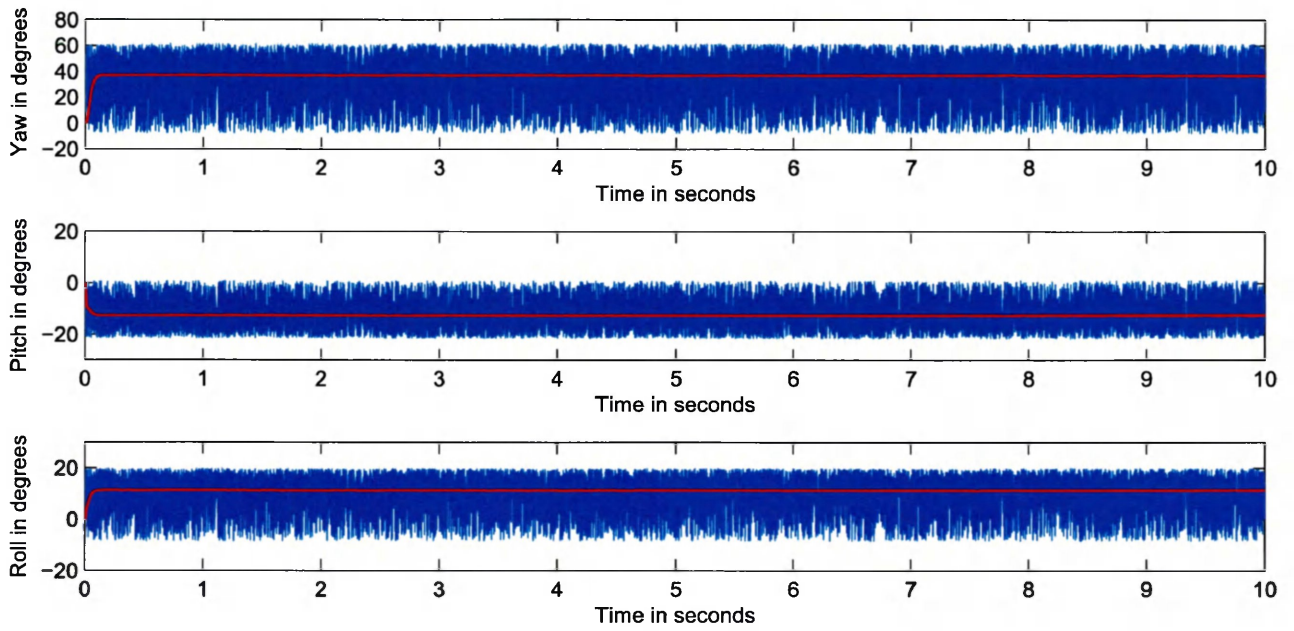


Figure 4.3: QUEST result 1

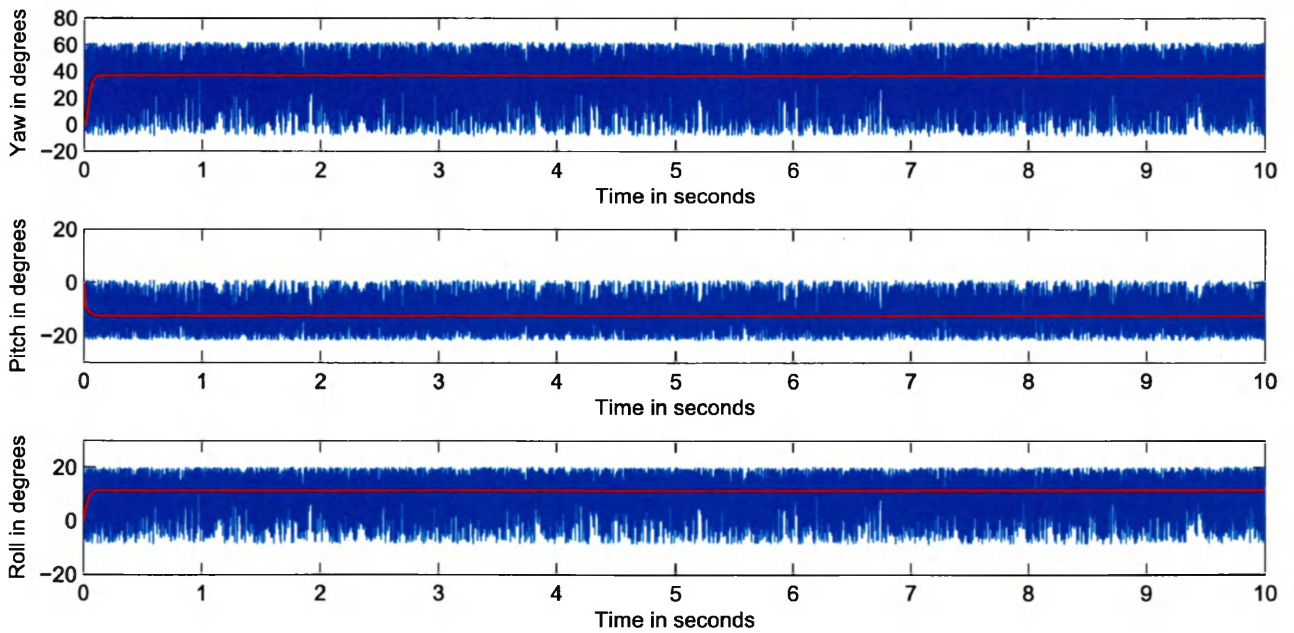


Figure 4.4: SVD Method result 1

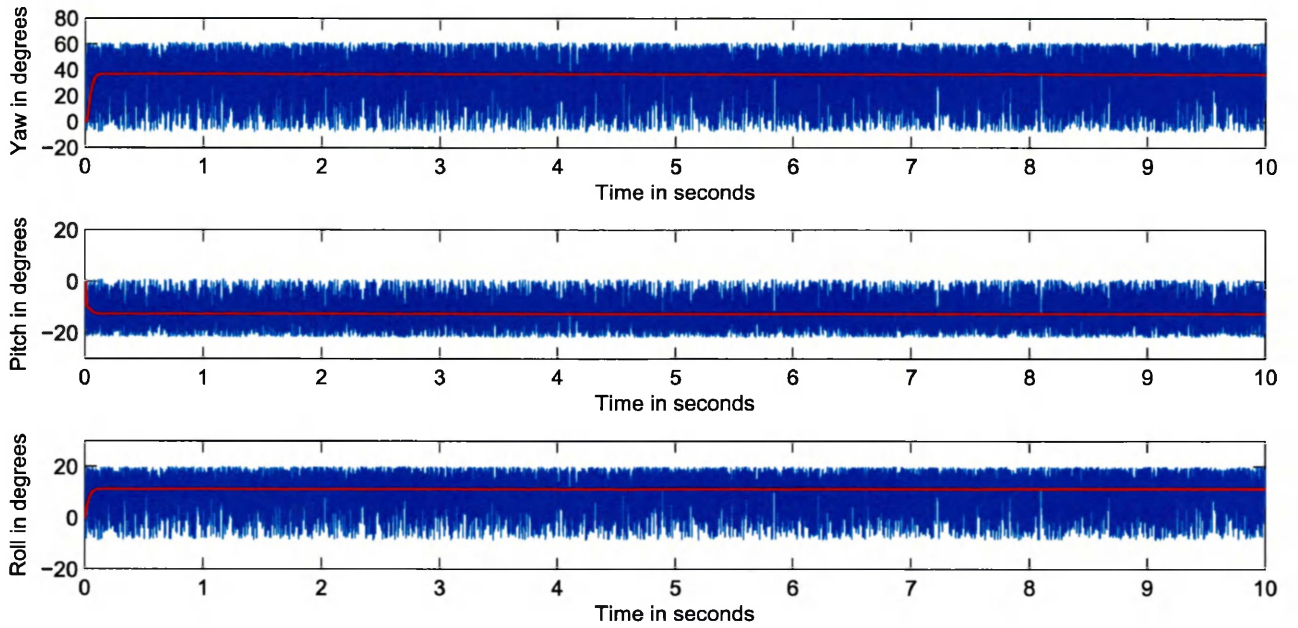


Figure 4.5: FOAM result 1

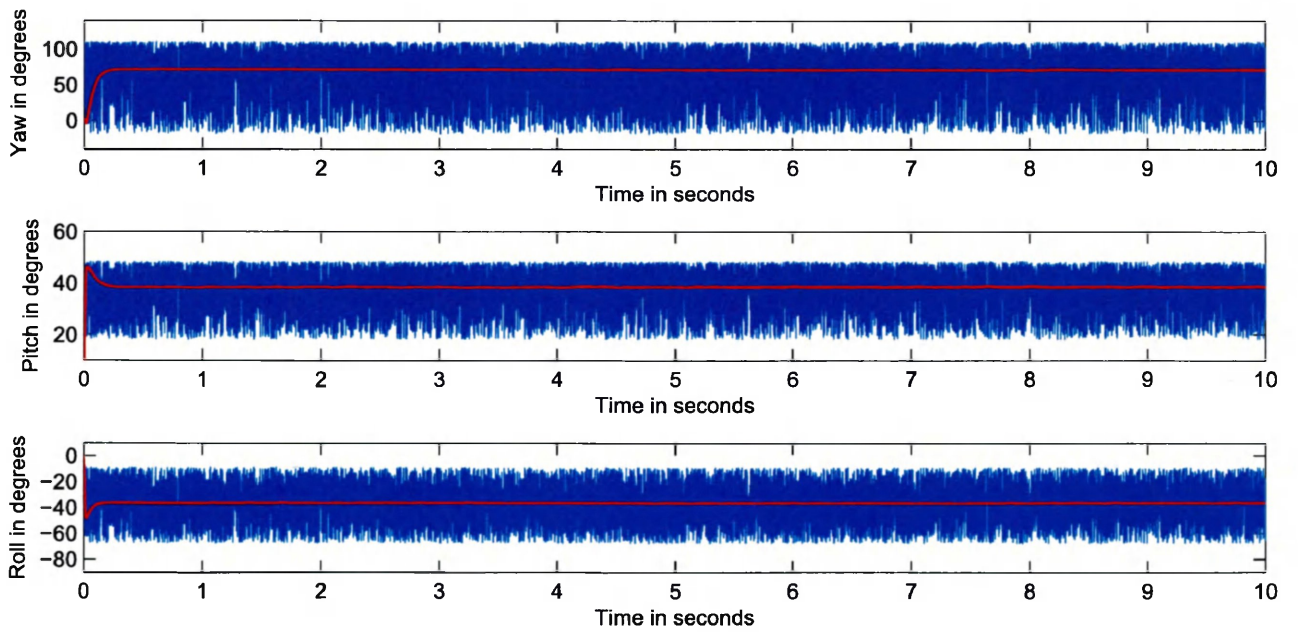


Figure 4.6: TRIAD result 2

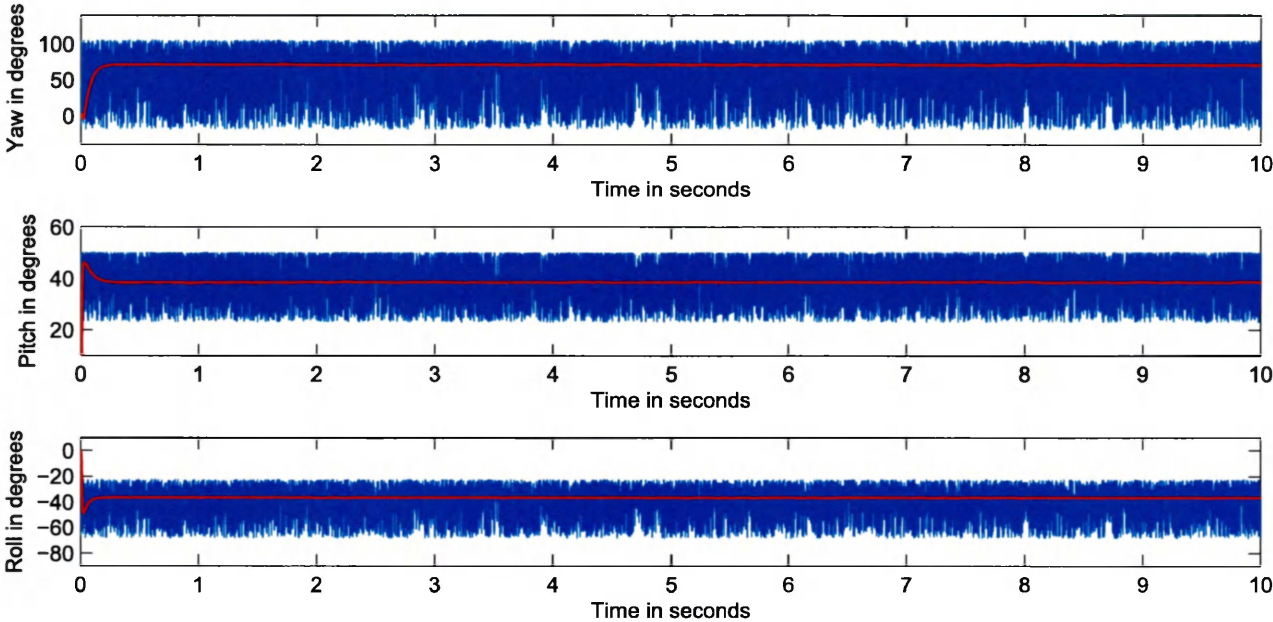


Figure 4.7: Q-method result 2

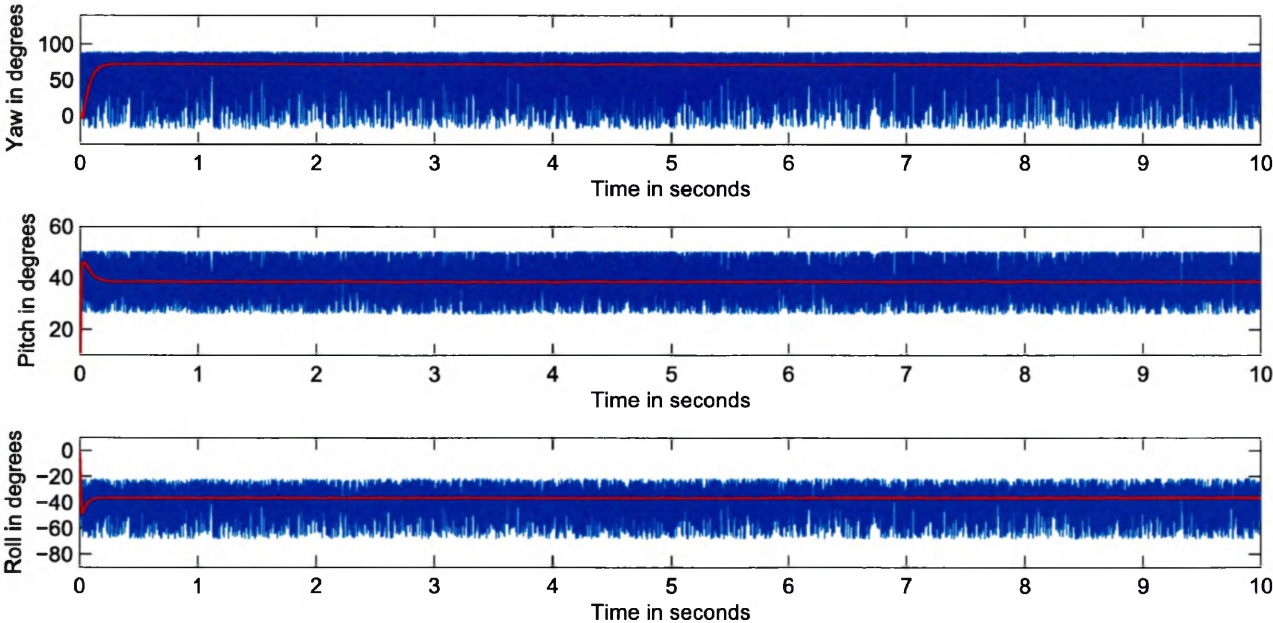


Figure 4.8: QUEST result 2

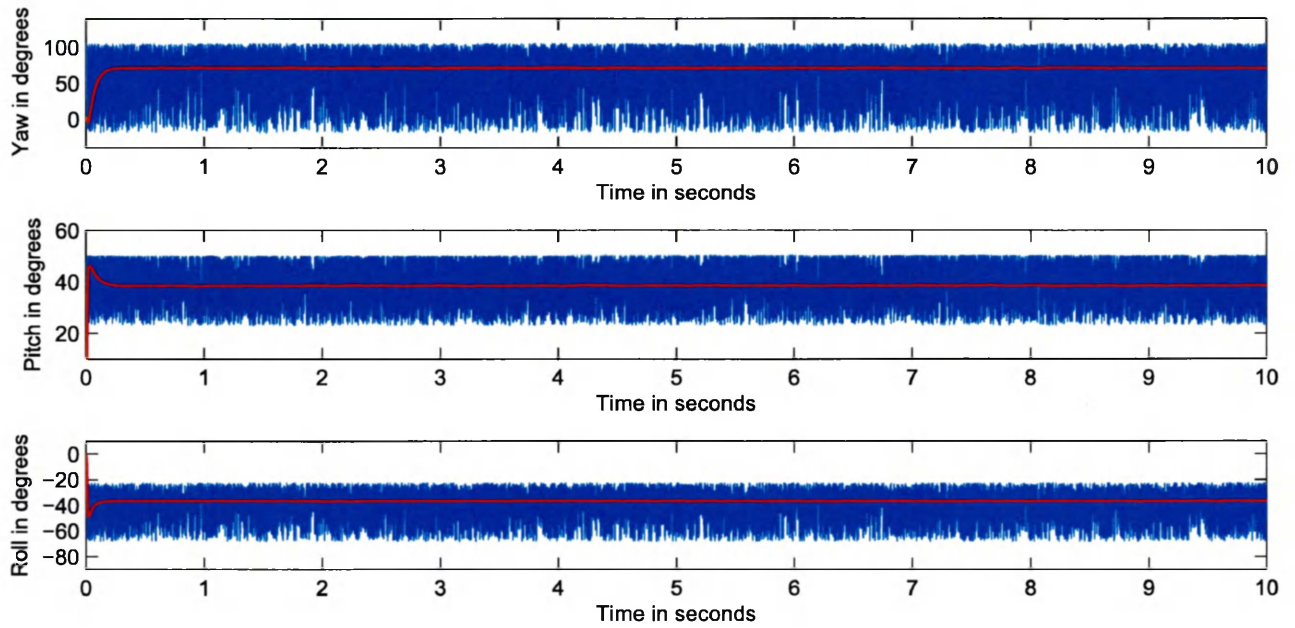


Figure 4.9: SVD Method result 2

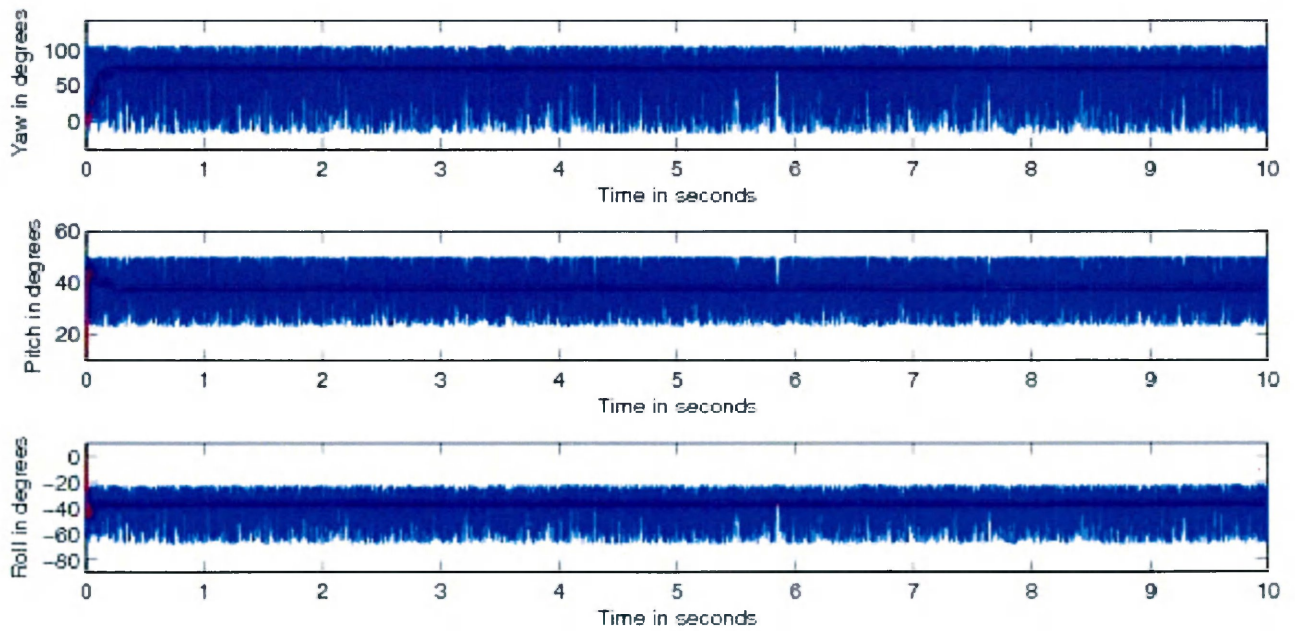


Figure 4.10: FOAM result 2

Figures 4.6 to 4.10 show the output of the attitude estimation algorithms when the orientation is changed.

For the next set of results, the orientation is kept the same. However, the accelerometer output is filtered as discussed in Section 3.5. The digital filter is set to have a cut-off frequency of 20 Hz. This results in a delay of 8.5 ms. The magnetometer output is left unchanged as it is already filtered on-board the HMC5883L and the calibrated magnetometer output does not exhibit high frequency disturbances. The results are shown in Figures 4.11 to 4.15 and the variation in steady state estimation error of yaw, pitch and roll angles is given in Table 4.1.

Algorithm	$\Delta(Yaw)$ in degrees	$\Delta(Pitch)$ in degrees	$\Delta(Roll)$ in degrees
TRIAD	57.374	14.6411	26.8686
Q-method	40.2985	11.7828	12.9442
QUEST	37.0666	11.2718	13.0508
SVD method	40.2839	11.7809	12.9512
FOAM	40.2734	11.7797	12.9561

Table 4.1: Variation of Euler angles estimated for results with accelerometer measurements filtering

Figures 4.16 to 4.20 show the result of the static attitude estimation techniques when the accelerometer output is filtered and the platform is rotated about all axes to simulate motion of the quadrotor in a flight.

It is interesting to note that while these algorithms have been extensively used with accurate sensors, their implementation is impeded by their inability to deliver reliable attitude estimates under noisy measurements. Even the results from filtered accelerometer measurements present a considerable variance in the estimates of attitude from the implemented algorithms. The figures showing the simulated motion of the quadrotor clearly depict that the static attitude estimators are unsuitable for implementation with filtered measurements as well.

The realization that static attitude estimation techniques are inefficient in the presence of measurement noise led to the development of filtering techniques incorporated into the estimation algorithms. These dynamic attitude estimation algorithms are discussed in the next chapter.

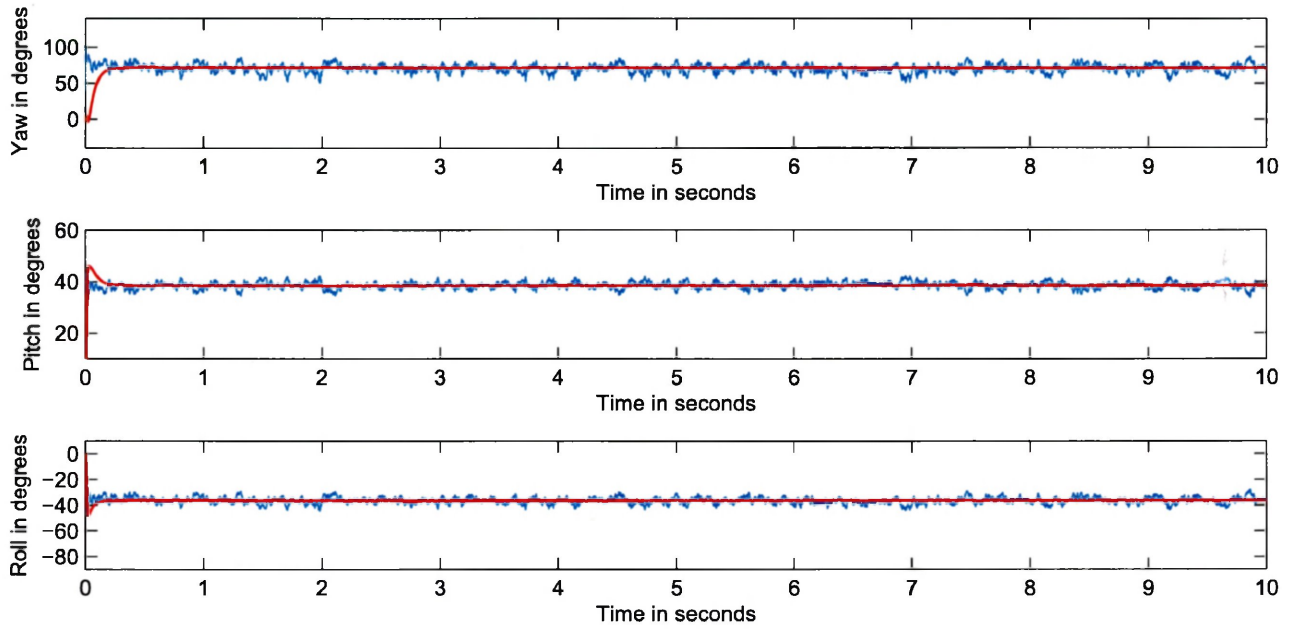


Figure 4.11: TRIAD result with accelerometer measurements filtering

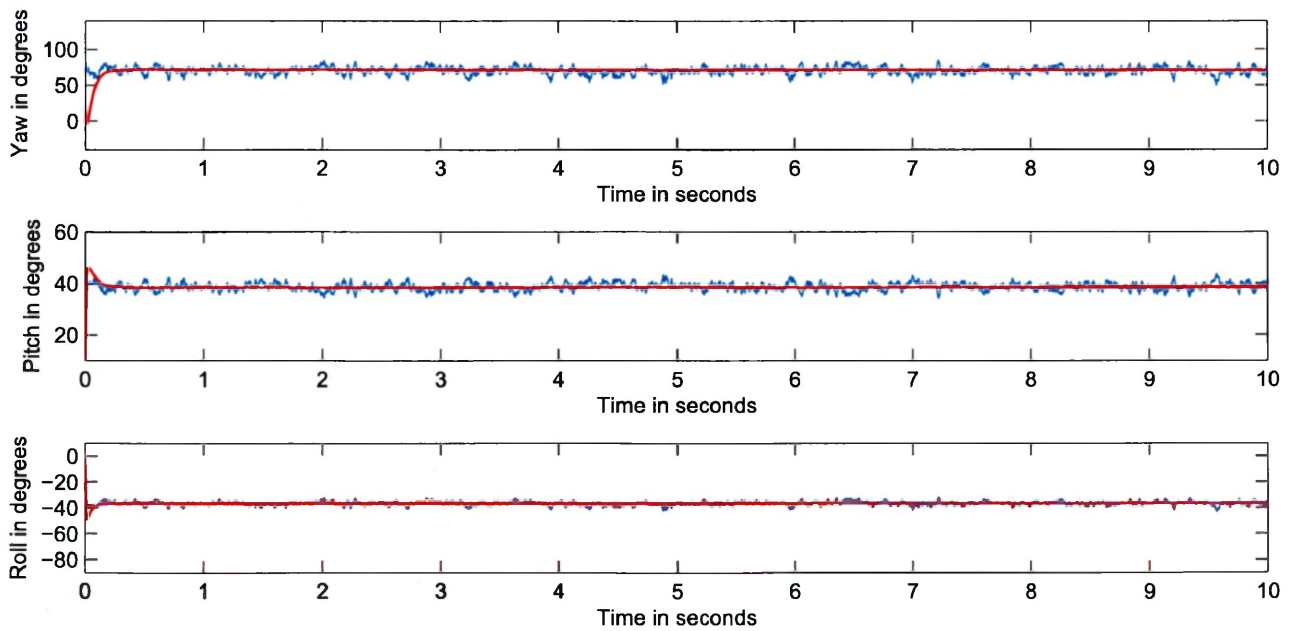


Figure 4.12: Q-method result with accelerometer measurements filtering

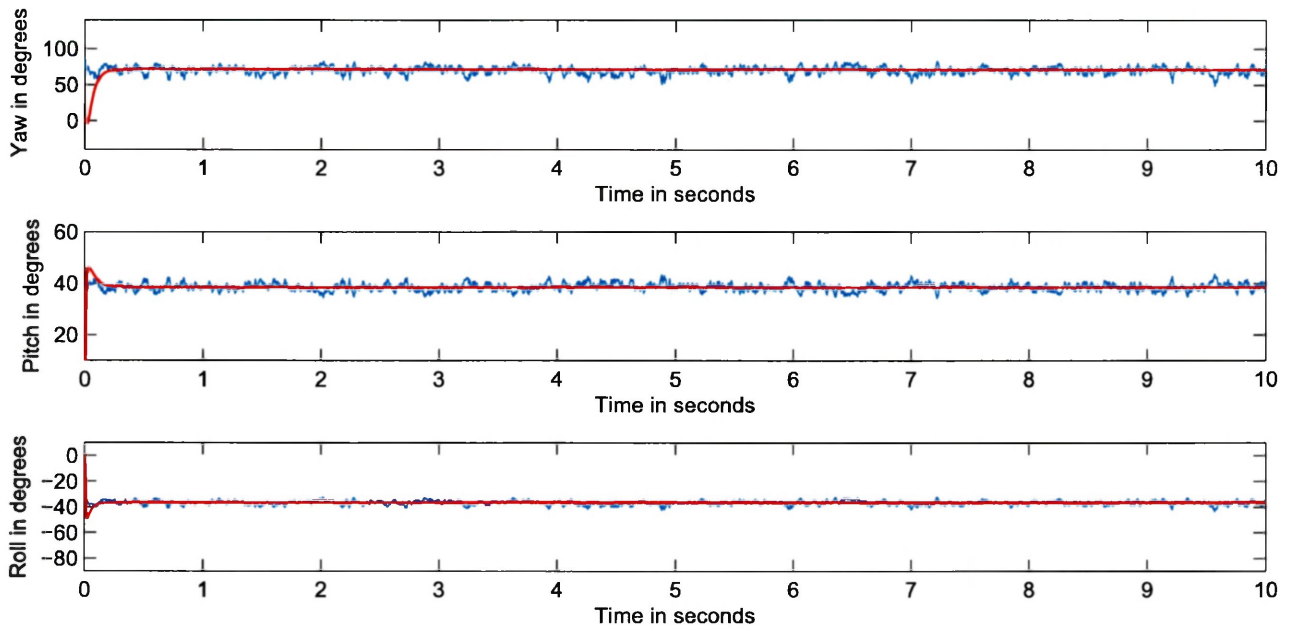


Figure 4.13: QUEST result with accelerometer measurements filtering

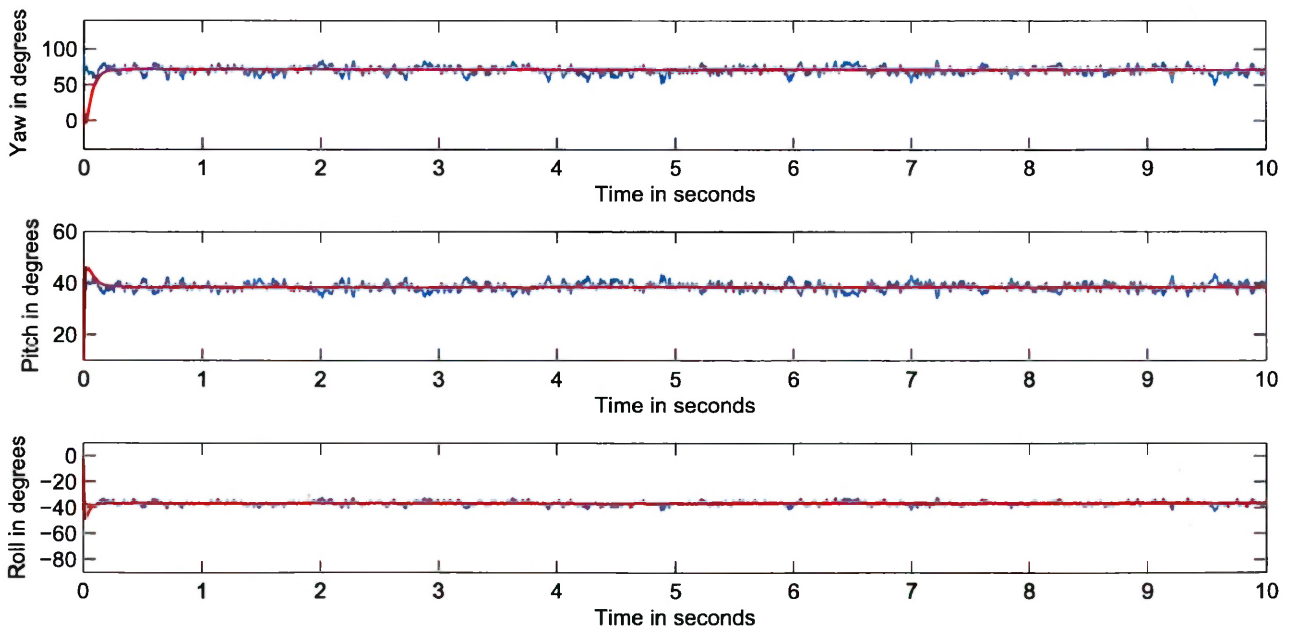


Figure 4.14: SVD Method result with accelerometer measurements filtering

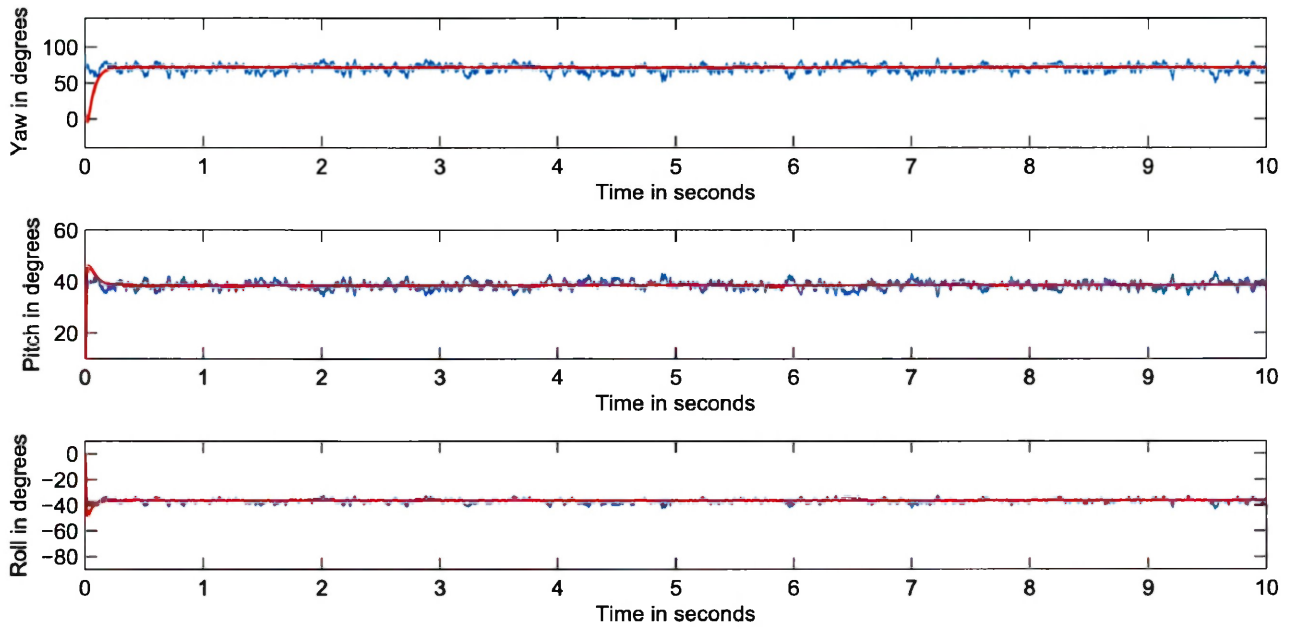


Figure 4.15: FOAM result with accelerometer measurements filtering

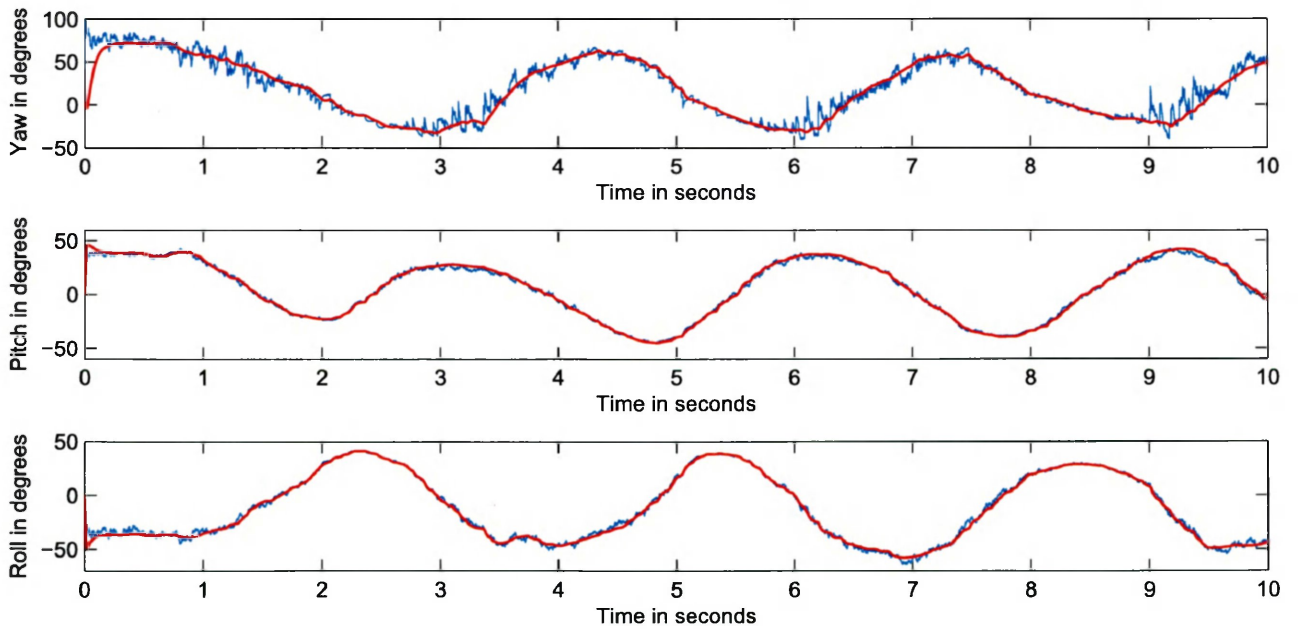


Figure 4.16: TRIAD result with accelerometer measurements filtering and simulated motion

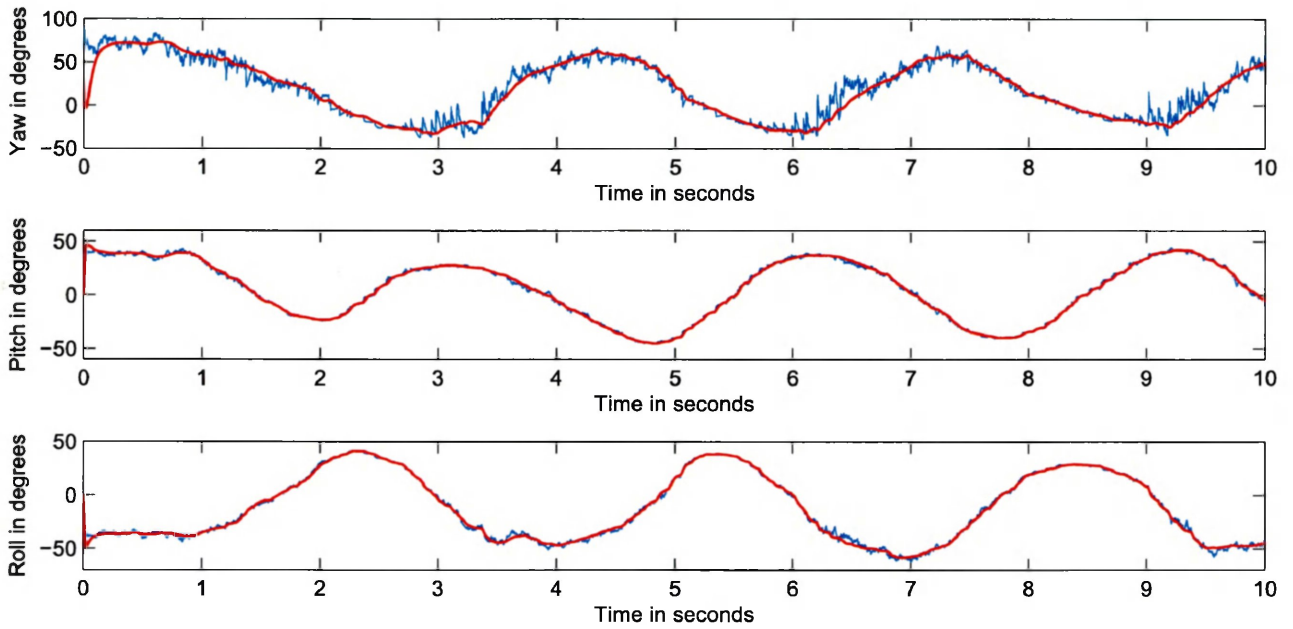


Figure 4.17: Q-method result with accelerometer measurements filtering and simulated motion

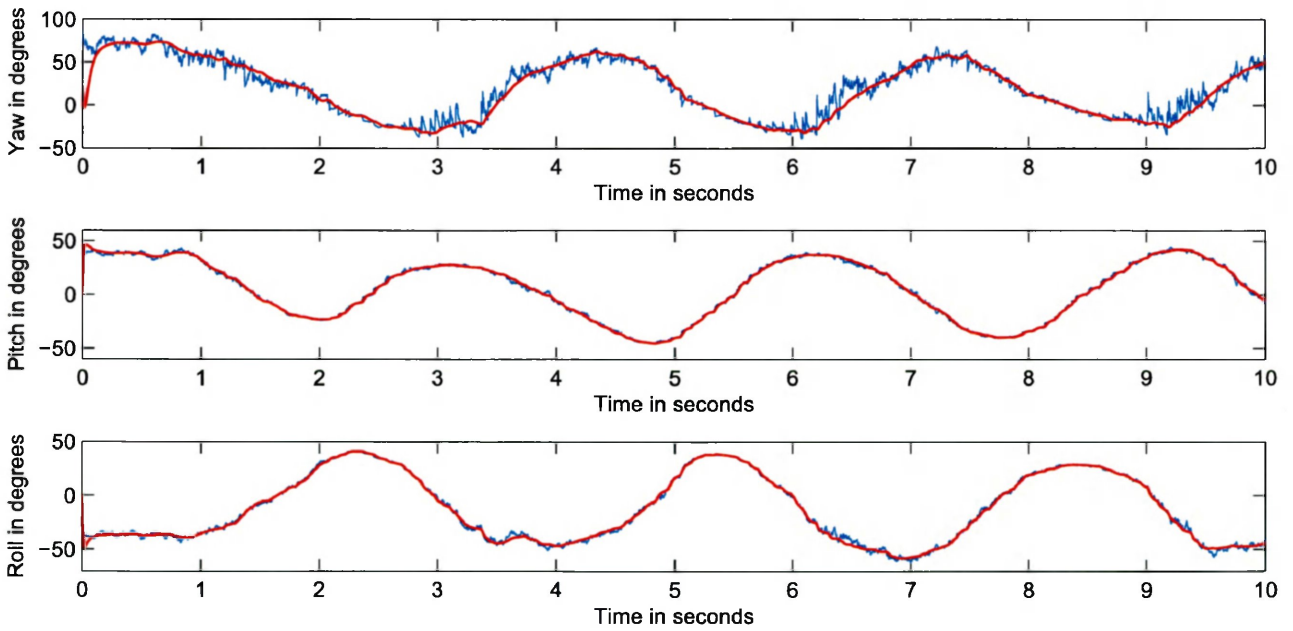


Figure 4.18: QUEST result with accelerometer measurements filtering and simulated motion

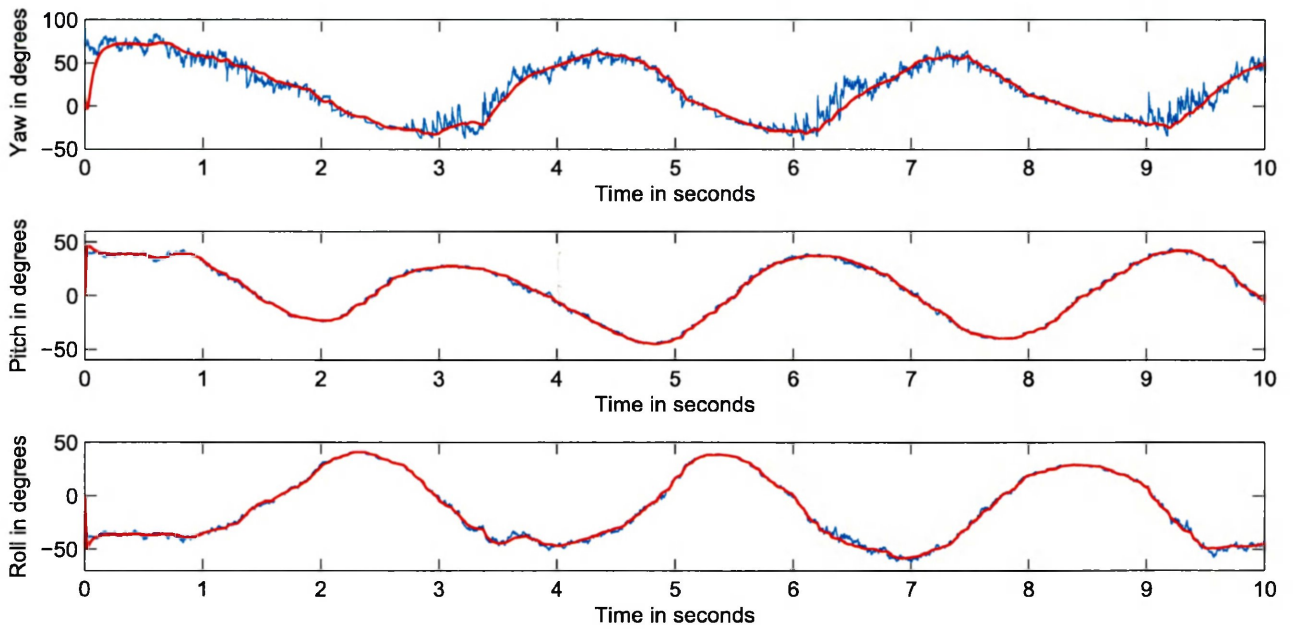


Figure 4.19: SVD Method result with accelerometer measurements filtering and simulated motion

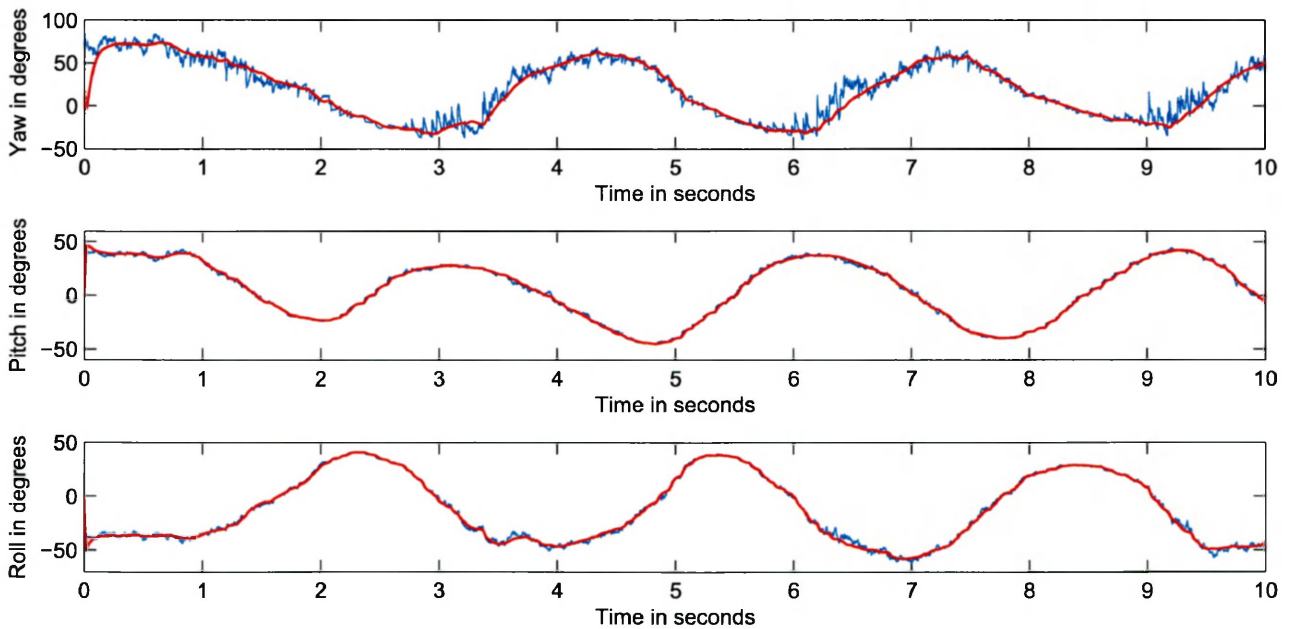


Figure 4.20: FOAM result with accelerometer measurements filtering and simulated motion

Chapter 5

Dynamic Attitude Estimation

As we have seen in the previous chapter, the static attitude estimators are sensitive to measurement noise. Thus, there is a need for attitude estimation algorithms that incorporate filtering techniques and provide reliable results in the presence of measurements noise and biases.

Theoretically, the static attitude estimation methods are aimed to be optimal solutions to Wahba's problem, which only consider the vector measurements and do not utilize the system dynamics. They are oblivious to the nonlinear structure of the system and hence, are very sensitive to disturbances. Thus, they perform admirably only when the sensor measurements are accurate. However, dynamic attitude estimation approaches rely on a process model considering motion dynamics and specific application properties to estimate attitude from noisy or disturbed sensor measurements.

Due to these noticeable drawbacks of the static attitude estimation algorithms, recursive algorithms incorporating the dynamics of the system were employed. Kalman filtering techniques [62] and recursive QUEST algorithms [63], [64] were the first to address these issues and present a solution to the attitude estimation problem with noisy measurements. Recently, nonlinear estimators involving complementary filters have been developed [65]. These are proven in the literature to be almost globally asymptotically stable. The most recent globally exponentially

stable nonlinear observers presented in [66] and [67] are also discussed and implemented.

5.1 Filter QUEST

Shuster noted in [68] that the *attitude profile matrix* B defined by Equation (4.3) contains the complete information about the current attitude of the rigid body. Thus, he proposed the Filter QUEST algorithm [63], by sequentially propagating and updating B as

$$B_k = \alpha \Phi_{k,k-1} B_{k-1} + \Delta B_k \quad (5.1)$$

where B_{k-1} is the previous iteration of B_k and can be initialized as a zero matrix. The forgetting factor $0 < \alpha < 1$ is a measure of the impact that past measurements have on the current estimate of attitude. For $\alpha = 0$ we recover the QUEST algorithm. The *state transition matrix* $\Phi_{k,k-1}$ relates the previous attitude and current attitude as

$$R_k = \Phi_{k,k-1} R_{k-1} \quad (5.2)$$

The current measurements b_i and their respective weights μ_i are incorporated as

$$\Delta B_k = \sum_{i=1}^N \frac{1}{\mu_i^2} b_i r_i^T \quad (5.3)$$

The state transition matrix can be obtained by converting the dynamic equation of a rigid body as given in Equation (2.13) to discrete time

$$R_k = e^{(-S(\omega_k))} R_{k-1} \quad (5.4)$$

Thus, Φ_k can be written as

$$\Phi_{k,k-1} = e^{(-S(\omega_k))} \quad (5.5)$$

where ω_k is the measured angular velocity provided by the gyroscope.

The updated matrix B_k is used in the original QUEST algorithm and the estimation technique continues as discussed earlier. Another similar algorithm called Recursive QUEST or REQUEST was proposed in [64]. However, it relies on propagating and updating the K matrix given in Davenport's Q-method. It was mathematically proven that the algorithm was equivalent to the

filter QUEST because the updated K matrix can also be derived from substituting the updated matrix B_k in Equation (4.13). Neither of these methods has been as popular as the Kalman filtering techniques, mainly because the unoptimized forgetting factor is constant as opposed to the Kalman gain.

5.2 Kalman Filter

The Kalman filter was formally introduced in [69] by Rudolf E. Kalman and it has gained immense popularity in the field of attitude estimation. Some note-worthy implementations include the guidance and navigation systems of NASA's Apollo program and Space Shuttle program, and U.S. Navy submarines and cruise missiles [70]. The filter operates recursively on a series of noisy measurements to produce an optimal estimate of the underlying system state. The Kalman filter was originally developed for a system defined by a set of linear differential equations.

The algorithm works in two steps. The first step of the Kalman filter predicts the current state variables based on the system dynamic model and the previous estimate. The next step involves updating the predicted states with weighted noisy measurements from the sensors to produce the current estimate of attitude. Due to this recursive nature of the Kalman filter, it is ideally suited to real-time applications involving corrupted sensor measurements.

Let us assume that the true state x_k of a linear system is described at time k in terms of the previous state x_{k-1} as

$$x_k = Fx_{k-1} + w_{k-1} \quad (5.6)$$

where F is the state transition matrix and w_{k-1} is the process noise. The Kalman filter attempts to estimate the state with measurement z_k that can be modeled as

$$z_k = Hx_k + v_k \quad (5.7)$$

where H and v_k are the measurement matrix and measurement noise respectively. Using the previously estimated state \hat{x}_{k-1} to predict the current state \bar{x}_k as shown by the following equations

$$\bar{x}_k = F\hat{x}_{k-1} \quad (5.8)$$

$$\bar{P}_k = F\hat{P}_{k-1}F^T + W \quad (5.9)$$

The process and measurement noise are assumed to be drawn from their normal probability distributions with covariance W and V respectively. \bar{P}_k is the predicted error covariance depending upon the previous estimate of the error covariance. The current optimal Kalman gain K_k can be computed as

$$K_k = \bar{P}_k H^T (H \bar{P}_k H^T + V)^{-1} \quad (5.10)$$

and the current state estimate \hat{x}_k and error covariance \hat{P}_k are given by

$$\hat{x}_k = \bar{x}_k + K_k (z_k - H \bar{x}_k) \quad (5.11)$$

$$\hat{P}_k = (I - K_k H) \bar{P}_k \quad (5.12)$$

The Kalman filter, however, was designed for linear systems and cannot be directly applied to nonlinear systems such as the quadrotor model. Its application has been extended to incorporate nonlinear systems and their state estimation.

5.2.1 Extended Kalman Filter

In simplistic terms, extended Kalman filter (EKF) is the nonlinear version of the Kalman filter. It linearizes the nonlinear system about an estimate of the current mean and covariance to obtain the Jacobian matrices in Kalman filter [71]. As opposed to Equation (5.6) the nonlinear system can be defined in discrete-time as

$$x_k = f(x_{k-1}) + w_{k-1} \quad (5.13)$$

$$z_k = h(x_k) + v_k \quad (5.14)$$

where all variables are defined in the same manner as Equation (5.6), and $f(x_{k-1})$ and $h(x_k)$ are the process nonlinear vector function and measurement nonlinear vector function respectively.

The Jacobian matrices F_k and H_k associated with $f(x_{k-1})$ and $h(x_k)$ respectively are given as

$$F_k = \left. \frac{\partial f(x)}{\partial x} \right|_{\hat{x}_{k-1}} \quad (5.15)$$

$$H_k = \left. \frac{\partial h(x)}{\partial x} \right|_{\hat{x}_{k-1}} \quad (5.16)$$

It can be seen that the Jacobian matrices are derived from the linearization of the nonlinear system at each instant of time around the best estimate of the system state. The remainder of the procedure follows from the original Kalman filter. The Jacobian matrices derived in this case are, however, just approximations and the higher-order terms have been truncated from the Taylor series expansion. A more accurate version employing second-order extended Kalman filters has been discussed in [72] and [73]. The EKF has been one of the most used attitude estimation techniques for UAVs owing to its merits in dealing with measurement noise. However, if the initial estimates are highly inaccurate, it may lead to divergence or poor estimation of the states. Therefore, global convergence of EKF is not guaranteed as suggested in [4, 74, 75]. A survey of stability analysis of EKF based attitude determination has been conducted in [76].

While many versions of the EKF are available in the literature [4], this thesis focuses on the Multiplicative EKF proposed in [62] and the Additive EKF proposed in [77] as they were the most widely implemented algorithms.

5.2.2 Multiplicative EKF

The Multiplicative Extended Kalman Filtering (MEKF) approach [62] was proposed by E. J. Lefferts, F. L. Markley and M. D. Shuster based on the unit quaternion attitude representation as given by Equation (2.19). Shuster suggested that the actual attitude in quaternion representation Q can be represented as the the quaternion product of the estimated unit quaternion \hat{Q} and an error in estimation given by the unit quaternion δQ . Thus the error quaternion can be defined as

$$\delta Q = Q \odot \hat{Q}^{-1} \quad (5.17)$$

An alternative form of representation can be used to define the error quaternion where the order of multiplication can be reversed. This has the advantage that the attitude error is represented in the inertial frame of reference rather than the body frame [78]. Let \mathbf{a} be a three-dimensional rotation vector by which $\delta Q(\mathbf{a})$ is parameterized.

$$\delta Q(\mathbf{a}) = \begin{bmatrix} \cos(a_0/2) \\ (\mathbf{a}/a_0) \sin(a_0/2) \end{bmatrix} \quad (5.18)$$

where $a_0^2 = \|\mathbf{a}\|^2$. Assuming that the body undergoes small rotations, this error quaternion can be approximated by a second-order Taylor series expansion and re-written as

$$\delta Q(\mathbf{a}) = \begin{bmatrix} 1 - a_0^2/8 \\ \mathbf{a}/2 \end{bmatrix} \quad (5.19)$$

The multiplication of two unit quaternions $P = [p_0, \mathbf{p}]^T$ and $R = [r_0, \mathbf{r}]$ is described in [79] as

$$P \otimes R = \begin{bmatrix} p_0 r_0 - \mathbf{p}^T \mathbf{r} \\ p_0 \mathbf{r} + r_0 \mathbf{p} - \mathbf{p} \times \mathbf{r} \end{bmatrix} \quad (5.20)$$

where (\times) denotes the cross product. The kinematics of the orientation Q can be redefined as

$$\dot{Q} = \frac{1}{2} \begin{bmatrix} 0 \\ \boldsymbol{\omega} \end{bmatrix} \otimes Q \quad (5.21)$$

where $\boldsymbol{\omega}$ is defined in terms of the gyroscope measurement ω_m , bias b and white noise n_ω as

$$\boldsymbol{\omega} = \omega_m - b - n_\omega \quad (5.22)$$

Let us assume that an estimate of Q is given by \hat{Q} as follows

$$\dot{\hat{Q}} = \frac{1}{2} \begin{bmatrix} 0 \\ \hat{\boldsymbol{\omega}} \end{bmatrix} \otimes \hat{Q} \quad (5.23)$$

where $\hat{\boldsymbol{\omega}}$ is defined in terms of the gyroscope measurement ω_m and an estimate of the gyroscope bias \hat{b} as

$$\hat{\boldsymbol{\omega}} = \omega_m - \hat{b} \quad (5.24)$$

Then the error quaternion δQ as given by [79] is

$$\delta Q(\mathbf{a}) = Q \otimes \hat{Q}^{-1} \quad (5.25)$$

Taking the derivative of the above equation with respect to time and considering Equation (5.21) and Equation (5.23) yields

$$\delta \dot{Q}(\mathbf{a}) = \dot{Q} \otimes \hat{Q}^{-1} + Q \otimes \dot{\hat{Q}}^{-1} \quad (5.26)$$

$$= \frac{1}{2} \begin{bmatrix} 0 \\ \boldsymbol{\omega} \end{bmatrix} \otimes \delta Q(\mathbf{a}) - \frac{1}{2} \delta Q(\mathbf{a}) \otimes \begin{bmatrix} 0 \\ \hat{\boldsymbol{\omega}} \end{bmatrix} \quad (5.27)$$

The nonlinear system is described by the state vector x in terms of the error rotation vector \mathbf{a} and the gyro bias b and given in [79] as

$$x = \begin{bmatrix} \mathbf{a} \\ b \end{bmatrix} \quad (5.28)$$

where w is the process noise assumed to be given by its normal probability distribution with covariance W

$$\dot{x} = Fx + Gw \quad (5.29)$$

$$F = \begin{bmatrix} -S(\hat{\omega}) & -I_{3 \times 3} \\ 0_{3 \times 3} & 0_{3 \times 3} \end{bmatrix} \quad (5.30)$$

$$G = \begin{bmatrix} -I_{3 \times 3} & 0_{3 \times 3} \\ 0_{3 \times 3} & 0_{3 \times 3} \end{bmatrix} \quad (5.31)$$

The covariance matrix P for the MEKF estimation algorithm that can be partitioned into 3×3 submatrices as

$$P = \begin{bmatrix} P_a & P_c \\ P_c^T & P_b \end{bmatrix} \quad (5.32)$$

and its time propagation is given by

$$\dot{P} = FP + PF^T + GWG^T \quad (5.33)$$

The measurements z for the MEKF algorithm as given in [79] are described as a function of \mathbf{a} as

$$z = h(\mathbf{a}) + v \quad (5.34)$$

where V is the normal probability distribution of the measurement noise v and the linearization of h results in the measurement sensitivity matrix H

$$H = \begin{bmatrix} \partial h / \partial \mathbf{a} & \partial h / \partial b \end{bmatrix} \quad (5.35)$$

However, the measurements from the accelerometer A_m and magnetometer M_m can be used to calculate a measurement unit quaternion Q_m using a static attitude estimation algorithm as discussed in Chapter 4. The advantage is that the measurement $\bar{\mathbf{z}}$ for the MEKF algorithm can

now be described as an error in the measured quaternion Q_m and the estimated quaternion \hat{Q} defined as

$$\delta Q(\bar{\mathbf{z}}) = Q_m \otimes \hat{Q}^{-1} \quad (5.36)$$

The measurement sensitivity matrix H can be shown to be $[I_{3 \times 3} \ 0_{3 \times 3}]$ as the measurement model is simply $h(\mathbf{a}) = \mathbf{a}$ (as shown in [79]). The recursive MEKF algorithm to be implemented in discrete-time for a sample period T is given as

$$\hat{\omega}_k = \omega_{m,k} + \hat{b}_k \quad (5.37)$$

$$\Omega(\hat{\omega}_k) = \frac{1}{2} \begin{bmatrix} 0 & -\hat{\omega}_k^T \\ \hat{\omega}_k & -S(\hat{\omega}_k) \end{bmatrix} \quad (5.38)$$

$$\phi_k = I + T\Omega(\hat{\omega}_k) \quad (5.39)$$

$$\hat{Q}_k = \phi_k Q_{k-1}^* \quad (5.40)$$

where Q_{k-1}^* is the most recent corrected estimate given by Equation (5.48). The prediction step is given as

$$\begin{bmatrix} \bar{\mathbf{a}}_k \\ \bar{b}_k \end{bmatrix} = (I + TF) \begin{bmatrix} \hat{\mathbf{a}}_{k-1} \\ \hat{b}_{k-1} \end{bmatrix} \quad (5.41)$$

$$P_k = P_{k-1}^* + T(FP_{k-1}^* + P_{k-1}^*F^T + GWG^T) \quad (5.42)$$

where P_{k-1}^* is the most recent estimate of the covariance given by Equation (5.47). $P_{a,k}$ and $P_{c,k}$ must be extracted from P_k as given by Equation (5.32) to compute the Kalman gains as follows

$$K_{a,k} = P_{a,k}(P_{a,k} + V)^{-1} \quad (5.43)$$

$$K_{b,k} = P_{c,k}^T(P_{a,k} + V)^{-1} \quad (5.44)$$

Equation (5.36) and Equation (5.19) are used to recover $\bar{\mathbf{z}}$ and the state estimate is updated as

$$\hat{\mathbf{a}}_k = \bar{\mathbf{a}}_k + K_{a,k}(\bar{\mathbf{z}} - \bar{\mathbf{a}}_k) \quad (5.45)$$

$$\hat{b}_k = \bar{b}_k + K_{b,k}(\bar{\mathbf{z}} - \bar{\mathbf{a}}_k) \quad (5.46)$$

The covariance of the MEKF algorithm is updated as

$$P_k^* = P_k - [P_{a,k} \ P_{c,k}]^T [P_{a,k} + V]^{-1} [P_{a,k} \ P_{c,k}] \quad (5.47)$$

The continuous time propagation is expected to maintain $\hat{\mathbf{a}}(t) = 0$, but the discrete measurement update assigns a finite post-update value $\hat{\mathbf{a}}_k$ to $\hat{\mathbf{a}}$. Immediately after the measurement update, the estimated quaternion still retains its preupdate value \hat{Q}_k , so that it no longer represents the optimal estimate. The following operation corrects this situation by moving the update information from $\hat{\mathbf{a}}_k$ to a post update estimate \hat{Q}_k^*

$$\hat{Q}_k^* = \delta Q(\hat{\mathbf{a}}_k) \otimes \hat{Q}_k \quad (5.48)$$

and $\hat{\mathbf{a}}_k$ is reset to zero to avoid the need to propagate two representations of the attitude. The reset does not modify the covariance, since it neither increases nor decreases the total information content of the estimate. The reset operation concludes the recursive filter algorithm and the process resumes from Equation (5.37).

The MEKF has an inherent advantage that the estimated quaternion \hat{Q} is a unit quaternion by definition. Therefore, it can be shown that for an initial estimate $\hat{Q}_0 \approx Q$ and small angular movements, the error quaternion $\delta Q \rightarrow 0$. Its simplicity and stability under the aforementioned restrictions led to its implementation in the Space Precision Attitude Reference System (SPARS) in 1969 [80]. It was later developed for NASA's Multimission Modular Spacecraft [81] and since then has been widely used in many practical applications [82], [83]. The MEKF algorithm has also been extended to incorporate GPS measurements to include the rigid body position and velocity in the state vector (see for instance [84] and [85]).

5.2.3 Additive EKF

The additive extended Kalman filter (AEKF) was introduced as an alternative to the MEKF by I. Y. Bar-Itzhack and Y. Oshman in [77]. Unlike the MEKF the true quaternion Q was defined as the sum of the quaternion error δQ and the estimated quaternion \hat{Q} . Mathematically, this can be written in discrete-time as

$$Q_k = \hat{Q}_k + \delta Q_k \quad (5.49)$$

However, the sum of two unit quaternions is not a unit quaternion and the resulting quaternion needs to be normalized. A collection of different methods for normalizing a quaternion are presented in [86]. One common method for quaternion normalization as presented in [77] is as

follows

$$Q_k^* = \frac{Q_k}{\|Q_k\|} \quad (5.50)$$

The rate of change of the actual quaternion Q is known to be a function of angular velocity $\omega = [\omega_x, \omega_y, \omega_z]^T$

$$\dot{Q} = \Omega(\omega)Q \quad (5.51)$$

where

$$\Omega(\omega) = \frac{1}{2} \begin{bmatrix} 0 & -\omega^T \\ \omega & -S(\omega) \end{bmatrix} \quad (5.52)$$

and $S(\cdot)$ is the skew-symmetric operator. Considering the gyroscope model given by Equation (2.21), we can re-write the above equation as

$$\dot{Q} = \Omega(\omega_m)Q + B\delta\omega \quad (5.53)$$

where ω_m and $\delta\omega$ are the gyroscope output and gyroscope bias respectively and B is given by

$$B = \frac{1}{2} \begin{bmatrix} q_1 & q_2 & q_3 \\ -q_0 & q_3 & -q_2 \\ -q_3 & -q_0 & q_1 \\ q_2 & -q_1 & -q_0 \end{bmatrix} \quad (5.54)$$

The estimated quaternion is propagated computationally according to

$$\dot{\hat{Q}} = \Omega(\omega_m)\hat{Q} \quad (5.55)$$

Subtracting Equation (5.55) from Equation (5.53) we have

$$\delta\dot{Q} = \Omega(\omega_m)\delta Q + B\delta\omega \quad (5.56)$$

It can be discretized for a sample period T by Euler integration to result in the following difference equation obtained for the propagation of δQ .

$$\delta Q_{k+1} = \phi_k \delta Q_k + B_k \delta \omega_k \quad (5.57)$$

where

$$\phi_k = I + T\Omega(\omega_m) \quad (5.58)$$

and

$$B_k = \frac{T}{2} \begin{bmatrix} \hat{q}_{k,1} & \hat{q}_{k,2} & \hat{q}_{k,3} \\ -\hat{q}_{k,0} & \hat{q}_{k,3} & -\hat{q}_{k,2} \\ -\hat{q}_{k,3} & -\hat{q}_{k,0} & \hat{q}_{k,1} \\ \hat{q}_{k,2} & -\hat{q}_{k,1} & -\hat{q}_{k,0} \end{bmatrix} \quad (5.59)$$

The AEKF algorithm calculates the estimated quaternion \hat{Q} and the error quaternion δQ , and can be summarized by the following recursive process.

Prediction step:

$$\hat{Q}_k = \phi_k Q_{k-1}^* \quad (5.60)$$

$$P_k = \phi_k P_{k-1}^* \phi_k^T + B_k W B_k^T \quad (5.61)$$

$$\delta Q_k^* = \phi_k \hat{Q}_{k-1} \hat{Q}_{k-1}^T \delta Q_{k-1} \quad (5.62)$$

The process and measurement noise are given by their normal probability distributions with covariance W and V respectively.

Optimal Kalman gain calculation step:

$$\hat{D}_k = R(\hat{Q}_k) \quad (5.63)$$

$$A_i = \left. \frac{\partial \hat{D}_k}{\partial q_i} \right|_{Q_k} \quad i = 0, 1, \dots, 3 \quad (5.64)$$

$$h_i = A_i u, \quad i = 0, 1, \dots, 3 \quad (5.65)$$

$$H_k = \begin{bmatrix} h_1 & h_2 & h_3 & h_4 \end{bmatrix} \quad (5.66)$$

$$K_k = P_k H_k^T (H_k P_k H_k^T + V)^{-1} \quad (5.67)$$

where $R(\hat{Q}_k)$ is the rotation matrix representation of the current estimate of attitude described in quaternion form and K_k is the optimal Kalman gain. The column vectors u and v consist of the reference vectors described in the inertial frame and body frame respectively. Explicitly,

A_0, A_1, A_2 and A_3 are given as

$$A_0 = 2 \begin{bmatrix} \hat{q}_{k,0} & \hat{q}_{k,3} & -\hat{q}_{k,2} \\ -\hat{q}_{k,3} & \hat{q}_{k,0} & \hat{q}_{k,1} \\ \hat{q}_{k,2} & -\hat{q}_{k,1} & \hat{q}_{k,0} \end{bmatrix} \quad (5.68)$$

$$A_1 = 2 \begin{bmatrix} \hat{q}_{k,1} & \hat{q}_{k,2} & \hat{q}_{k,3} \\ \hat{q}_{k,2} & -\hat{q}_{k,1} & \hat{q}_{k,0} \\ \hat{q}_{k,3} & -\hat{q}_{k,0} & -\hat{q}_{k,1} \end{bmatrix} \quad (5.69)$$

$$A_2 = 2 \begin{bmatrix} -\hat{q}_{k,2} & \hat{q}_{k,1} & -\hat{q}_{k,0} \\ \hat{q}_{k,1} & \hat{q}_{k,2} & \hat{q}_{k,3} \\ \hat{q}_{k,0} & \hat{q}_{k,3} & -\hat{q}_{k,2} \end{bmatrix} \quad (5.70)$$

$$A_3 = 2 \begin{bmatrix} -\hat{q}_{k,3} & \hat{q}_{k,0} & \hat{q}_{k,1} \\ -\hat{q}_{k,0} & -\hat{q}_{k,3} & \hat{q}_{k,2} \\ \hat{q}_{k,1} & \hat{q}_{k,2} & \hat{q}_{k,3} \end{bmatrix} \quad (5.71)$$

State update step:

The error in current measurements e_k is given as

$$e_k = v_k - \hat{D}_k u \quad (5.72)$$

$$\delta Q_k = \delta Q_k^* + K_k(e_k - H_k \delta Q_k^*) \quad (5.73)$$

Quaternion normalization and covariance update step:

$$Q_k = \hat{Q}_k + \delta Q_k \quad (5.74)$$

$$Q_k^* = \frac{Q_k}{\|Q_k\|} \quad (5.75)$$

$$P_k^* = (I - K_k H_k^*) P_k (I - K_k H_k^*)^T + K_k V K_k^T \quad (5.76)$$

The asterisk on H_k^* denotes that it is recomputed using the normalized estimated quaternion Q_k^* .

A comparison of AEKF and MEKF can be found in [87] and [88]. It argues that although the quaternion error is added to the estimated quaternion, the process noise and dynamic parameters enter the kinematic equation multiplicatively. Thus, it is not entirely similar to the linear Kalman

filter. Also, a comparative study provided in [4] suggests that MEKF is computationally more efficient than the AEKF as the latter involves reconstructing the rotation matrix.

5.3 Complementary Filter

The complementary filter provides a much simpler algorithm to provide better estimates from noisy measurements of the same signal which are fused together to complement each other. Earlier implementations focused on retrieving the velocity from position and acceleration measurements. Thus, the complementary filter can be modified to use measurements from sensors that are related to the original signal by differential signals [89]. This is specifically advantageous in attitude estimation techniques where the system is described by nonlinear equations in terms of the gyroscope measurement [65, 90].

5.3.1 Linear Complementary Filter

The implementation of linear complementary filter on the proposed experimental apparatus requires the knowledge of the Euler angles at specific intervals of time. For this purpose, the accelerometer is used to provide the roll ϕ and pitch θ . Assuming that the quadrotor doesn't undergo any high linear accelerations, the calibrated accelerometer A_c can be normalized and re-written as

$$A_n = \frac{A_c}{\|A_c\|} = \begin{bmatrix} A_x \\ A_y \\ A_z \end{bmatrix} = \begin{bmatrix} \sin \theta \\ -\cos \theta \sin \phi \\ -\cos \theta \cos \phi \end{bmatrix} \quad (5.77)$$

The roll and pitch can be calculated algebraically from A_n as follows

$$\phi = \arctan 2(-A_y, -A_z) \quad (5.78)$$

$$\theta = \arctan 2(A_x, A_y \sin \phi + A_z \cos \phi) \quad (5.79)$$

However, the accelerometer cannot be used to determine the yaw ψ of the rigid body. The magnetometer, as discussed earlier is the only sensor on-board capable of providing accurate yaw information. The calibrated magnetometer reading M_c can be described by a set of rotations about x , y and z axes as

$$M_c = R_x^T(\phi)R_y^T(\theta)R_z^T(\psi)m_I \quad (5.80)$$

where m_I is the unit vector of the local magnetic field in the inertial frame of reference. Let m_p denote the projection of the magnetometer reading on the $x - y$ plane given by

$$m_p = R_y(\theta)R_x(\phi)M_c \quad (5.81)$$

Then the magnetometer, utilizing the roll and pitch values provided by the accelerometer, can be used to compute the yaw angle as

$$\psi = \arctan 2(m_I^y m_p^x - m_I^x m_p^y, m_I^x m_p^x + m_I^y m_p^y) \quad (5.82)$$

A similar method to estimate the Euler angles using linear observers was proposed in [92]. Whereas, the original paper discussed the design and implementation of a complementary filter using two inclinometers and a rate gyro, it can easily be extended to work with a three-axis accelerometer, magnetometer and gyroscope.

Assume that the system is described by the state vector $x = [x_1^T, x_2^T]^T$, where $x_1 = [\phi, \theta, \psi]^T$ and $x_2 = [y_1, y_2, y_3]^T$ and the output y . Using Equation (2.20), the system dynamics can be written as

$$\dot{x}_1 = \rho\omega = \begin{bmatrix} 1 & \sin\phi \tan\theta & \cos\phi \tan\theta \\ 0 & \cos\phi & -\sin\phi \\ 0 & \sin\phi \sec\theta & \cos\phi \sec\theta \end{bmatrix} \begin{bmatrix} \omega_x \\ \omega_y \\ \omega_z \end{bmatrix} \quad (5.83)$$

$$\dot{x}_2 = \begin{bmatrix} \tau_1 & 0 & 0 \\ 0 & \tau_2 & 0 \\ 0 & 0 & \tau_3 \end{bmatrix} (x_1 - x_2) \quad (5.84)$$

$$y = Cx = \begin{bmatrix} 0_{3 \times 3} & I_{3 \times 3} \end{bmatrix} \begin{bmatrix} x_1 \\ x_2 \end{bmatrix} \quad (5.85)$$

where τ_1 , τ_2 and τ_3 are the filter time constants for roll pitch and yaw calculated from the accelerometer and magnetometer. The authors suggest an observer based on the assumption that the gyroscope measurements are ideal

$$\dot{\hat{x}} = f(\hat{x}, \omega) + L(y - C\hat{x}) \quad (5.86)$$

The linear complementary filter proposed in [93] is shown to be uniformly asymptotically stable assuming that the pitch described by the quadrotor is bounded as $|\theta| \leq \theta_{max} < \pi/2$. This means that the estimation error resulting from Equation (5.87) can be described as the difference in Euler angles defining the true orientation of the rigid body and their estimates. Lyapunov stability analysis based on these error definitions proves that the origin of the estimation error dynamics is uniformly asymptotically stable.

5.3.2 Non-linear Complementary Filter

The nonlinear complementary filtering has become immensely popular due its ability to truly capture the nonlinear nature of the rotational dynamics of a rigid body. The nonlinear observer reinforced with strong Lyapunov theory arguments assures that the estimated states are more accurate as compared to linear estimators. While previous observers focused on linearizing the system dynamics to obtain an estimate about the linearized model, the nonlinear complementary filter design is based on the nonlinear structure of the system.

One of the earliest works is nonlinear observer design is presented in [94]. The author proposes a novel solution to the problem of angular velocity measurement from torque and orientation measurements only. The observer for estimation of angular velocity of the rigid body is described using a mechanical energy function and it is shown to be globally exponentially convergent. Works such as [95], [96], [97], [98], [99] and [100] suggest that the literature is rich in research based on the nonlinear complementary filtering technique for attitude estimation. Also, the authors provide rigorous proof of stability through Lyapunov analysis.

However, these filtering techniques are often described by means of theoretical representations and fail to represent the observers as a function of sensors outputs from the IMU. The estimation algorithm presented in [65] explicitly defines the observer in terms of the sensors. Let us consider that a set of vectors r_i and b_i for $i = 1, \dots, n$ are available in inertial and body reference frames respectively and the angular velocity measurement ω_c is available in the body frame. Then a

simple and efficient observer with bias correction is given as

$$\dot{\hat{R}} = \hat{R}S(\omega_c - \hat{b}_g + k_P\sigma_r) \quad (5.90)$$

$$\dot{\hat{b}}_g = k_I\sigma_r \quad (5.91)$$

$$\sigma_r = \sum_{i=1}^n k_i b_i \times \hat{b}_i \quad (5.92)$$

where $\hat{b}_i = \hat{R}^T r_i$ is an estimate of a known inertial vector in the body-fixed frame. The gains k_P and k_I are positive scalar gains and k_i are positive coefficients influencing the individual contribution of sensors to the estimation algorithm.

The authors prove that the attitude and bias estimation errors are locally exponentially stable, assuming that at least two non-parallel vector measurements are available for feedback and $M_0 = \sum_{i=1}^n k_i r_i r_i^T$ has three distinct eigenvalues. The equilibrium points are identified and undesirable equilibria are shown to be unstable using Chetaev's Theorem. It is proven using Lyapunov analysis that for all initial conditions, except the unstable equilibria, the estimated attitude and bias converge to the actual values.

However, it is evident that decoupling of sensor measurements to ensure that the roll and pitch estimates are not disturbed by deviation in magnetometer measurements should be considered for higher accuracy and faster convergence. The modifications presented in [101] and [102] account for local decoupling of the roll and pitch estimation from the magnetometer measurements and present results to verify the overall improvement in quality of the attitude estimate. Another issue with bias estimation revolves around the integral wind-up in the presence of measurement noise.

With these considerations in perspective, a modified nonlinear complementary filter design has been proposed in [103] that is almost-globally stable and locally exponentially stable, and that ensures the global decoupling of the dynamics of the roll and pitch estimates from magnetic disturbances and from the dynamics of the yaw estimate. Moreover, a gyro-bias compensation technique is proposed that incorporates a saturation function to effectively work as an anti-wind-up nonlinear integrator.

Let us assume that IMU provides the calibrated accelerometer and magnetometer values in the body-fixed frame, given as A_c and M_c respectively. The gyroscope measurement is available for feedback, although the constant gyroscope bias \hat{b}_g is unknown. Then, the proposed observer in [103] estimates the quaternion representing the attitude of the rigid body \hat{Q} and can be given in discrete-time as

$$\hat{Q}_{k+1} = e^{\frac{T}{2}A(\hat{\Omega}_k)}\hat{Q}_k \quad (5.93)$$

$$\hat{b}_{g,k+1} = T(-k_b\hat{b}_{g,k} + k_b \text{sat}_\Delta(\hat{b}_{g,k}) + \sigma_{b,k}) + \hat{b}_{g,k}, \quad |\hat{b}_g(0)| < \Delta \quad (5.94)$$

$$\hat{\Omega}_k = \omega_{c,k} - \hat{b}_{g,k} + \sigma_{r,k} \quad (5.95)$$

$$A(\hat{\Omega}_k) = \frac{1}{2} \begin{bmatrix} 0 & -\hat{\Omega}_k^T \\ \hat{\Omega}_k & S(\hat{\Omega}_k) \end{bmatrix} \quad (5.96)$$

$$\sigma_{r,k} = k_1 A_{c,k} \times \hat{A}_k + k_2 \hat{A}_k \hat{A}_k^T (M_k \times \hat{M}_k) \quad (5.97)$$

$$\sigma_{b,k} = -k_3 A_{c,k} \times \hat{A}_k - k_4 M_{c,k} \times \hat{M}_k \quad (5.98)$$

where \hat{A} and \hat{M} are the estimates of the gravity field vector and magnetic field vector in the body-fixed frame and T is the sampling time period. The gains k_1, k_2, k_3, k_4 and k_b are positive scalars such that $k_4 < k_3$. The saturation function $\text{sat}_\Delta(\cdot)$ can be defined as $\text{sat}_\Delta(x) = x \min(1, \Delta/|x|)$, where x is a vector and Δ is a positive number.

Assuming that the gyroscope measurement is bounded and the gyro-bias is bounded in norm by Δ , the error dynamics are shown to have only four isolated equilibria of which three undesirable equilibria are proven to be unstable and the desirable equilibrium is proven to be locally exponentially stable. Thus, almost global exponential convergence of the attitude estimates is guaranteed. Furthermore, the gyroscope bias estimate \hat{b}_g is shown to be bounded and the estimation of roll and pitch angles does not depend upon the magnetic field measurement.

5.4 Globally Exponentially Stable Observers Non-evolving in SO3

Attitude estimation algorithms so far have been plagued with drawbacks such as lack of convergence guarantees, topological limitations for achieving global asymptotic stability, and slow convergence to a stable equilibrium [4]. The previously discussed nonlinear attitude observers

were designed to have a structure that imposed a topological restriction on the estimates themselves. Thus, $\hat{R} \in SO(3)$ or $\hat{Q} \in \mathbb{S}^3$ were the constraints on the estimated rotation matrix or quaternion respectively, so that the attitude estimate would essentially be a member of the rotation group itself.

Some recent papers such as [66,67,104,105] present an interesting approach. The authors suggest that the definition of the estimated attitude may be extended and allowed to evolve in Euclidean spaces (as discussed in detail in [106,107]) and finally converge to a value that lies within the $SO(3)$. This not only enables them to overcome the topological hurdle encountered in the attitude observers evolving in $SO(3)$, but also helps in guaranteeing exponential convergence. One of the most recent papers found in the literature dealing with such problems is [67].

Let us recall the rotational dynamics of a rigid body as given by Equation (2.13). Assume that a pair of non-collinear vectors A_I and M_I in the inertial frame are known and their projections in the body-fixed frame are A_B and M_B respectively can be measured by an accelerometer and a magnetometer. Let the accelerometer and magnetometer measurements be scaled and calibrated appropriately to give A_c and M_c respectively. Then, an estimate of the attitude \hat{R} is proposed in [67] as

$$\dot{\hat{R}} = R S(\omega) + \Gamma J \quad (5.99)$$

$$J = A_n A_b^T - \hat{R} A_b A_b^T \quad (5.100)$$

$$A_b = [A_c \quad A_c \times M_c \quad A_c \times (A_c \times M_c)] \quad (5.101)$$

$$A_n = [A_I \quad A_I \times M_I \quad A_I \times (A_I \times M_I)] \quad (5.102)$$

where Γ is a symmetric positive-definite gain matrix. Note that \hat{R} is not necessarily a rotation matrix. It is only a rotation matrix when the matrix J is a null matrix or in other words, the estimation error given by

$$\tilde{R} = R - \hat{R} \quad (5.103)$$

is a null matrix. The Lyapunov analysis of this observer yields that the origin of \tilde{R} is globally exponentially stable, provided that ω is known and bounded. However, the gyroscope measurement is affected by a constant bias b .

In order to maintain consistency and receive comparable results, an observer for the bias estimation needs to be developed. For this purpose we modify the Equation (5.99) such that $\omega = \omega_c - \hat{b}$. This can be seen as

$$\dot{\hat{R}} = RS(\omega_c - \hat{b}) + \Gamma J \quad (5.104)$$

$$\dot{\hat{b}} = -K \text{Vex}(M - M^T) \quad (5.105)$$

$$M = \hat{R}^T (A_b A_b^T)^{-1} J \quad (5.106)$$

where $\text{Vex}(\cdot)$ is the anti-skew symmetric operator defined as

$$\text{Vex}(S(x)) = x \quad (5.107)$$

The bias estimation error can be defined as

$$\tilde{b} = b - \hat{b} \quad (5.108)$$

The dynamics of the estimation error can be re-written using equations 2.13, 5.103 and 5.104 as

$$\begin{aligned} \dot{\tilde{R}} &= RS(\omega_c - b) - \hat{R}S(\omega_c - b + b - \hat{b}) - \Gamma J \\ &= \tilde{R}S(\omega) - \hat{R}S(\tilde{b}) - \Gamma J \end{aligned} \quad (5.109)$$

Proposition 1: *Assuming that ω is uniformly bounded, the origin of the dynamics of the estimation error as given by Equation (5.109), for the observer described in Equation (5.104), is globally exponentially stable.*

Proof: Let us recapitulate a few properties of the trace of a matrix given by

$$\text{tr}(X^T Y) = \text{tr}(X Y^T) \quad (5.110)$$

$$\text{tr}(X + Y) = \text{tr}(X) + \text{tr}(Y) \quad (5.111)$$

$$\text{tr}(XY) = \text{tr}(YX) \quad (5.112)$$

$$\text{tr}(X) = \text{tr}(X^T) \quad (5.113)$$

$$\text{tr}(S(a)X) = -a^T \text{Vex}(X - X^T) \quad (5.114)$$

Let us consider the following positive definite Lyapunov function candidate

$$\begin{aligned} V(\tilde{R}, \tilde{b}) &= \frac{1}{2} \|\tilde{R}\|^2 + \frac{1}{2} \tilde{b}^T K^{-1} \tilde{b} \\ &= \frac{1}{2} \text{tr}(\tilde{R}^T \tilde{R}) + \frac{1}{2} \tilde{b}^T K^{-1} \tilde{b} \end{aligned} \quad (5.115)$$

where K is a symmetric positive definite gain matrix. The time derivative of the Lyapunov function candidate is given by

$$\dot{V} = \frac{1}{2} \text{tr}(\tilde{R}^T \dot{\tilde{R}} + \dot{\tilde{R}}^T \tilde{R}) + \tilde{b}^T K^{-1} \dot{\tilde{b}} \quad (5.116)$$

Substituting Equation (5.103) and Equation (5.109), and using the properties of trace, we have

$$\dot{V} = \text{tr}(\tilde{R}^T \tilde{R} S(\omega)) - \text{tr}(\tilde{R}^T \Gamma \tilde{R} A_b A_b^T) + \text{tr}(S(\tilde{b}) \hat{R}^T \tilde{R}) + \tilde{b}^T K^{-1} \dot{\tilde{b}} \quad (5.117)$$

Taking the derivative of Equation (5.108) and remembering that b is assumed to be constant with respect to time, we can say that

$$\dot{\tilde{b}} = -\dot{b} \quad (5.118)$$

Since $A_n = R A_b$, we can rewrite J as

$$J = R A_b A_b^T - \hat{R} A_b A_b^T = \tilde{R} A_b A_b^T \quad (5.119)$$

Rearranging to describe \tilde{R} in terms of J , we have

$$\tilde{R} = (A_b A_b^T)^{-1} J \quad (5.120)$$

Let us substitute Equation (5.118) and Equation (5.120) in Equation (5.117). This results in

$$\dot{V} = \text{tr}(\tilde{R}^T \tilde{R} S(\omega)) - \text{tr}(\tilde{R}^T \Gamma \tilde{R} A_b A_b^T) + \text{tr}(S(\tilde{b}) \hat{R}^T (A_b A_b^T)^{-1} J) - \tilde{b}^T K^{-1} \dot{\tilde{b}} \quad (5.121)$$

Let us consider

$$\text{tr}(S(\tilde{b}) \hat{R}^T (A_b A_b^T)^{-1} J) - \tilde{b}^T K^{-1} \dot{\tilde{b}} = 0 \quad (5.122)$$

This implies that

$$\begin{aligned} \tilde{b}^T K^{-1} \dot{\tilde{b}} &= \text{tr}(S(\tilde{b}) \hat{R}^T (A_b A_b^T)^{-1} J) \\ &= \text{tr}(S(\tilde{b}) M) \end{aligned} \quad (5.123)$$

Using property 5.114, it can be shown that

$$\tilde{b}^T K^{-1} \dot{\tilde{b}} = -\tilde{b}^T \text{Vex}(M - M^T) \quad (5.124)$$

which leads to Equation (5.105). Under this condition, the derivative of the Lyapunov function is reduced to

$$\dot{V} = \text{tr}(\tilde{R}^T \tilde{R} S(\omega)) - \text{tr}(\tilde{R}^T \Gamma \tilde{R} A_b A_b^T) \quad (5.125)$$

Noting that $\text{tr}(S(x)X) = 0$ for any $x \in \mathbb{R}^3$ and symmetric $X \in \mathbb{R}^{3 \times 3}$, we have

$$\dot{V} \leq -\lambda_{\min}(A_b A_b^T) \lambda_{\min}(\Gamma) \|\tilde{R}\|^2 \quad (5.126)$$

(see [108], for the relevant trace inequalities). Let us write $A_b = N\Lambda$, where the columns of N are the normalized columns of A_b and Λ is a diagonal matrix with elements corresponding to the column norms of A_b . Since A_c and M_c are non-collinear, i.e. $\|A_c \times M_c\| > 0$ it can be said that N is an orthogonal matrix. It follows that $\lambda_{\min}(A_b A_b^T) = \lambda_{\min}(N\Lambda^2 N^T) = \lambda_{\min}(\Lambda^2)$. Thus, $\dot{V} \leq -\lambda_{\min}(\Gamma) \lambda_{\min}(\Lambda^2) \|\tilde{R}\|^2$ and we can say that the origin of the dynamics of the estimation error as given by Equation (5.109), for the observer described in Equation (5.104), is globally exponentially stable.

The concept of observers non-evolving in $SO(3)$ is interesting as it opens up new horizons for improvement and innovation. Whereas, classical nonlinear observers evolving in $SO(3)$ can only achieve almost global results, these observers face no such restrictions. Also, they claim to have faster convergence as they are not restricted by the topological definition of a rotation matrix or unit quaternion. However, despite these theoretical advantages, global attitude estimators have yet to be extensively tested on physical systems. One of the major concerns is that the the estimated attitude matrix is not a direction cosine matrix. This implies that the estimated attitude matrix may not retain its orthogonal nature. A simple orthogonalization process as given by [109] is

$$\hat{R}_n = \frac{1}{2}(\hat{R} + \hat{R}^{-1}) \quad (5.127)$$

Under the assumption that the accelerometer and magnetometer are not affected by noise, the algorithm operates flawlessly. In practice, both the vector observations are subjected to a variety

of noises as discussed in Chapter 3. This results in the loss of orthogonality of the attitude estimate and leads to inaccurate measurements.

5.5 Experimental Results

The experimental apparatus is configured and calibrated as discussed in Chapter 3. The dynamic attitude estimation algorithms discussed in this chapter have been implemented on the quadrotor platform and their performance under the effect of noisy sensor measurements is recorded and discussed. The actuators were run at fifty per cent capacity with the propeller removed. This produced the necessary vibrations and magnetic disturbances to simulate an actual flight. The results are compared to the attitude provided by the 3DM-GX1 IMU as discussed earlier. These results were visualized in SIMULINK by transmitting the data via UDP packets, in real-time. The estimated attitude is indicated in blue color and the attitude measurement from 3DM-GX1 module is shown in red color.

The parameters in the dynamic attitude estimators can be varied to change the extent of influence that the sensors have on measurements. Therefore, careful tuning of these gains in the estimation algorithms is necessary. Decreasing the influence of accelerometer and magnetometer helps to reduce the noise effecting the estimates, but it also leads to much slower dynamics and larger transient delays. On the other hand, increasing the influence of accelerometer and magnetometer results in faster convergence rates by compromising the efficiency of the filter to reduce noise in estimates.

The 3DM-GX1 module output is noted to have an approximate delay of 0.1 seconds to converge to a steady state value. This serves as a benchmark to achieve comparable delays in the estimated attitude. However, upon implementation, the loop execution time for attitude estimation algorithms was in the approximate range of 0.0091 seconds to 0.0115 seconds depending on the functions being called by the main loop. This meant that the linear estimation methods would be incapable of converging to a steady state value within 10 loops if the initial errors are too large.

The gains are adjusted in order to minimize the noise from sensor measurements while maintaining a reasonable amount of delay. The output of the estimation algorithms is recorded as shown in Figures 5.2 to 5.7 where the platform is held at approximately yaw = 36.63 degrees, pitch = -15.11 degrees and roll = 15.06 degrees. The variation in steady state estimation error Δ of an angle α , in degrees, can be defined as

$$\Delta(\alpha) = |\max(\alpha) - \min(\alpha)| \quad (5.128)$$

Table 5.1 gives an indication of the variation in steady state attitude estimation error for the first set of results. Then the orientation is changed to approximately yaw = 95.35 degrees, pitch = -30.68 degrees and roll = 63.07 degrees and the results are recorded as shown in Figures 5.2 to 5.7 and Table 5.2. For the third set of results the platform is rotated about all axes to simulate motion of the quadrotor in an agile flight manoeuvre.

Algorithm	$\Delta(Yaw)$ in degrees	$\Delta(Pitch)$ in degrees	$\Delta(Roll)$ in degrees
Filter QUEST	15.2845	4.5225	4.4286
MEKF	1.8007	0.1810	0.1788
AEKF	1.8185	0.1898	0.1865
LCF	1.7893	0.1429	0.1438
NCF	1.7062	0.1381	0.1394
GES Observer	1.7107	0.1370	0.1336

Table 5.1: Variation of Euler angles estimated for results set 1

Algorithm	$\Delta(Yaw)$ in degrees	$\Delta(Pitch)$ in degrees	$\Delta(Roll)$ in degrees
Filter QUEST	14.2202	4.5183	4.6700
MEKF	1.8572	0.1947	0.1906
AEKF	1.8956	0.1966	0.1937
LCF	1.8136	0.1581	0.1520
NCF	1.6718	0.1403	0.1414
GES Observer	1.7247	0.1497	0.1478

Table 5.2: Variation of Euler angles estimated for results set 2

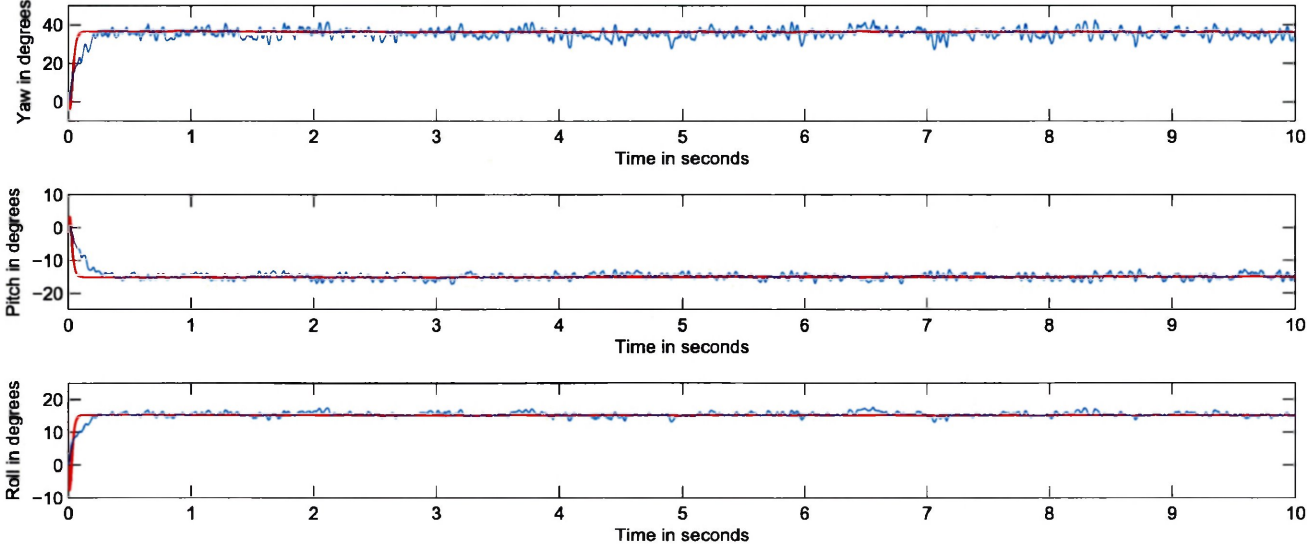


Figure 5.2: Filter QUEST result 1

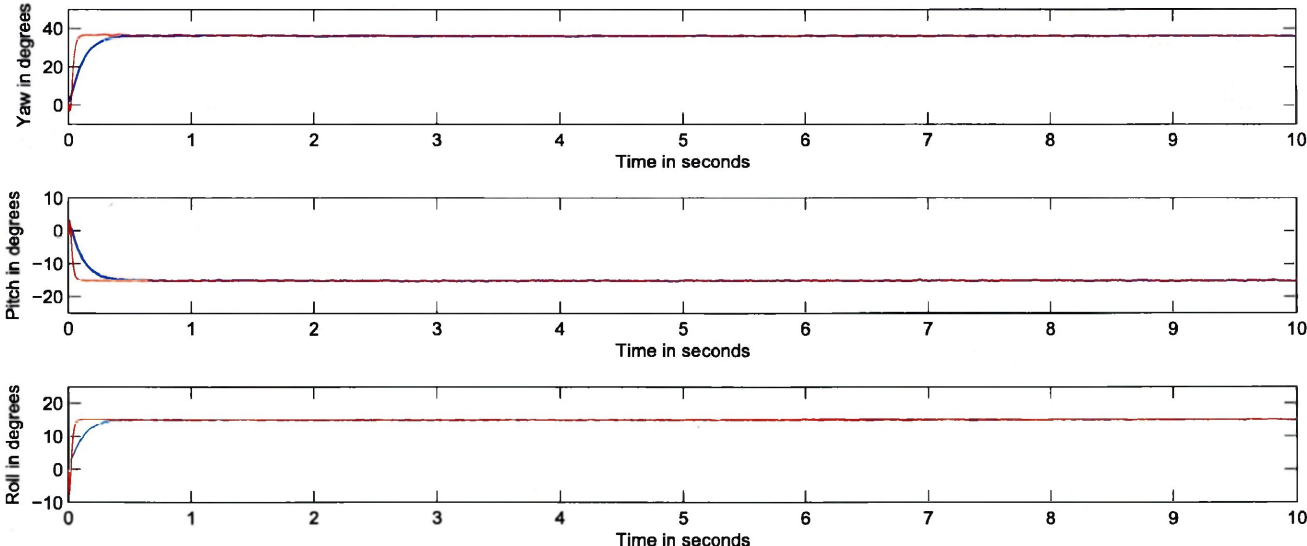


Figure 5.3: MEKF result 1

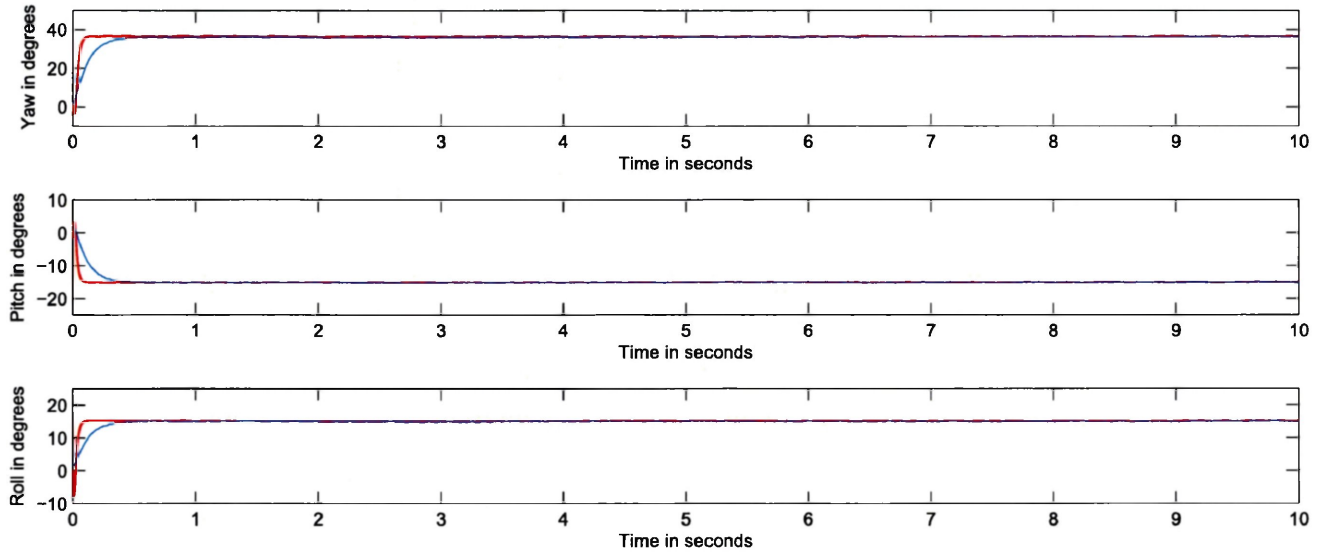


Figure 5.4: AEKF result 1

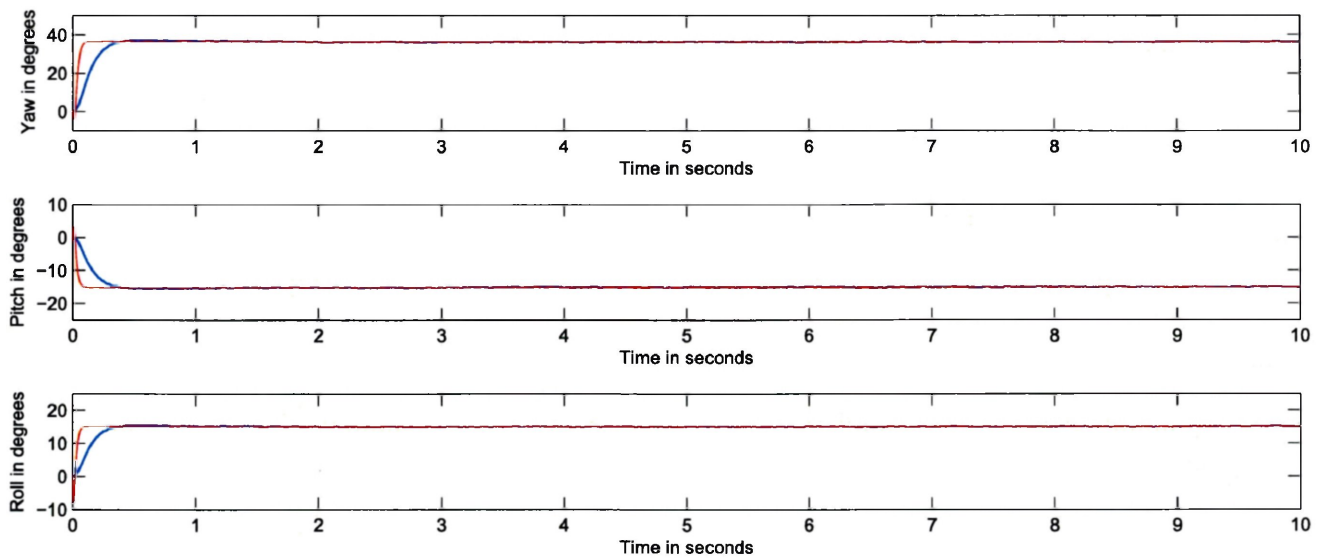


Figure 5.5: Linear complementary filter result 1

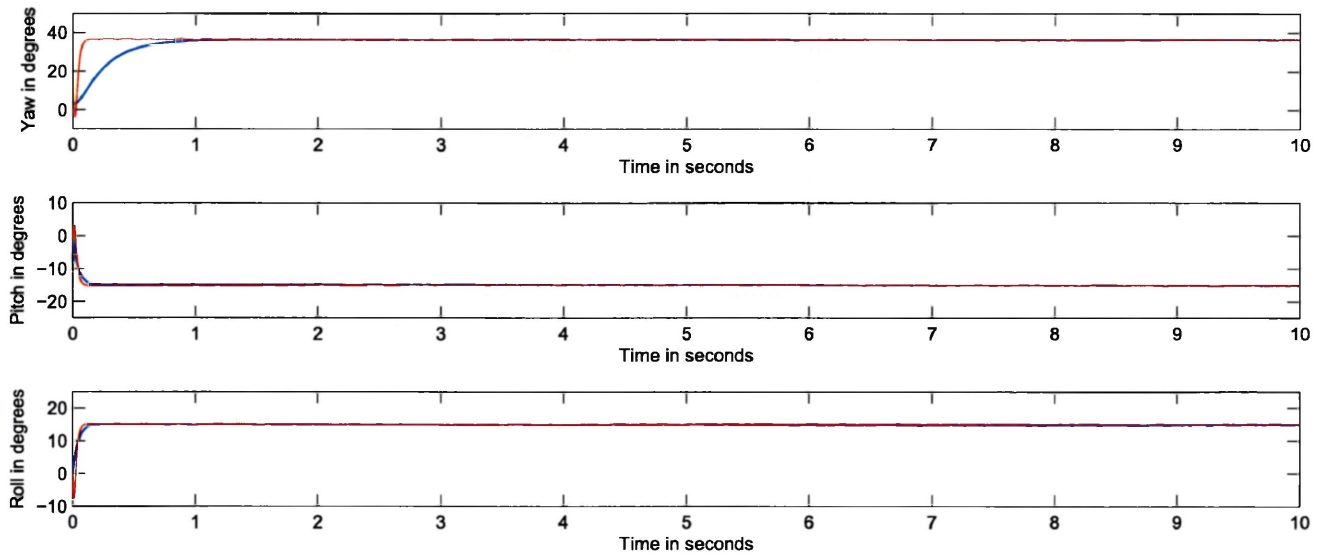


Figure 5.6: Nonlinear complementary filter result 1

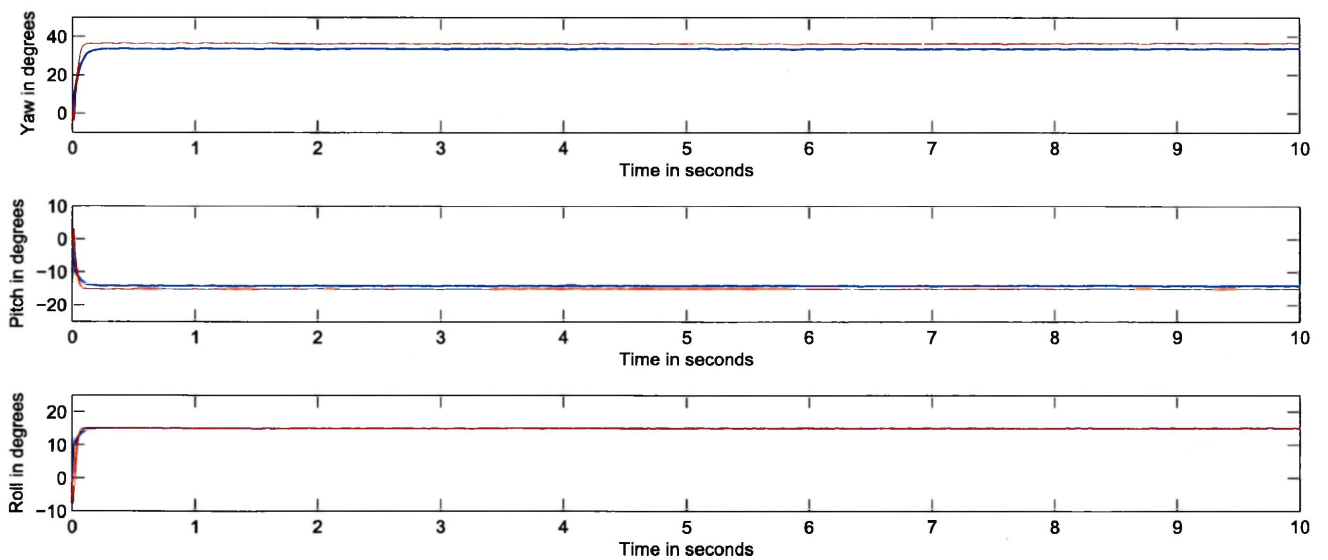


Figure 5.7: Globally exponentially stable Observer result 1

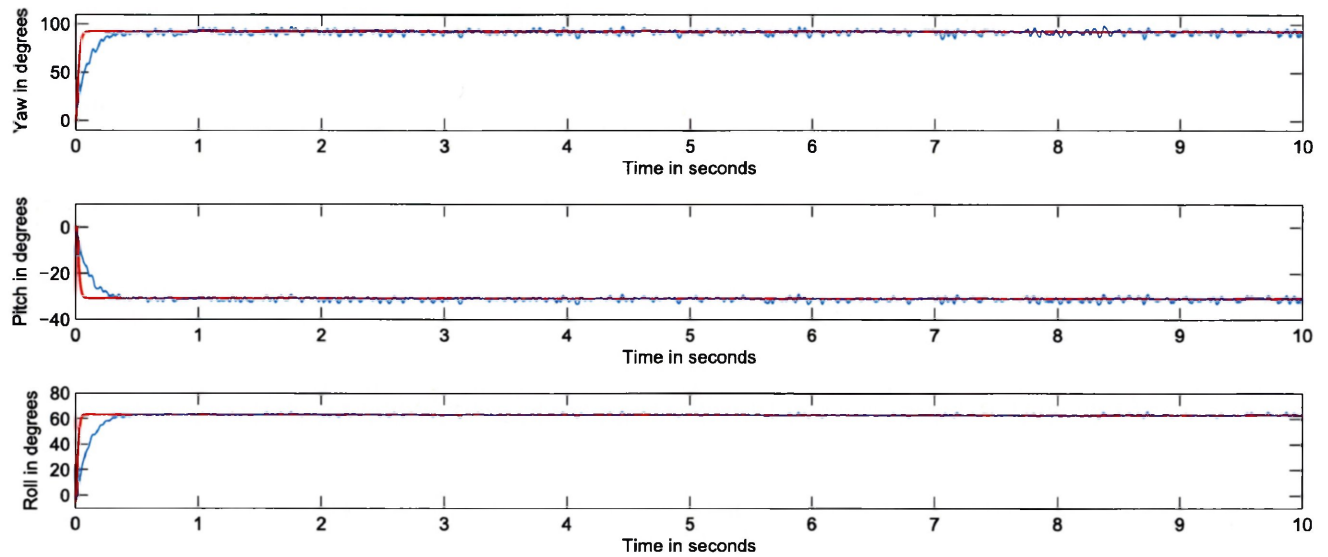


Figure 5.8: Filter QUEST result 2

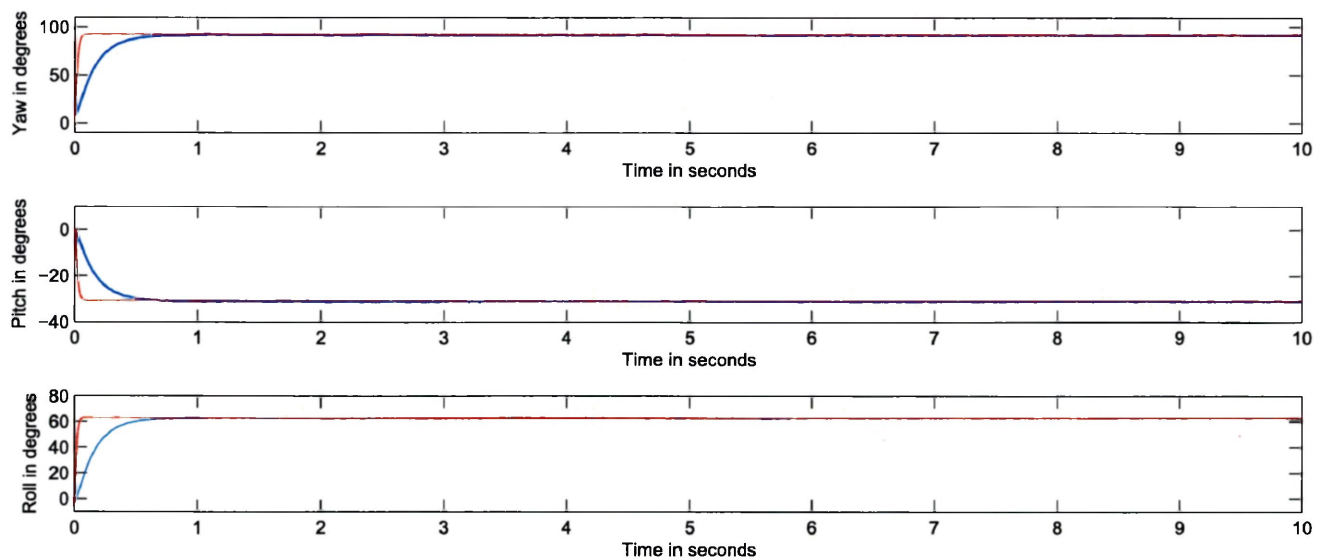


Figure 5.9: MEKF result 2

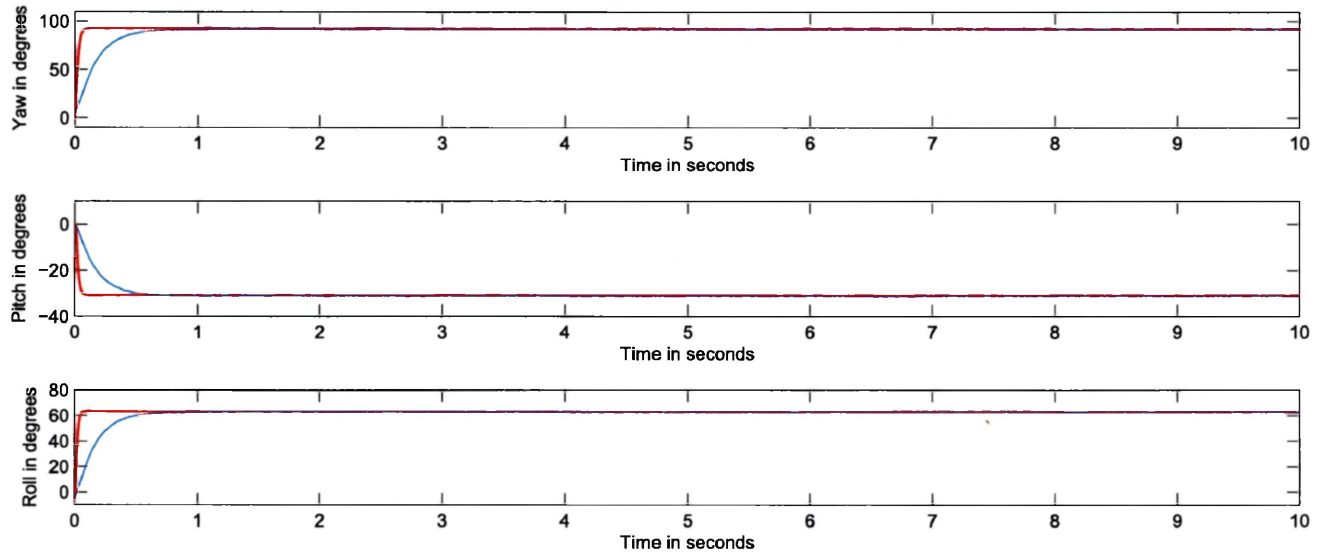


Figure 5.10: AEKF result 2

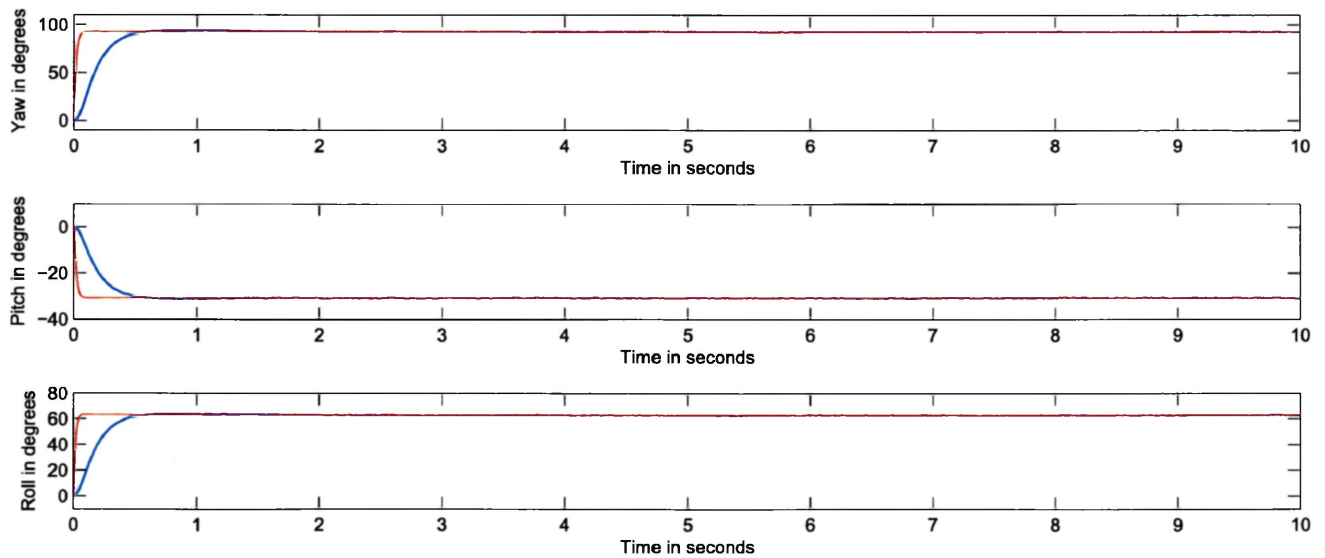


Figure 5.11: Linear complementary filter result 2

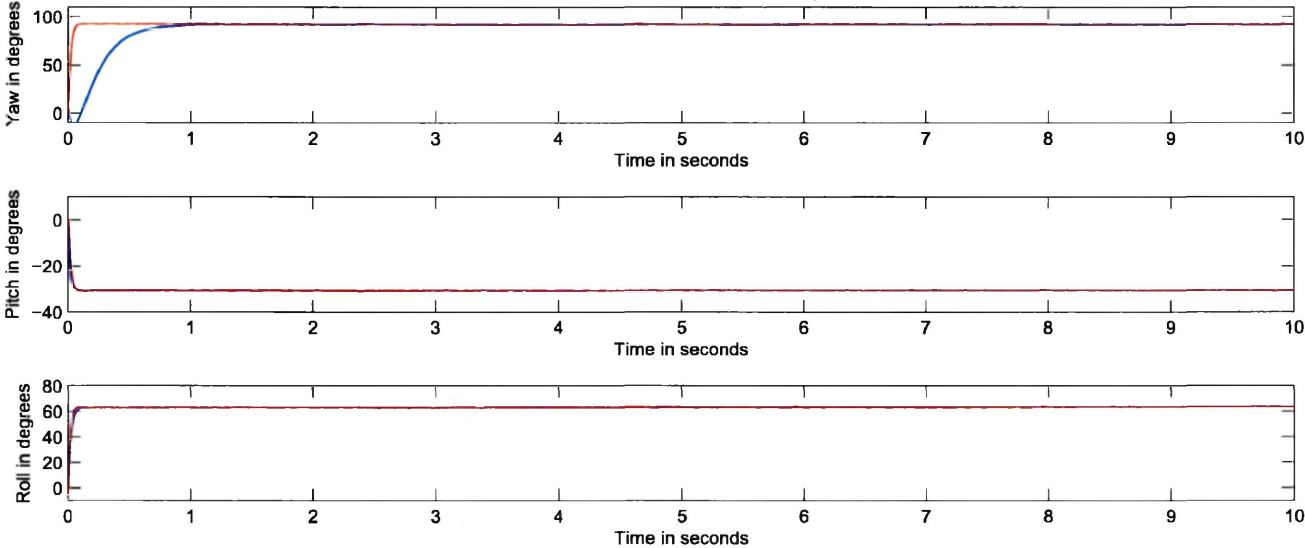


Figure 5.12: Nonlinear complementary filter result 2

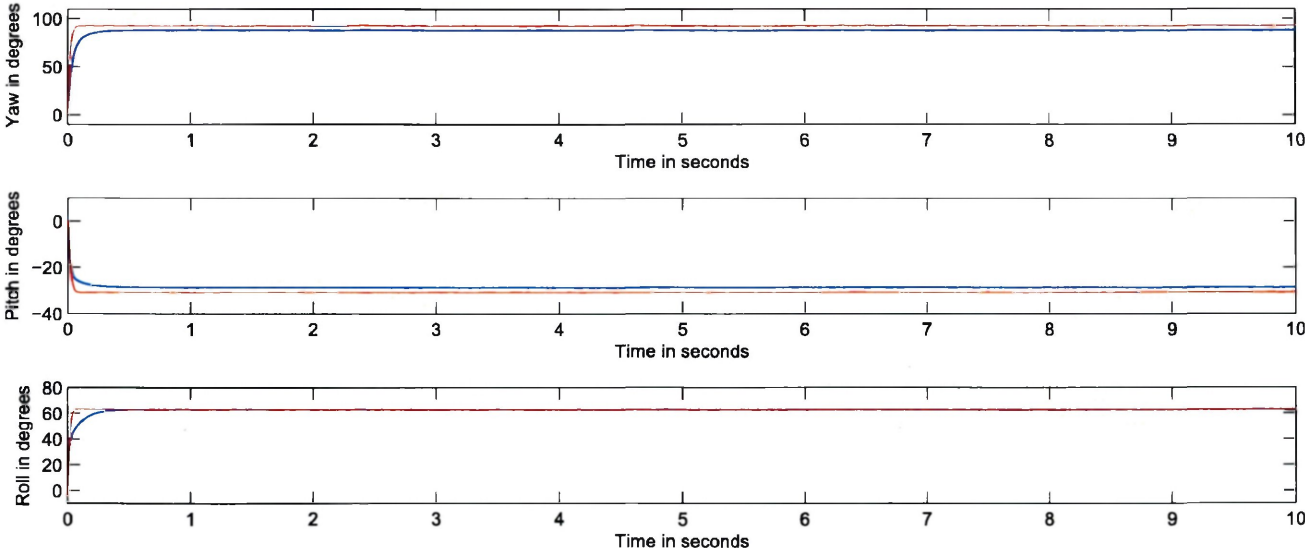


Figure 5.13: Globally exponentially stable Observer result 2

The first two sets of results clearly show that the Filter QUEST algorithm performs better than the static attitude estimation algorithms as indicated by comparison of Tables 5.1, 5.2 and 4.1. However, the variation Δ is still too large to be used for practical implementation of an estimation algorithm. We also observe in Figure 5.14 that there is a noticeable transient delay. This shows that the noise affecting the estimates is not due to a small filter parameter, but the inability of the algorithm to effectively tackle measurement noise.

The MEKF and AEKF techniques have been used extensively in the past and the reason is clear from tables 5.1 and 5.2. We notice that the noise from the accelerometer and magnetometer has been dealt with almost completely and we see a very small variation in the estimates. However, it is interesting to note that the time delay to reach a steady state value in Figures 5.3 and 5.4 is approximately 0.5 seconds. This is due to the fact that the MEKF and AEKF algorithms are based on the linearization of an underlying nonlinear model. This delay is larger as we move further away from the equilibrium point. This is demonstrated by the Figures 5.9 and 5.10 where the convergence to a steady state value takes approximately as long as 0.8 seconds. For sufficiently large deviations in initial conditions from the equilibrium point the algorithm may not even converge to the true attitude. This is the major drawback of a Kalman filter based attitude estimation algorithm.

The linear complementary filter algorithm shows similar results as the MEKF and AEKF with a marginal improvement in performance. The transient delay also follows a similar trend and convergence time increases as the initial conditions deviate from the equilibrium point. The nonlinear complementary filter however exhibits much more favorable results. The convergence time for roll and pitch axes is approximately 0.2 seconds and 1 second for the yaw estimate as shown in Figures 5.6 and 5.12. The convergence time is independent of the initial condition.

The globally exponentially stable observer results as shown in 5.7 and 5.13 provide an interesting insight into the effectiveness of such nonlinear observers. While the variation in steady state error in estimation is of a similar magnitude as the complementary filter based algorithms, the attitude estimates do not converge to the values provided by the 3DM-GX1. This can be attributed to the definition of observer. As discussed earlier, the attitude estimate is not strictly constrained within

the $SO(3)$ domain and fails to be an orthogonal matrix. Without this constraint, the estimated attitude needs to be orthogonalized and we note an error in the estimated Euler angles.

Figures 5.14 to 5.19 show the result of the dynamic attitude estimation techniques when the platform is rotated about all axes to simulate motion of the quadrotor in a flight. We note that the estimates follow the 3DM-GX1 output with a reasonable degree of accuracy. This suggests that the gains have been adjusted appropriately to meet the needs of aggressive manoeuvres and quasi-stationary flights alike.

It can be argued that the gains for the globally exponentially stable observer can be decreased in order for the attitude estimates to converge to the values provided by the 3DM-GX1. A trial and error approach is adopted for this purpose and the gains are reduced till the estimates converge to the desired value. This can be seen in Figure 5.20

In the presence of noisy measurements from the accelerometer, magnetometer and gyroscope, the nonlinear complementary filter presents the most favorable results amongst the attitude observers discussed within the scope of this thesis. Its nonlinear structure coupled with the Lyapunov analysis guaranteeing almost global convergence are the reason behind its success.

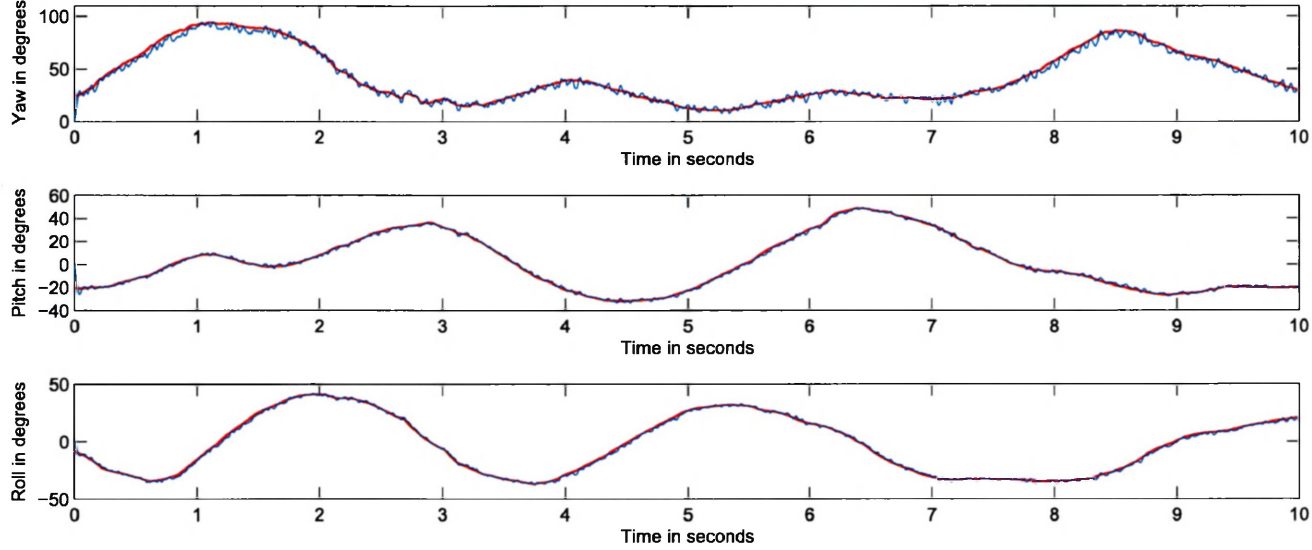


Figure 5.14: Filter QUEST result 3

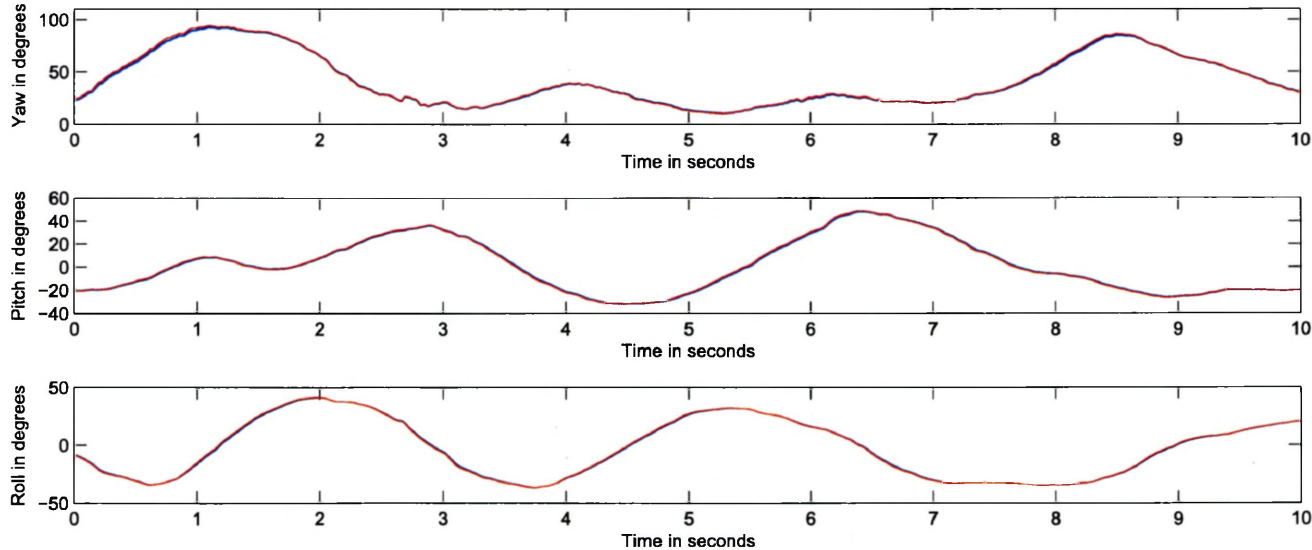


Figure 5.15: MEKF result 3

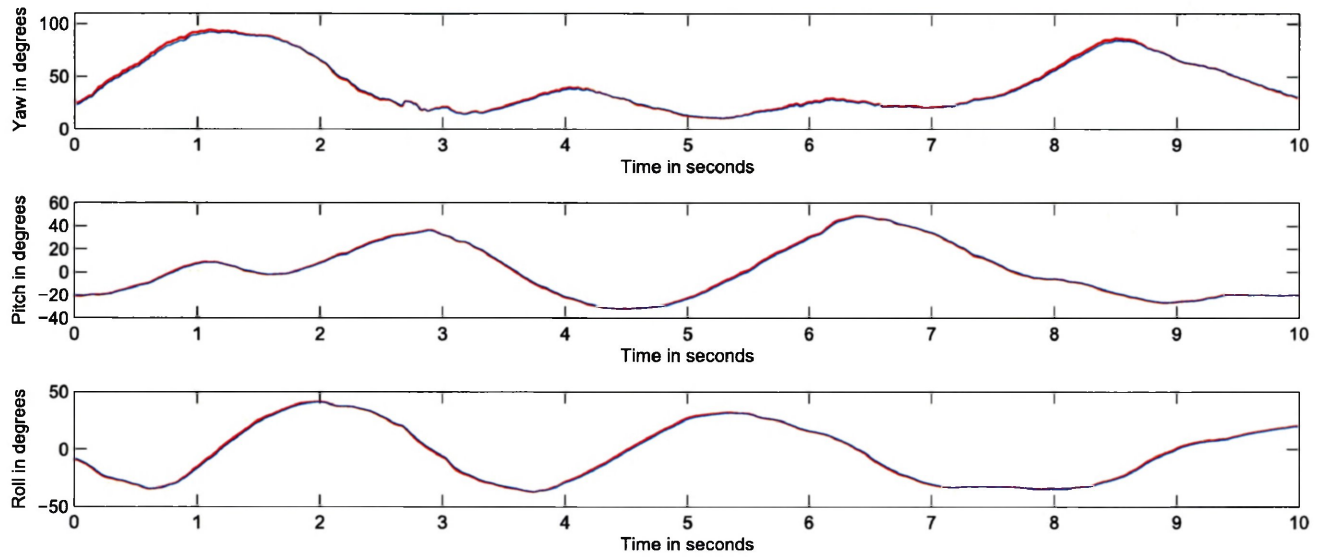


Figure 5.16: AEKF result 3

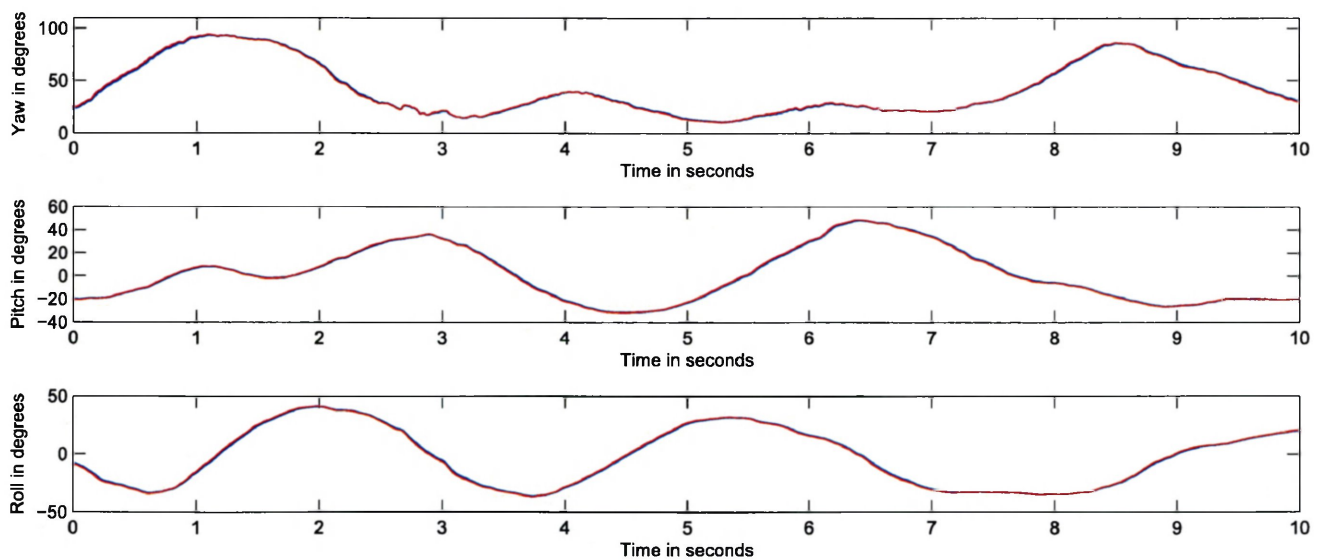


Figure 5.17: Linear complementary filter result 3

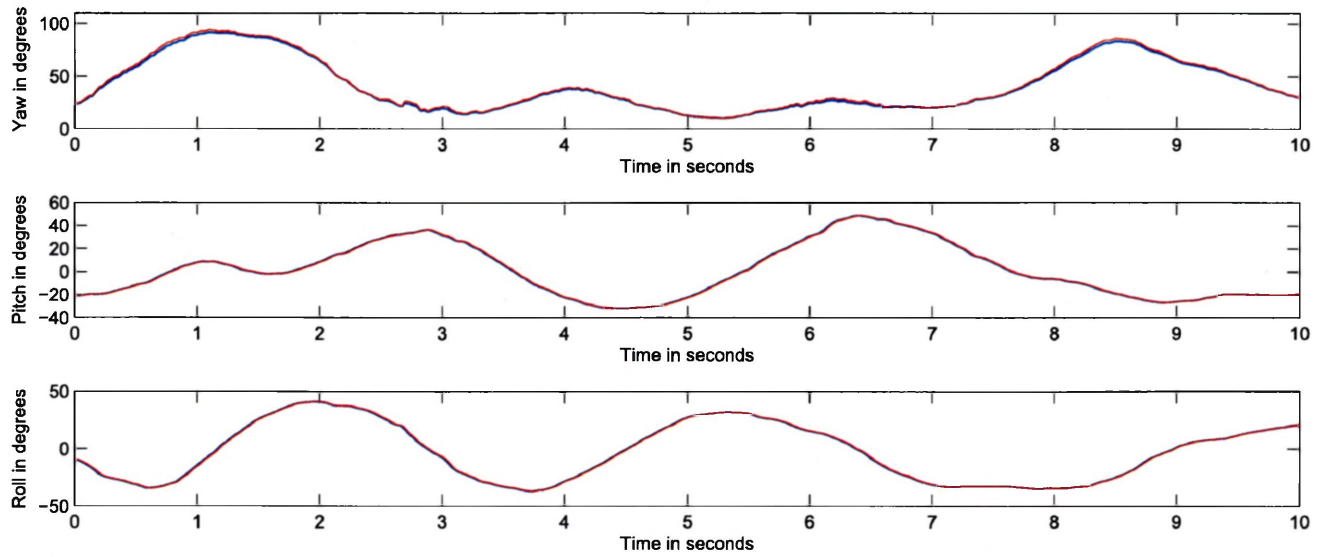


Figure 5.18: Nonlinear complementary filter result 3

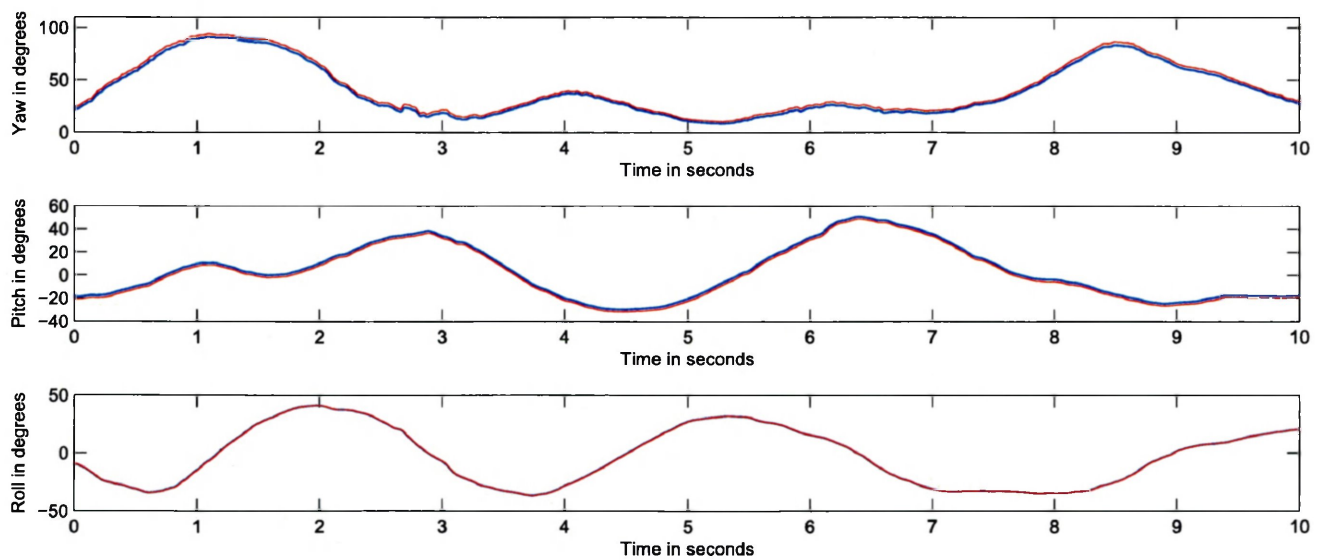


Figure 5.19: Globally exponentially stable Observer result 3

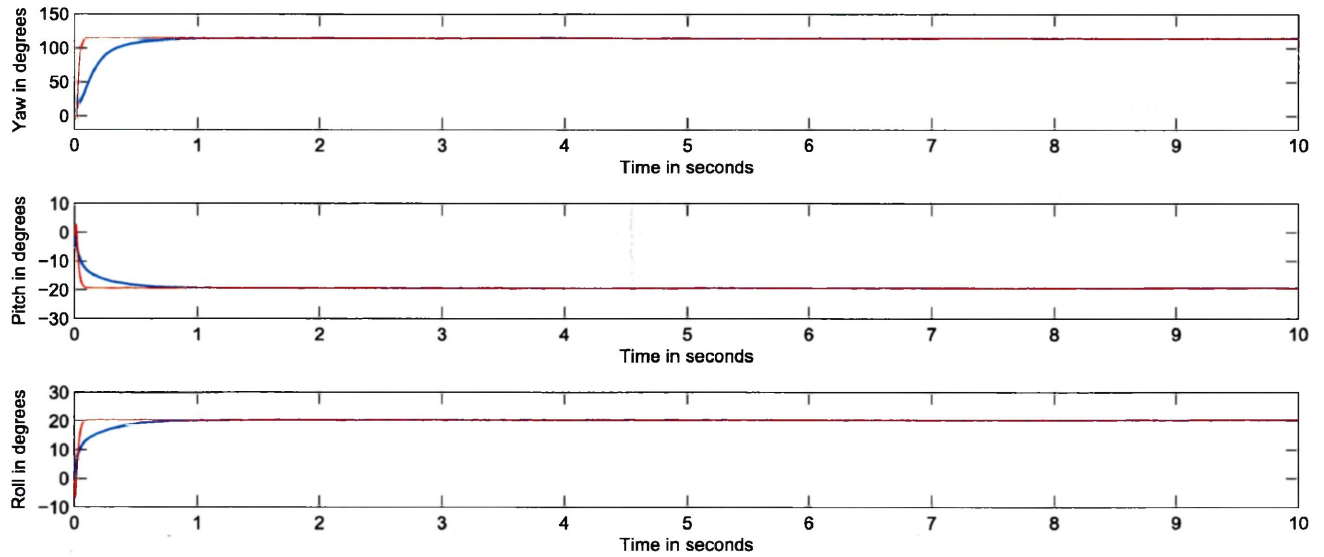


Figure 5.20: Globally exponentially stable Observer result 4

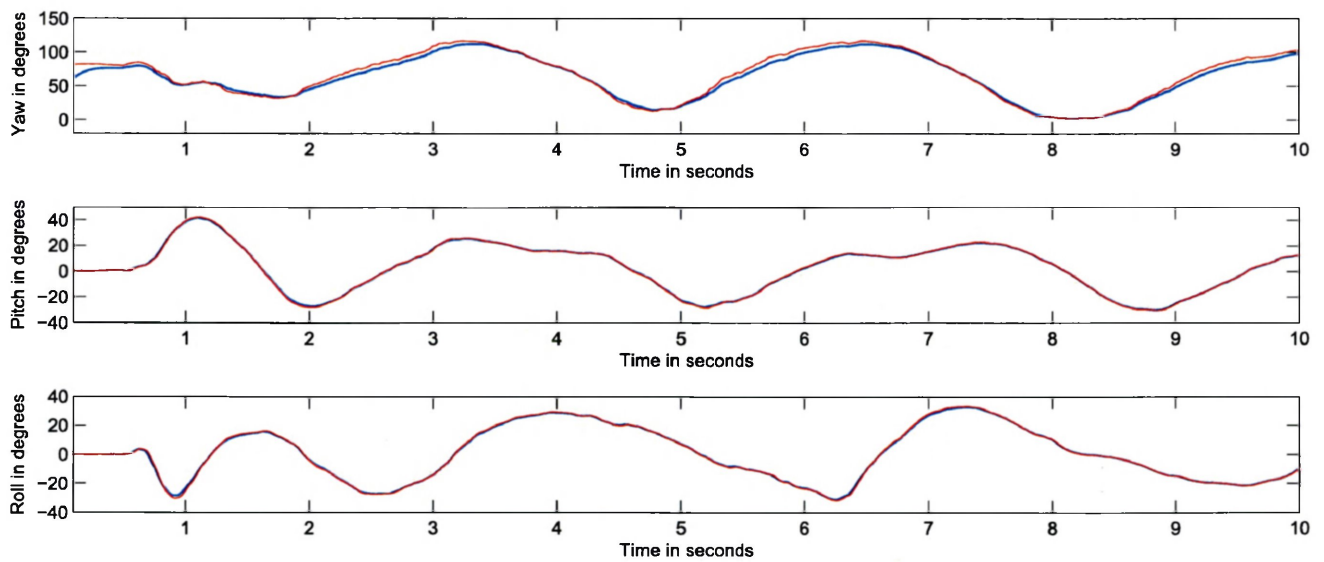


Figure 5.21: Globally exponentially stable Observer result 5

Chapter 6

Conclusion

Unmanned aerial vehicles have been the prime focus for many researchers due to their suitability to applications where human presence may not be feasible. However, autonomous stable flight, requires control strategies that rely on accurate attitude estimations. Moreover, noise and uncertainties due to low-cost sensor measurements and the inherent instability of aerial robots make it an exciting and interesting field of research. Therefore, rigorous and reliable attitude estimation techniques are required to produce good estimations in a real-time environment.

Various configurations of flying vehicles have evolved over the years. The quadrotor concept has proven to be one of the most desirable configurations among rotary wing aircrafts due to its maneuverability, efficient design and capability to land and take-off vertically. These features coupled with light-weight MEMS sensors, make it an ideal research platform. Quadrotor mathematical modelling and parameterization has been reviewed to understand the dynamics governing the motion of the aerial vehicle.

A suitable quadrotor platform with an on-board three-axis gyroscope, accelerometer and magnetometer has been used to serve as a reliable test-bed for the comparative study of some prominent attitude estimation techniques. Configuration of the experimental apparatus was given prime importance and sensor calibration techniques were employed to provide reliable measurements.

Key components of the experimental apparatus have been discussed to present a clear view of their roles and limitations.

The on-board IMU consists of integrated digital low pass filters and ADCs and can be utilized in a large variety of attitude estimation techniques. The earliest static estimation algorithms take advantage of the body vector observations to numerically determine the attitude without necessarily considering its kinematics. They are intended to be used with accurate sensor measurements and it is evident from the implementation results that they are not well suited with noisy sensor measurements.

The motivation behind the dynamic attitude estimation methods is discussed and various prominent techniques are presented. Their practical implementation is discussed and experimental results are studied to better understand their relative advantages and disadvantages.

Whereas, extended Kalman filtering techniques have been in use for a few decades, the lack of global convergence proofs and sub-optimal performance for large errors in initial estimates, have motivated the search for other reliable attitude estimation techniques. Complimentary filters are among the promising candidates to replace them, due to their simplicity, accuracy and larger domain of convergence.

More recently unconstrained nonlinear observers have evolved with lucrative properties such as exponential global convergence. However, experimental results suggest that their performance deteriorates with noisy measurements and we observe a large choice of observer gain results in high estimation error and smaller gains produce slower convergence rates. Although from a theoretical perspective, they seem promising and provide newer avenues for innovation and improvement.

Future development could involve comparison of attitude estimation algorithms incorporating position estimation using GPS sensors. GPS is limited by the fact that it is only usable outdoors and usually offers a small bandwidth range. For indoor applications where GPS signal is not available, optical flow sensors can be utilized. Proximity sensors such as rangefinders using LADAR technology or sonar detection can also be added to the platform. Each of these im-

provements may be added to the experimental platform to facilitate in attaining a higher degree of autonomy.

Bibliography

- [1] W.F. Phillips, C.E. Hailey, and G.A. Gebert. Review of attitude representations used for aircraft kinematics. *Journal of Aircraft*, 38(4):718–737, 2001.
- [2] Malcolm D Shuster. A survey of attitude representations. *Journal of Astronautical Sciences*, 41:439–517, 1993.
- [3] Mark W Spong and Mathukumalli Vidyasagar. *Robot dynamics and control*. John Wiley & Sons, Inc., 2008.
- [4] John L Crassidis, F Landis Markley, and Yang Cheng. Survey of nonlinear attitude estimation methods. *Journal of Guidance, Control, and Dynamics*, 30(1):12–28, 2007.
- [5] A. Tayebi, A. Roberts, and A. Benallegue. Inertial measurements based dynamic attitude estimation and velocity-free attitude stabilization. In *Proc. of American Control Conference (ACC), 2011*, pages 1027–1032. IEEE, 2011.
- [6] M.D. Hua. Attitude observers for accelerated rigid bodies based on gps and ins measurements. In *Decision and Control, 2009 held jointly with the 2009 28th Chinese Control Conference. CDC/CCC 2009. Proceedings of the 48th IEEE Conference on*, pages 8071–8076, 2009.
- [7] J Gordon Leishman. Principles of helicopter aerodynamics. 2006. *Cambridge Aerospace Series*, 2000.

- [8] Kenneth Munson and John William Wood. *Helicopters and other Rotorcraft since 1907*. Blandford Press, 1973.
- [9] R.J. Brown. *Planes that go straight up open new fields for aviation*. Popular Science Monthly 126, 1935.
- [10] Erdinc Altug. *Vision based control of unmanned aerial vehicles with applications to an autonomous four-rotor helicopter, quadrotor*. PhD thesis, Pensilvania University, 2004.
- [11] Charles Gablehouse. *Helicopters and autogiros: a history of rotating-wing and V/STOL aviation*. J.B. Lippincott Company, 1969.
- [12] G. Hoffmann, D.G. Rajnarayan, S.L. Waslander, D. Dostal, Jung Soon Jang, and C.J. Tomlin. The stanford testbed of autonomous rotorcraft for multi agent control (starmac). In *Digital Avionics Systems Conference, 2004. DASC 04. The 23rd*, volume 2, pages 12.E.4–121–10, 2004.
- [13] <http://www.rctoys.com/>.
- [14] [Online]. <http://aero.stanford.edu/Reports/AHSPaper.pdf>.
- [15] [Online]. <http://hybrid.eecs.berkeley.edu/starmac/>.
- [16] S. J. McGilvray. Attitude stabilization of a quadrotor aircraft. Master’s thesis, Lakehead University, 2004.
- [17] A. D. Roberts. Attitude estimation and control of a ducted fan vtol uav. Master’s thesis, Lakehead University, 2007.
- [18] F. Ghashghaee. Attitude estimation and stabilization of a quadrotor aircraft. Master’s thesis, Lakehead University, 2011.
- [19] F Landis Markley and Daniele Mortari. How to estimate attitude from vector observations. In *Proceedings of the AAS/AIAA Astrodynamics Specialist Conference*, volume 103, pages 1979–1996, 1999.
- [20] [Online]. www.mathworks.com.

-
- [21] N. Madinehi. Rigid body attitude estimation: An overview and comparative study. Master's thesis, University of Western Ontario, 2013.
- [22] John Stuelpnagel. On the parametrization of the three-dimensional rotation group. *SIAM review*, 6(4):422–430, 1964.
- [23] Peter Carlisle Hughes. *Spacecraft attitude dynamics*. Dover Publications, 2012.
- [24] John Stuelpnagel. On the parametrization of the three-dimensional rotation group. *SIAM review*, 6(4):422–430, 1964.
- [25] A. Tayebi, A. Roberts, and A. Benallegue. Inertial vector measurements based velocity-free attitude stabilization. *IEEE Transactions on Automatic Control*, 58(11):2893–2898, 2013.
- [26] Tarek Hamel, Robert Mahony, Rogelio Lozano, and James Ostrowski. Dynamic modeling and configuration stabilization for an x4-flyer. *Proceedings of the 15th IFAC World Congress*, 15(1):846–846, 2002.
- [27] Abdelhamid Tayebi and Stephen McGilvray. Attitude stabilization of a vtol quadrotor aircraft. *Control Systems Technology, IEEE Transactions on*, 14(3):562–571, 2006.
- [28] Jonathan Bernstein. An overview of mems inertial sensing technology. *Corning IntelliSense Corp.*, 2003.
- [29] Haiyang Chao, C. Coopmans, Long Di, and Yang-Quan Chen. A comparative evaluation of low-cost imus for unmanned autonomous systems. In *Multisensor Fusion and Integration for Intelligent Systems (MFI), 2010 IEEE Conference on*, pages 211–216, 2010.
- [30] T.K. Sethuramalingam and A. Vimalajuliet. Design of mems based capacitive accelerometer. In *Mechanical and Electrical Technology (ICMET), 2nd International Conference on*, pages 565–568. IEEE, 2010.
- [31] M. Schneider and S. Hubschmann. Magneto resistive sensors: principles of operation and application. *ZETEX Co. application note 20*, 1996.
- [32] <https://code.google.com/p/arducopter/>.

- [33] <http://www.asctec.de/uav-applications/research/products/asctec-pelican/>.
- [34] <http://www.dji.com/product/phantom/>.
- [35] <http://www.draganfly.com/>.
- [36] <http://ardrone2.parrot.com/>.
- [37] Hyon Lim, Jaemann Park, Daewon Lee, and H Jin Kim. Build your own quadrotor: Open-source projects on unmanned aerial vehicles. *Robotics & Automation Magazine, IEEE*, 19(3):33–45, 2012.
- [38] Datasheet: Atmel ATmega2560.
- [39] Datasheet: Atmel ATmega32U2.
- [40] Datasheet: Invensense MPU-6000.
- [41] Datasheet: Honeywell HMC5883L.
- [42] <http://www.microstrain.com/inertial/3DM-GX1>.
- [43] C.C. Foster and G.H. Elkaim. Extension of a two-step calibration methodology to include nonorthogonal sensor axes. *Aerospace and Electronic Systems, IEEE Transactions on*, 44(3):1070–1078, 2008.
- [44] CC Finlay, S Maus, CD Beggan, TN Bondar, A Chambodut, TA Chernova, A Chulliat, VP Golovkov, B Hamilton, M Hamoudi, et al. International geomagnetic reference field: the eleventh generation. *Geophysical Journal International*, 183(3):1216–1230, 2010.
- [45] Stefan Maus, Susan Macmillan, Susan McLean, B. Hamilton, A. Thomson, M. Nair, and C. Rollins. The us/uk world magnetic model for 2010-2015. *NOAA Technical Report NESDIS/NGDC*, 2010.
- [46] Harold D. Black. A passive system for determining the attitude of a satellite. *AIAA Journal*, 2(7):1350–1351, 1964.
- [47] G. Wahba. A least squares estimate of spacecraft attitude. *SIAM Review*, 7(3):409, 1965.

-
- [48] M. D. Shuster and S. D. Oh. Three-axis attitude determination from vector observations. *Journal of Guidance, Control, and Dynamics*, 4(1):70–77, 1981.
- [49] J. E. Brock. A least squares estimate of spacecraft attitude. *SIAM Review*, 8(3):384–386, 1966.
- [50] J. R. Velman. A least squares estimate of spacecraft attitude. *SIAM Review*, 8(3):384–386, 1966.
- [51] R. H. Wessner. A least squares estimate of spacecraft attitude. *SIAM Review*, 8(3):384–386, 1966.
- [52] J. L. Farrell and J. C. Stuelpnagel. A least squares estimate of spacecraft attitude. *SIAM Review*, 8(3):384–386, 1966.
- [53] James E Keat. Analysis of least-squares attitude determination routine doaop. *Technical report, Computer Sciences Corporations*, 1977.
- [54] G. M. Lerner. *Spacecraft Attitude Determination and Control, Chapter: Three-Axis Attitude Determination*. D. Reidel, Dordrecht, Holland, 1978.
- [55] Roger A. Horn and Charles R. Johnson. *Matrix Analysis*. Cambridge University Press, 2012.
- [56] Gene H Golub and Charles F Van Loan. *Matrix computations*, volume 3. The Johns Hopkins University Press, Baltimore, MD, 2012.
- [57] Daniele Mortari. Esoq: A closed-form solution to the wahba problem. *Journal of the Astronautical Sciences*, 45(2):195–204, 1997.
- [58] Daniele Mortari. Second estimator of the optimal quaternion. *Journal of Guidance, Control, and Dynamics*, 23(5):885–888, 2000.
- [59] F Landis Markley and Daniele Mortari. Quaternion attitude estimation using vector observations. *Journal of the Astronautical Sciences*, 48(2):359–380, 2000.

- [60] F Landis Markley. Attitude determination using vector observations and the singular value decomposition. *The Journal of the Astronautical Sciences*, 36(3):245–258, 1988.
- [61] F Landis Markley. Attitude determination using vector observations: A fast optimal matrix algorithm. *Journal of the Astronautical Sciences*, 41(2):261–280, 1993.
- [62] Ern J. Lefferts, F. Landis Markley, and Malcolm D. Shuster. Kalman filtering for spacecraft attitude estimation. *Journal of Guidance, Control, and Dynamics*, 5(5):417–429, 1982.
- [63] M. D. Shuster. Maximum likelihood estimation of spacecraft attitude. *Journal of the Astronautical Sciences*, 37(1):89–106, 1989.
- [64] Itzhack Y Bar-Itzhack. Request-a recursive quest algorithm for sequential attitude determination. *Journal of Guidance, Control, and Dynamics*, 19(5):1034–1038, 1996.
- [65] Robert Mahony, Tarek Hamel, and J-M Pfimlin. Nonlinear complementary filters on the special orthogonal group. *Automatic Control, IEEE Transactions on*, 53(5):1203–1218, 2008.
- [66] Pedro Batista, Carlos Silvestre, and Paulo Oliveira. Globally exponentially stable cascade observers for attitude estimation. *Control Engineering Practice*, 20(2):148–155, 2012.
- [67] H. F. Grip, Ali Saberi, and Tor A Johansen. Observers for interconnected nonlinear and linear systems. *Automatica*, 48(7):1339–1346, 2012.
- [68] M. D. Shuster. Maximum likelihood estimation of spacecraft attitude. *Journal of the Astronautical Sciences*, 37(1):79–88, 1989.
- [69] Rudolph Emil Kalman et al. A new approach to linear filtering and prediction problems. *Journal of basic Engineering*, 82(1):35–45, 1960.
- [70] Mohinder S Grewal and Angus P Andrews. Applications of kalman filtering in aerospace 1960 to the present [historical perspectives]. *Control Systems, IEEE*, 30(3):69–78, 2010.
- [71] Andrew H Jazwinski. *Stochastic processes and filtering theory*. Academic Press, New York, 1970.

- [72] S. Vathsal. Spacecraft attitude determination using a second-order nonlinear filter. *Journal of Guidance, Control, and Dynamics*, 10(6):559–566, 1987.
- [73] Michael Roth and Fredrik Gustafsson. An efficient implementation of the second order extended kalman filter. In *Information Fusion (FUSION), 2011 Proceedings of the 14th International Conference on*, pages 1–6. IEEE, 2011.
- [74] Yongkyu Song and Jessy W. Grizzle. The extended kalman filter as a local asymptotic observer for discrete-time nonlinear systems. *Journal of Mathematical Systems, Estimation and Control*, 5(1):59–78, 1995.
- [75] Mark L Psiaki. Backward-smoothing extended kalman filter. *Journal of Guidance, Control, and Dynamics*, 28(5):885–894, 2005.
- [76] Karianne Knutsen Tønne. Stability analysis of ekf-based attitude determination and control. Master’s thesis, Norwegian University of Science and Technology, 2007.
- [77] I. Y. Bar-Itzhack and Y. Oshman. Attitude determination from vector observations: Quaternion estimation. *Aerospace and Electronic Systems, IEEE Transactions on*, AES-21(1):128–136, 1985.
- [78] Charles W Gray. Star tracker/iru attitude determination filters. In *AAS Guidance and Control Conference*, pages 459–478, 2001.
- [79] F Landis Markley. Attitude error representations for kalman filtering. *Journal of Astronautical Sciences*, 52(1):221–238, 2004.
- [80] N. F. Toda, J. L. Heiss, and F. H. Schlee. Hubble space telescope angular velocity estimation during the robotic servicing mission. *Report TR0066 (5306)-12, Proceedings of the Symposium on Spacecraft Attitude Determination*, 1:361–370, 2007.
- [81] James W. Murrell. Precision attitude determination for multimission spacecraft. *AIAA Guidance and Control Conference*, 78:1248, 1978.

- [82] KJ Ernandes, BE Joseph, and PJ Cefola. Implementation of a multiplicative extended kalman filter (mekf) for spinning spacecraft attitude determination in the astrodynamics environment (ade). *Advances in the Astronautical Sciences*, 129(2), 2007.
- [83] Johan Bijker and Willem Steyn. Kalman filter configurations for a low-cost loosely integrated inertial navigation system on an airship. *Control Engineering Practice*, 16(12):1509–1518, 2008.
- [84] S. Bonnabel, P. Martin, and E. Salaun. Invariant extended kalman filter: theory and application to a velocity-aided attitude estimation problem. In *Decision and Control, 2009 held jointly with the 2009 28th Chinese Control Conference. CDC/CCC 2009. Proceedings of the 48th IEEE Conference on*, pages 1297–1304, 2009.
- [85] Philippe Martin and Erwan Salaün. Generalized multiplicative extended kalman filter for aided attitude and heading reference system. In *Proc. AIAA Guidance, Navigation and Control Conference*, pages 1–13, 2010.
- [86] Julie Deutschmann, Itzhack Bar-Itzhack, and Ken Galal. Quaternion normalization in spacecraft attitude determination. In *AIAA/AAS Astrodynamics Conference Technical Papers (A92-52051 22-13)*, pages 27–37, 1992.
- [87] F Landis Markley. Attitude estimation or quaternion estimation. *Journal of Guidance, Control, and Dynamics*, 26(2):311–317, 2003.
- [88] F Landis Markley. Multiplicative vs. additive filtering for spacecraft attitude determination. *Proceedings of the Sixth Conference on Dynamics and Control of Systems and Structures in Space(DCSSS)*, 2004.
- [89] F. Daum. Nonlinear filters: beyond the kalman filter. *Aerospace and Electronic Systems Magazine, IEEE*, 20(8):57–69, 2005.
- [90] Mark Euston, Paul Coote, Robert Mahony, Jonghyuk Kim, and Tarek Hamel. A complementary filter for attitude estimation of a fixed-wing uav. In *Intelligent Robots and Systems, 2008. IEEE/RSJ International Conference on*, pages 340–345. IEEE, 2008.

- [91] A-J Baerveldt and Robert Klang. A low-cost and low-weight attitude estimation system for an autonomous helicopter. In *Intelligent Engineering Systems, 1997. INES'97. Proceedings., 1997 IEEE International Conference on*, pages 391–395. IEEE, 1997.
- [92] Henrik Rehbinder and Xiaoming Hu. Nonlinear state estimation for rigid-body motion with low-pass sensors. *Systems & control letters*, 40(3):183–190, 2000.
- [93] J. F. Vasconcelos, Bruno Carneira, Carlos Silvestre, Paulo Oliveira, and Pedro Batista. Discrete-time complementary filters for attitude and position estimation: Design, analysis and experimental validation. *Control Systems Technology, IEEE Transactions on*, 19(1):181–198, 2011.
- [94] S Salcudean. A globally convergent angular velocity observer for rigid body motion. *Automatic Control, IEEE Transactions on*, 36(12):1493–1497, 1991.
- [95] B. Vik and Thor I. Fossen. A nonlinear observer for gps and ins integration. In *Decision and Control, 2001. Proceedings of the 40th IEEE Conference on*, volume 3, pages 2956–2961. IEEE, 2001.
- [96] W.F. Guerrero-Sanchez, J.F. Guerrero-Castellanos, R. Juarez-Salazar, and B.B. Salmeron-Quiroz. Nonlinear observer for real-time attitude estimation. In *Electrical Engineering, Computing Science and Automatic Control, CCE, 2009 6th International Conference on*, pages 1–6, 2009.
- [97] J.D. Boskovic, Sai-Ming Li, and R.K. Mehra. A globally stable scheme for spacecraft control in the presence of sensor bias. In *Aerospace Conference Proceedings, 2000 IEEE*, volume 3, pages 505–511, 2000.
- [98] J. Thienel and Robert M. Sanner. A coupled nonlinear spacecraft attitude controller and observer with an unknown constant gyro bias and gyro noise. *Automatic Control, IEEE Transactions on*, 48(11):2011–2015, 2003.
- [99] Julie K. Thienel and Robert M. Sanner. Hubble space telescope angular velocity estimation during the robotic servicing mission. *Journal of Guidance, Control, and Dynamics*, 30(1):29–34, 2007.

-
- [100] A. Tayebi, S. McGilvray, A. Roberts, and M. Moallem. Attitude estimation and stabilization of a rigid body using low-cost sensors. In *Proceedings of the 46th IEEE Conference on Decision and Control*, pages 6424–6429. IEEE, 2007.
- [101] M. D. Hua, Konrad Rudin, Guillaume Ducard, Tarek Hamel, and Robert Mahony. Non-linear attitude estimation with measurement decoupling and anti-windup gyro-bias compensation. In *Proceedings of the 18th IFAC World Congress*, page 29722978, 2011.
- [102] Philippe Martin and Erwan Salaün. Design and implementation of a low-cost observer-based attitude and heading reference system. *Control Engineering Practice*, 18(7):712–722, 2010.
- [103] M.D. Hua, Guillaume Ducard, Tarek Hamel, Robert Mahony, and Konrad Rudin. Implementation of a nonlinear attitude estimator for aerial robotic vehicles. *IEEE Transactions on Control Systems Technology*, 2013.
- [104] M. D. Hua. Attitude estimation for accelerated vehicles using gps/ins measurements. *Control Engineering Practice*, 18(7):723–732, 2010.
- [105] P. Batista, C. Silvestre, and P. Oliveira. Sensor-based complementary globally asymptotically stable filters for attitude estimation. In *Decision and Control, 2009 held jointly with the 2009 28th Chinese Control Conference. CDC/CCC 2009. Proceedings of the 48th IEEE Conference on*, pages 7563–7568, 2009.
- [106] Sanjay P Bhat and Dennis S Bernstein. A topological obstruction to continuous global stabilization of rotational motion and the unwinding phenomenon. *Systems & Control Letters*, 39(1):63–70, 2000.
- [107] N.A. Chaturvedi, A.K. Sanyal, and N.H. McClamroch. Rigid-body attitude control. *Control Systems, IEEE*, 31(3):30–51, 2011.
- [108] D. Kleinman and Michael Athans. The design of suboptimal linear time-varying systems. *Automatic Control, IEEE Transactions on*, 13(2):150–159, 1968.

-
- [109] Itzhack Y Bar-Itzhack and Jeffrey Meyer. On the convergence of iterative orthogonalization processes. *Aerospace and Electronic Systems, IEEE Transactions on*, 12(2):146–151, 1976.